

# AN ANALYTICAL STUDY ON THE ULTIMATE TENSILE STRENGTH OF ANCHOR BOLTS IN CONCRETE UNDER THE PULL-OUT LOADING

ハリヤディ

<https://doi.org/10.15017/1543948>

---

出版情報：九州大学, 2015, 博士（工学）, 課程博士  
バージョン：  
権利関係：全文ファイル公表済

**AN ANALYTICAL STUDY  
ON THE ULTIMATE TENSILE STRENGTH OF ANCHOR BOLTS  
IN CONCRETE UNDER THE PULL-OUT LOADING**



**GRADUATE SCHOOL OF ENGINEERING  
KYUSHU UNIVERSITY**

**H A R I Y A D I**

Department of Civil and Structural Engineering  
KYUSHU UNIVERSITY

A thesis submitted for the degree of  
*Doctor of Engineering*  
March, 2015



DEPARTMENT OF CIVIL AND STRUCTURAL ENGINEERING  
GRADUATE SCHOOL OF ENGINEERING  
**KYUSHU UNIVERSITY**  
Fukuoka, Japan

**CERTIFICATE**

The undersigned hereby certify that they have read and recommended to the Graduate School of Engineering for the acceptance of this thesis entitled, “*An Analytical Study on the Ultimate Tensile Strength of Anchor Bolts in Concrete under the Pull-out Loading*” by **Hariyadi** in partial fulfillment of the requirements for the degree of **Doctor of Engineering**.

Dated: March, 2015

Thesis Supervisor:

---

Professor Yoshimi SONODA, Dr. Eng.

Examining Committee:

---

Professor Masuhiro BEPPU, Dr. Eng.

---

Assoc. Professor Yukihide KAJITA, Dr. Eng.



## ACKNOWLEDGEMENTS

---

Thanks to the Almighty Alloh S.W.T. (God) because of His blessing I can finish my study. I would like to gratefully and sincerely thank Prof. Yoshimi Sonoda for his impeccable guidance, knowledge, and most importantly, his invaluable support and motivation during my graduate studies at Kyushu University.

I also wish to thank Assoc. Prof. Dr Mitsuteru Asai, Dr. Hiroki Tamai, Mr. Susumu Moriya, Mr. Cheon, Dr. Abd. Raheem, Dr. Satoru Menemoto, Mr. Kohei Kiyonari, Mr. Hamidun, Mrs. Nur Ain and all the Structural Analysis Laboratory members for their never-ending support and guidance. Thanks also to all my families who had been supporting me from the beginning of the study until its completion.

I really thank the Directorate General of Higher Education (DGHE) of the Ministry of Education and Culture of Indonesia for the full scholarship (BLN-Dikti scholarship) of this study. I also thank the University of Mataram (Unram) for giving me the chance to continue my study.

Finally, I am also grateful to all parties who have directly and indirectly given their fullest cooperation to ensure a successful completion of my doctoral research.

*Hariyadi*

## **DEDICATED**

---

*Specially dedicated to*

*our parents*

*Melia Rifa Afina*

*Muhammad Zaki Mubarak Hariyadi*

*Haula Aulia Tazkia Hariyadi*

*for*

*the prayers, patience, support, sacrifice, tears and laughter*

## ABSTRACT

---

Generally, the design of pull-out strength of the anchor bolt structure in concrete is based on standards with some parameters and limitations which is generally assumed that the load applied is static load, its failure is a single crack, and the stress is uniform stress. Many efforts have been done to analyze and get a better prediction of strength and behavior of anchor, by numerical analysis and experimental program. However, a numerical analysis, giving a better on figuring the failure modes and on the calculation result still need to explore. Hence, the experimental program and numerical analysis conducted in this study can give a better understanding of failure mechanism of anchor bolt and on strength analyzing. Predicting the performance of anchor bolt structures against pullout loading through full-scale tests is expensive and time consuming to perform. On the other hand, numerical analysis of anchor bolt structures generally based on Finite Element Method (FEM) is limited due to the mesh based technique. Furthermore, the numerical analysis is rather difficult to develop when working with non-elastic materials such as reinforced concrete. Smoothed Particle Hydrodynamics (SPH) method with particle based technique can be more reliable on figuring a large deformation of particles when the material deforms and moreover they can be accurately tracked. According to the characteristic of concrete is non-elastic material, the pressure dependent criterion is more appropriate to evaluate the accuracy of material strength and the plastic failure behavior of concrete/mortar under pull-out loads. In this analysis, the two-parameter pressure dependent model, Drucker-Prager (DP) is applied to concrete materials, whereas the pressure independent (von Mises -VM) criterion is employed to steel anchor bolt. Anchor bolt structure is one case of hybrid/composite structures, so when the different properties materials combined, the problem of bond character assumption between them arises. For further analysis, the developed bond character is applied to model specifically on the contact surface between concrete and steel anchor bolt. The simulated results using SPH conform to the design standard in term of the maximum loading capacity. Even though the loading capacity of numerical analysis results is in accordance with the design standards, however, it is still higher than the experimental result. Consequently a



certain correction/ safety factor should be used when the numerical analysis will be applied to the design and analysis of anchor bolt structure. Finally, the numerical analysis using SPH method, applying the von Mises and Drucker-Prager constitutive model, and considering the bond character model is reliable to predict the failure mode and loading capacity of the anchor bolt in concrete under pull-out load.

## TABLE OF CONTENT

---

CERTIFICATE .....	iii
ACKNOWLEDGEMENTS .....	v
DEDICATED.....	vi
ABSTRACT.....	vii
TABLE OF CONTENT.....	ix
LIST OF FIGURES .....	xiii
LIST OF TABLES .....	xvi
LIST OF SYMBOLS .....	xvii
LIST OF APPENDIXES .....	xix
CHAPTER I.....	1
<b>INTRODUCTION</b> .....	1
1.1 Anchor bolts and the pull-out failure.....	1
1.2 Analysis and design assumption problem and computational modelling phenomena ....	5
1.2.1 Design standard equations of anchor bolt and assumption problem .....	5
1.2.2 Computational modeling phenomena.....	8
1.3 Problem definition .....	10
1.4 Objective of the research .....	12
1.5 Scope and limitations of research .....	12
1.6 Organization of the thesis .....	13
1.7 References.....	15
CHAPTER II.....	17
<b>EXPERIMENTAL TESTS</b> .....	17
2.1 Introduction.....	17
2.2 Materials, mix proportion, anchor bolt depth .....	18
2.2.1 Preparation of materials.....	18
2.2.2 Mix proportioning design of mortar. ....	18
2.2.3 Anchor bolt depth and sample size of mortar block.....	19

2.3	Experimental set up, equipment and procedures .....	20
2.3.1	Wooden moulds preparation.....	20
2.3.2	Testing of mechanical properties of steel anchor bolt.....	22
2.3.3	Testing of mechanical properties of mortar.....	22
2.3.4	Testing of pull-out load test.....	23
2.4	Mixing and casting .....	25
2.5	Experimental results .....	27
2.5.1	Tensile strength of anchor bolt.....	27
2.5.2	Compressive strength and modulus elasticity of mortar. ....	27
2.5.3	Tensile strength of mortar. ....	29
2.5.4	Anchor bolt structures under pull-out load test .....	30
2.5.4.1	Reaction force and displacement.....	30
2.5.4.2	Failure mode, cone failure area and concrete cone surface stress.....	30
2.6	Comparison between experimental result and standard design.....	33
2.6.1	Comparison of cone stress.....	33
2.6.2	Comparison of maximum pull-out loading capacity.....	34
2.7	Conclusion .....	36
2.8	References.....	37
CHAPTER III .....		39
<b>SPH METHOD AND NUMERICAL CALCULATION SETTING.....</b>		<b>39</b>
3.1	Introduction.....	39
3.2	Review of mesh-free method.....	39
3.3	Smoothed particle hydrodynamics (SPH) method .....	41
3.4	Conservation equations and its approximation forms .....	49
3.4.1	Conservation of mass equation.....	50
3.4.2	Conservation of momentum equation .....	51
3.5	Calculation scheme of SPH to the solid-state analysis.....	54
3.6	Constitutive model.....	56
3.6.1	Elastic-plastic constitutive equation von Mises criteria .....	56

3.6.2	Elastic-plastic constitutive equation Drucker Prager criteria .....	63
3.7	Combination of von Mises (VM) and Drucker-Prager (DP) failure criterion .....	74
3.8	Tensile softening – elastic degradation.....	75
3.9	Boundary condition problem on SPH.....	79
3.9.1	Boundary condition on the free surface.....	79
3.9.2	Dummy particles and its effect to the numerical stability .....	80
3.10	Conclusion .....	82
3.11	References.....	83
<b>CHAPTER IV .....</b>		<b>87</b>
<b>NUMERICAL ANALYSIS WITH PERFECT BOND OF ANCHOR AND CONCRETE</b>		<b>87</b>
4.1	Introduction.....	87
4.2	Numerical analysis of pull-out simulation models .....	88
4.2.1	Tensile failure mechanism of anchor bolt with various anchor depth.....	88
4.2.1.1	Pull-out simulation models .....	88
4.2.1.2	Analysis result and discussion .....	91
4.3	Conclusion .....	98
4.4	References.....	99
<b>CHAPTER V .....</b>		<b>101</b>
<b>NUMERICAL ANALYSIS WITH CONSIDERING THE BOND CHARACTER .....</b>		<b>101</b>
5.1	Introduction.....	101
5.2	Bonding character model .....	101
5.3	Comparison between the analysis model with and without considering bonding character .....	107
5.3.1	Load carrying capacity .....	107
5.3.2	Failure mode .....	109
5.4	Conclusion .....	120
5.5	References.....	121

CHAPTER VI.....	123
<b>NUMERICAL-EXPERIMENTAL COMPARISON .....</b>	<b>123</b>
6.1 Introduction.....	123
6.2 Bonding mechanism .....	124
6.3 Numerical analysis of experimental model .....	126
6.3.1 Numerical analysis of experimental model with and without considering the bond character .....	127
6.3.1.1 Loading capacity and displacement.....	127
6.3.1.2 Failure mode of anchor bolt structure .....	128
6.3.2 Comparison between experimental results and numerical model .....	132
6.4 Conclusion .....	134
6.5 References.....	135
CHAPTER VII.....	137
<b>CONCLUSIONS AND RECOMMENDATIONS FOR FUTURE RESEARCH .....</b>	<b>137</b>
7.1 Conclusions.....	137
7.2 Recommendations for future research .....	140

## LIST OF FIGURES

---

Figure 1-1: Expected failure modes and formulas under pull-out load .....	3
Figure 1-2: Anchor failure on the bridge restrainer system and column due to pull-out load....	4
Figure 1-3: Cone failure mode of anchor.....	6
Figure 1-4: Maximum pull-out strength based on failure mode .....	7
Figure 1-5: Computational meshes for the pul-out analysis using grid-based method .....	11
Figure 2-1: The size of anchor bolt specimen.....	20
Figure 2-2: The wooden moulds preparation.....	21
Figure 2-3: Laboratory works of tensile test of anchor bolt .....	22
Figure 2-4: Compression and split tensile test of mortar.....	23
Figure 2-5: The structure of test equipment for pull-out test of anchor bolt .....	25
Figure 2-6: The mixing and casting process .....	26
Figure 2-7: Tensile test of anchor bolt.....	27
Figure 2-8: The compression test of mortar concrete .....	28
Figure 2-9: The split tensile test of mortar concrete .....	29
Figure 2-10: Load-displacement of anchor bolt under Pull-out load test.....	31
Figure 2-11: Cracking line on the concrete surface after pull-out load test .....	31
Figure 2-12: The side view of anchor failure and detail of failure sizes .....	31
Figure 2-13: The comparison of cone failure stress between experimental and standard design .....	34
Figure 2-14: The comparison of pull-out loading capacity between experimental and standard design .....	35
Figure 3-1: Particle approximation in in a three-dimensional problem domain $\Omega$ .....	42
Figure 3-2: The smoothing function and its derivative $W'$ of Bell-shaped function .....	46
Figure 3-3: The smoothing and its first $W'$ of Gaussian function .....	46
Figure 3-4: The smoothing function and its first derivative $W'$ of B-(cubic) spline function ..	47
Figure 3-5: The smoothing function and its first derivative $W'$ of quartic function.....	48
Figure 3-6: The smoothing function and its first derivative $W'$ of quintic function.....	49
Figure 3-7: Calculation flow of the SPH method algorithm.....	55
Figure 3-8: Graphic of VM cylinder with hardening criteria .....	57
Figure 3-9: Uniaxial stress-strain curve.....	58
Figure 3-10: Graphic of DP cylinder with hardening criteria.....	64
Figure 3-11: Calculation of the parameter $k$ using $J_2 - I_1$ plot .....	66
Figure 3-12: Typical uniaxial stress-strain curve .....	69
Figure 3-13: Envelope for DP and VM models.....	74
Figure 3-14: Linear tensile strain-softening and fracture energy, $G_f$ .....	75
Figure 3-15: Numerical method of cone failure .....	76
Figure 3-16: Principal stress and strain calculation .....	76
Figure 3-17: The chronology of calculation for damage parameter .....	77
Figure 3-18: Damage-health level of material .....	78
Figure 3-19: SPH kernel and particle approximation for interior and boundary particles. ....	79
Figure 3-20: Dummy particle on the outside of the boundary.....	80
Figure 3-21: Initial position of dummy particles .....	81
Figure 3-22: Strain in z-direction.....	81
Figure 3-23: Stress in z-direction.....	82

Figure 4-1: Analytical model.....	90
Figure 4-2: Detail of particle arrangement as support .....	90
Figure 4-3: Stress-strain relation of concrete and steel .....	91
Figure 4-4: Pull-out analysis result of anchor bolt ( $h / d = 2$ ) .....	92
Figure 4-5: Pull-out analysis result of anchor bolt ( $h / d = 4$ ) .....	93
Figure 4-6: Pull-out analysis result of anchor bolt ( $h / d = 6$ ) .....	93
Figure 4-7: Pull-out analysis result of anchor bolt ( $h / d = 8$ ) .....	94
Figure 4-8: Pull-out analysis result of anchor bolt ( $h / d = 10$ ) .....	95
Figure 4-9: Influence of embedment depth into load-bearing ability based on the analysis....	97
Figure 4-10: Influence of embedment depth into load-bearing ability based on the design equation.....	98
Figure 5-1: Schematic of bond link element and slip boundary .....	102
Figure 5-2: Schematic of cross product vector of normal and slip vectors .....	102
Figure 5-3: Schematic of cross product vector in local coordinate .....	103
Figure 5-4: Transformation of bond stress and bond strain from local to global coordinate .	103
Figure 5-5: Particle pair of bonding particle.....	104
Figure 5-6: Procedures of bond failure judgement .....	104
Figure 5-7: Stress-strain relation of bond shear and bonding shear softening of mortar...	105
Figure 5-8: Maximum loading capacity of various anchor bolt depths.....	107
Figure 5-9: Ratio of loading capacity between with and without considering bond character .....	108
Figure 5-10: Load-displacement of Model $h/d = 2$ .....	110
Figure 5-11: Displacement on the maximum load of Model $h/d = 2$ .....	111
Figure 5-12: Failure mode analysis considering bond character for Model $h/d = 2$ .....	111
Figure 5-13: Load-displacement of Model $h/d = 4$ .....	112
Figure 5-14: Displacement on the maximum load of Model $h/d = 4$ .....	112
Figure 5-15: Failure mode analysis considering bond character for Model $h/d = 4$ .....	113
Figure 5-16: Load-displacement of Model $h/d = 6$ .....	114
Figure 5-17: Displacement on the maximum load of Model $h/d = 6$ .....	114
Figure 5-18: Failure mode analysis considering bond character for Model $h/d = 6$ .....	115
Figure 5-19: Load-displacement of Model $h/d = 8$ .....	116
Figure 5-20: Displacement on the maximum load of Model $h/d = 8$ .....	116
Figure 5-21: Failure mode analysis considering bond character for Model $h/d = 8$ .....	117
Figure 5-22: Load-displacement of Model $h/d = 10$ .....	117
Figure 5-23: Displacement on the maximum load of Model $h/d = 10$ .....	118
Figure 5-24: Failure mode analysis considering bond character for Model $h/d = 10$ .....	118
Figure 5-25: Maximum loading capacity considering to various of the anchor depths .....	119
Figure 6-1: Mechanism of load transfer of anchor bolt .....	125
Figure 6-2: Model of the anchor bolt structure .....	127
Figure 6-3: Stress-strain relation of mortar and steel anchor. ....	127
Figure 6-4: Load-displacement of the experimental model anchor bolt under pull-out load.	128
Figure 6-5: Displacement on the maximum load of the experimental model .....	129
Figure 6-6: Failure mode analysis without considering bond character for the experimental model .....	130
Figure 6-7: Failure mode analysis considering bond character for the experimental model..	131

Figure 6-8: The comparison of pull-out loading capacity between experimental, numerical and design standard.....	133
Figure A-1: Relationships between stress cracking zone and crack opening .....	151
Figure A-2: Stress-strain relation of bond shear and bonding shear softening of mortar ..	154



## LIST OF TABLES

---

Table 2-1: Mortar mix proportion and expected compressive strength <sup>*)</sup> .....	18
Table 2-2: Mechanical properties of mortar .....	29
Table 2-3: The detail of failure sizes of the inner side area of anchor bolt cone failure .....	32
Table 2-4: The detail of failure sizes of the outside area of anchor bolt cone failure .....	32
Table 2-5: The stress of concrete cone surface by experimental .....	32
Table 2-6: Comparison of tensile cone failure stress between experimental and standard design .....	34
Table 2-7: Comparison of pull-out loading capacity between experimental and standard design .....	35
Table 4-1: Material properties of each material .....	91

## LIST OF SYMBOLS

---

$h$	influence area
$A$	denote the given particle $A$
$B$	denote the given particle $B$
$dV, \Omega$	volume of the integral that contains all particles
$\delta_{ij}, \delta^{AB}$	kronecker-delta
$S$	surface of support domain
$f(x^A)$	functions of target particle $A$
$f(x^B)$	function of neighbouring particle $B$
$kh$	support domain
$W^{AB}$	kernel function
$m$	mass of particle
$\rho$	density
$v, \hat{v}$	velocity, average velocity
$W'$ and $\nabla W$	first derivative of kernel function
$R$	relative distance between two point particles
$N$	number of particles in influence domain
$d/dt$	total time derivative operator
$\sigma_{ij}$	stress tensor
$\sigma'_{ij}$	deviatoric stress tensor
$I_1$	first invariant of stress tensor
$\dot{\varepsilon}_{ij}$	strain rate tensor
$\dot{R}_{ij}$	rotation rate tensor
$\varepsilon_v$	volumetric strain
$K, P, V$	bulk modulus, normal force, volume
$d\varepsilon_{ij}, d\varepsilon^e_{ij}, d\varepsilon^p_{ij}$	total strain increment, elastic strain increment, plastic strain increment
$f_{VM}, f_{DP}$	function of von Mises model, function of Drucker Prager model
$d\sigma_{eqs}, d\varepsilon^p_{eqs}$	increment of equivalent stress, increment of equivalent plastic strain
$dW^p$	plastic work
$d_x^L, d_y^L, d_z^L$	damage parameter in the local coordinate
$\alpha, k$	slope of failure line, intercept of failure line
$H', H$	hardening modulus for von Mises and Drucker Prager

$\sigma_c, \sigma_t$	yield stress (compressive) and yield stress (tensile)
$J_2$	second invariant of deviatoric stress tensor
$E$	young's modulus
$\varepsilon_v^p$	volumetric plastic strain
$\lambda_{vm}, \lambda_{dp}$	plastic multiplier for von Mises and Drucker Prager
$\lambda, \mu$	Lamè constant
$G_f$	fracture energy
$\varepsilon_{crc}, \varepsilon_{cru}$	cracking strain limit and crushing strain limit
$\varphi_x, \varphi_y, \varphi_z$	integrity tensor corresponds to the x, y, z direction
$D$	scalar damage parameter
$[D]^e, [D]^p, [D]^{ep}$	elastic, plastic, elastic-plastic stiffness matrix
$D_{ijkl}^e, D_{ijkl}^p$	fourth-tensor of elastic stiffness, fourth-tensor of plastic stiffness
$h_{ef}$	effective depth of anchor bolt
$\tau$	shear stress between concrete and anchor bolt
$\gamma$	shear strain between concrete and anchor bolt

## LIST OF APPENDIXES

---

APPENDIX 1 - Derivation of notation.....	143
APPENDIX 2 - Calculation of ultimate strain, $\varepsilon_{cr}$ .....	151



## CHAPTER I

### INTRODUCTION

#### 1.1 Anchor bolts and the pull-out failure

Concrete is the most widely used construction material in the world with over 25 billion tons constructed every year. This number is predicted will continuously increase along with infrastructure developments (Schokker, 2010). Since Portland cement introduced by Aspadin, concrete to be the most important building material and widely used in numerous types of engineering structures. Its application in structures is mainly used as column, beam, slab, wall, deck and roof. Considering the availability of concrete material constituent at everywhere and simplicity of mixing and casting process promotes on using concrete material for many applications around the world. Furthermore, the strength and stiffness and the efficiency of concrete structures make it a suitable material for a broad range of structural application. Nowadays, due to a limited construction area, quality control necessity, reducing cost, technological development, and limited resource availability stimulate the concrete precast system and composite/hybrid structures.

Anchorage of the steel bolt in concrete has gained special attention due to some global trends in the construction industry, such as, increasing use of pre-fabricated structural element (precast system) and hybrid structures, increased interest on structural retrofitting earthquake resistance, increased on strengthening and maintenance of existing or historical buildings, and other particular anchorage demands (Solomos and Berra, 2006). The purpose of anchor bolt used is to get a structure with a good strength and stability. In order to connect the other structural members to the concrete structures, the anchorage system (anchor bolt) is necessary

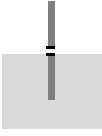
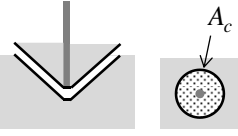

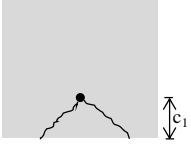
and plays an important role in many cases, for structural as well as nonstructural applications. Anchors are used for transferring load between concrete and other members (such as steel or wood element), and it is useful to improve the flexibility in the design of concrete structures. However, typically concrete or mortar (cementitious material) is a brittle material that performs well in compression but is significantly lower in tension. Thus, it should be deeply evaluated when tensile load is applied.

The demand for the ability to connect components with each other is as old as building itself. The solution for the concrete and masonry construction offer different attachment methods, which are essentially the type of load transfer (positive locking, frictional and adhesive bond) as also differ by the type of installation (Eligehausen *et al.*, 2006a). Anchorage systems comprise of a bolt element (anchor bolt) embedding in and the concrete base material. There are two anchorages to concrete classification, i.e. (i) cast-in-place and (ii) post installed. The post installed anchors may be either bonded or mechanical anchors (screw, expansion sleeve, and undercut types) (Eligehausen *et al.*, 2006b). Based on provision codes and technical paper (ACI Committee 349, 2001; ACI Committee 318, 2011; and Fuchs *et al.*, 1995) the failure modes of anchor under tensile loading are categorized as:

1. *Anchor bolt failure*: the stress of anchor bolt reaches its yield limit resulted from a sufficient embedment depth of anchor, confinement of concrete, and low ratio of the bolt diameter to the resistance of concrete.
2. *Concrete cone failure*: the concrete surrounding the embedded anchor fails in tension originating from the head of anchor and propagating towards the surface which is in conical form. The inclination of the failure surface corresponding to the axis of anchor varies depending on the effective embedment depth of anchor, the diameter of anchor and the concrete behavior (Yang and Ashour, 2009).
3. *Anchor pullout*: the concrete around the head of anchor fails in compression and from this point the fracture propagates shearing towards the surface. *Anchor pull-through*: the anchor bolt slides out of the anchor sleeve commonly due to the shearing adhesion of concrete and anchor is low.

4. *Concrete splitting*: the tensile failure along one or more surface planes of concrete surrounding the embedded anchor originating from the head of anchor and sides and propagating transversely with respect to the axis of anchor.

Figure 1-1 shows an illustration of failure modes of anchor structures under pull-out load and general formulas to determine the maximum loading capacity. Concrete splitting failure is a special case when the anchors located close to an edge or to a corner, particularly when the thickness of the member is small (Huer and Eligehausen, 2007). Hence, the splitting failure will not consider in this thesis. Among these failure modes, concrete cone failure is the most common to be studied. Therefore, a proper estimation of the concrete cone capacity under tensile loads would be controlled by ductile yielding and the nominal strength of anchor (Yang and Ashour, 2009). Under static load, concrete cone failure is commonly estimated by the concrete capacity design (CCD) method (Fuchs *et al.*, 1995) on which design provisions for anchorage systems of ACI 318-11 are referred.

Bolt failure $T_{a1}$	Cone failure $T_{a2}$	Bond failure $T_{a3}$	Split failure $T_{a4}$
			
$T_{a1} = f_y a_0$	$T_{a2} = 0.23(f'c)^{(2/3)} A_c$	$\tau_a = 10\sqrt{f'c/21}$ $T_{a3} = \tau_a \pi d_a l_e$	$T_{a4} = k_p (\pi d_a l_e)^{1/2} c_1^{3/7} h_{cr,sp}^{1/6} f_c^{1/2}$
$f_y$ : Yield strength of the bolt $A_c$ : Effective horizontal projected area	$a_0$ : Nominal cross-sectional area of the bolt $d_a$ : Bolt diameter	$f'c$ : Compressive strength of concrete $l_e$ : Effective length of embedded bolt	$h_{cr,sp}$ : characteristic thickness $k_p$ : product factor

**Figure 1-1:** Expected failure modes and formulas under pull-out load

The anchor bolt structure undergoes various loading conditions during their service life, all of which can produce the failure of the structure. In a real application the anchor bolt receives some load types, mainly: tensile, shear, and combination load. One of the important considerations for the effective use of structural materials is pull-out loading. However, to



simplify this thesis is focused to analyze the anchor structure on concrete under the pull-out loading. Generally, a pull-out loading predominantly one of the accountability focuses for anchor structure both in steel anchor and concrete. In fact, an anchor structure under pull-out loading shows the dissimilar behavior due to differences the mechanical properties of steel anchor and concrete. Thus, loading type is one of the factors that should consider in the analysis and design of anchor structures. Figure 1-2 shows two samples of tensile failures of anchors, that are bridge restrainer systems on concrete pier and base plate of column.



(a) Bridge restrainer system  
(Munemoto and Sonoda, 2012)



(b) Base plate of column  
([https://www.osha.gov/doc/engineering/2012\\_r\\_04.html](https://www.osha.gov/doc/engineering/2012_r_04.html))

**Figure 1-2:** Anchor failure on the bridge restrainer system and column due to pull-out load

The aim of the present work is to contribute to a deeper understanding of the structural behavior of anchors in uncracked concrete under pull-out load. Therefore, in order to describe the maximum loads of the failure modes it is necessary to identify the main factors influencing the structural behavior. The structural behavior is theoretically investigated using the finite-element method and experimentally in single bonded anchors and fasteners group. The state of research on anchor bolt in the concrete and the proposed analysis and design concepts is discussed in detail, evaluated and extended. From the prior knowledge and the newly acquired theoretical and experimental results, a simple, user-friendly, economical and

sufficiently safe design model for individual with anchor bolt shall be developed under tensile loading in uncracked concrete.

With regards to this, there has been a growing interest in the past few decades among the engineering community to understand the response of anchorage structures subjected to pull-out loads. The evaluation on pull-out load will affect jointed elements has been investigated experimentally in the study of Hoehler *et al.* (2011), Solomos and Berra (2006), Eligehausen *et al.* (2006b), Ozbolt *et al.* (1999), Primavera *et al.* (1997), Fujikake *et al.* (2003), Jang and Suh (2006), and Cook and Konz (2001). It also has been examined numerically in the study of Etse (1998), Ozbolt *et al.* (2006), Periskic *et al.* (2007) and Ozbolt *et al.* (2014).

## 1.2 Analysis and design assumption problem and computational modelling phenomena

### 1.2.1 Design standard equations of anchor bolt and assumption problem

There are currently two main design method available to compute the cone failure strength of embedded anchor bolt under static tensile loading, namely Concrete-Cone Method (CCM) (Eligehausen *et al.*, 2006a) and Concrete-Capacity Design (CCD) methods (Fuchs *et al.*, 1995). In the CCM method, the tensile resistance can be expressed by a general basic equation of,

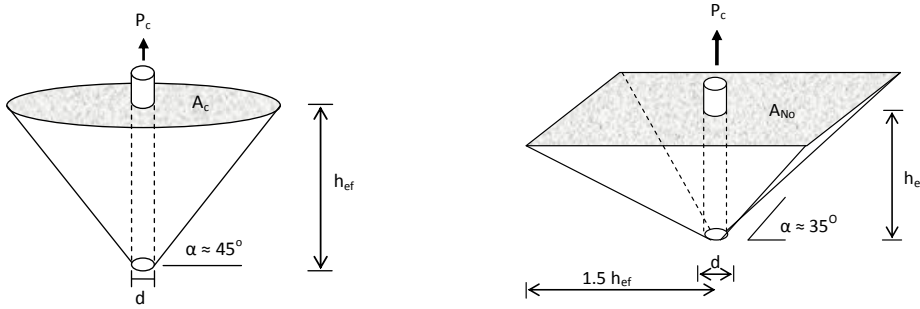
$$P_c = A_c \cdot f_{ct} \quad 1.1$$

where  $A_c$  is projected area of the cone failure of concrete and  $f_{ct}$  is concrete tensile strength. Then, CCM method generally considers a  $45^\circ$  lateral failure cone, so for embedment depth  $h_{ef}$  and the tensile strength expressed by the cube strength of concrete as  $f_{ct} = k \cdot f_c^{0.5}$ , the equation can be written,

$$P_c = k \cdot \pi \cdot f_c^{0.5} \cdot h_{ef}^2 \cdot \left( 1 + \frac{d}{h_{ef}} \right) \quad 1.2$$

The parameter  $k$  is units independent and to simplify the equation to be (Eligehausen, 2006a),

$$P_c = 0.96 \cdot f_c^{0.5} \cdot h_{ef}^2 \cdot \left( 1 + \frac{d}{h_{ef}} \right) \quad 1.3$$



(a) Concrete-Cone Method (CCM)    (b) Concrete-Capacity Design Method (CCD)

**Figure 1-3:** Cone failure mode of anchor

In the Japanese standard, however, the tensile strength of concrete is  $f_{ct} = 0.23 \cdot f_c^{(2/3)}$  (JSCE, 2010), so the equation to be,

$$P_c = 0.72 \cdot f_c^{(2/3)} \cdot h_{ef}^2 \cdot \left( 1 + \frac{d}{h_{ef}} \right) \quad 1.4$$

The CCD method is intended to the concrete capacity of arbitrary fastenings under tension or shear load. The concrete capacity of single anchor under tension is calculated by assuming an inclination between the concrete surface and the failure surface of about  $35^\circ$ . The widespread failure surface should be observed about three times the effective embedment ( $h_{ef}$ ). In the CCD method, it was assumed that there are several factors affected to the breakout resistance, such as: the nominal tensile strength of concrete and the projected failure area, with additional some calibration factors. Based on the proposed basic idea, the ultimate tensile strength is calculated as,

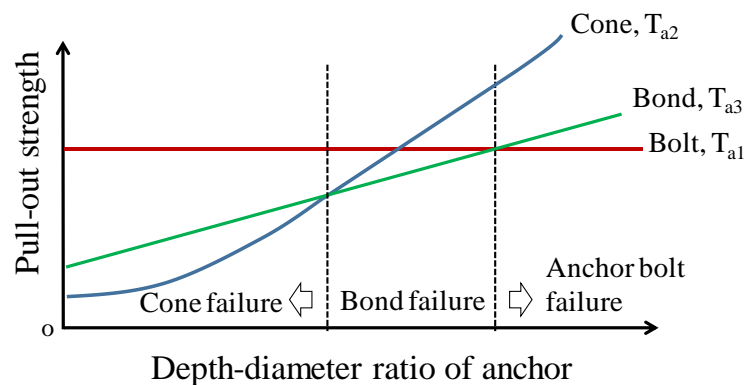
$$P_c = k_1 \cdot f_c^{0.5} \cdot k_2 \cdot h_{ef}^2 \cdot k_3 \cdot h_{ef}^{-0.5} \quad 1.5$$

where  $k_1$ ,  $k_2$ ,  $k_3$  are calibration factors (calibration for tensile strength of concrete, cone failure projected area and size effect, respectively) and they are simplified to be  $k_{nc}$ , so the equation becomes,

$$P_c = k_{nc} \cdot f_c^{0.5} \cdot h_{ef}^{1.5} \quad 1.6$$

where  $k_{nc} = 10$  for cast in situ anchor bolt and 7 for post-installed anchor bolt (ACI 318, 2011). The CCD method was created to predict the failure loads of cast-in-place anchors and postinstalled concrete breakout failure (Eligehausen et al., 2006). Moreover, the CCD and CCM method assume that the tensile strength of concrete is  $f_{ct} = 0.48 \cdot f_c^{0.5}$ .

In current design formulas, there is some problem related to the failure assumption of anchor bolt structure. First, on anchor bolt failure the standard assumed that the pull-out strength is affected by yield stress of anchor only. So, when the certain embedment depth used, the maximum strength due to the anchor bolt failure is constant even the depth of anchor increase. Some parameters affected is neglected in this assumption, such as size effect, tension softening, and other parameters.



**Figure 1-4:** Maximum pull-out strength based on failure mode

Second, for the cone failure of concrete, the standard assumed that the tensile stress of concrete is uniform stress throughout the cracking concrete surface ( $A_c$ ). In addition, standard design formula assumed that the crack path of concrete under pull-out load is only a single crack, starting from the end of effective depth and propagate to the surface of concrete with a certain degree's inclination. However, in real phenomena the cone failure developed may differ from design load, because several cracks may grow at the same time.

Third, for the bond failure, the standard assumed that the shear stress is uniform over the breaking surface of concrete and parallel to the anchor. On the other hand, the bond stress may vary in accordance to the depth anchor. And also some parameters may affect to the bond characteristic such as adhesion, friction, and mechanical interlocking. NCHRP (2008) classifies factors affecting bond performance in two main categories, such as member properties and material properties. Some member property factors are transfer length, splice length, transverse of anchor bolt, casting position, and concrete cover and spacing of anchor bolts. Whereas, anchor bolt properties and concrete properties are classified as material properties.

### **1.2.2 Computational modeling phenomena**

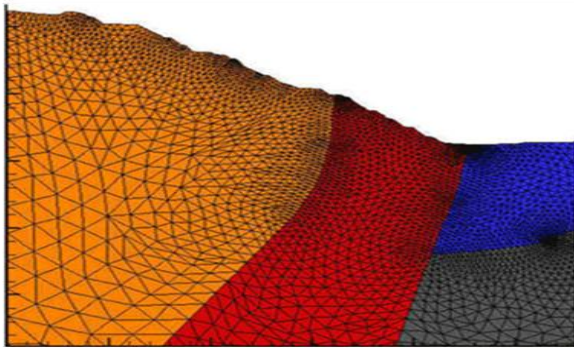
It is costly and time consuming to estimate the response of concrete structures under pull-out loading through full-scale in terms of providing the necessary test equipment, test material, and time to perform. Nowadays, the estimation of the anchorage concrete structure response under pull-out load by implementing numerical analyses is becoming more accurate and reliable. By combining between modern computer hardware and numerical hydrocodes, the accurate result and real figure has shown to a satisfactory level. The computer program that is currently developing in this field, the numerical models for the pull-out load assessment on concrete anchor bolt are fairly quick to obtain. Moreover, the computational simulation delivers a better understanding of the failure mode phenomena and it can be investigated thoroughly.

The analysis and design behavior of anchorage structures under pull-out loading are frequently rather complex. The complicated analysis is found when working with non-elastic materials such as the reinforced concrete. Thus, the conventional approach of structural analysis is not long enough to define the real behavior of concrete element under pull-out load. Therefore, solving problems in the computational solid mechanics using various grids or mesh-based methods such as finite-element method (FEM), finite-difference method (FDM) or finite-volume method (FVM) have been explored. The FEM, as one of the most popular numerical methods, has achieved great success in various areas. The FEM also has been widely employed for solving the linear-elastic and elastic-plastic failure problems, as well as has become a popular technique in civil engineering for predicting the response of structures and materials. In general, Finite element (FE) is a structural analysis method in which the problem in continuum mechanics is approximated by the analysis of an assemblage of FEs, which is interconnected at a finite number of nodal points and represents the solution to the problem.

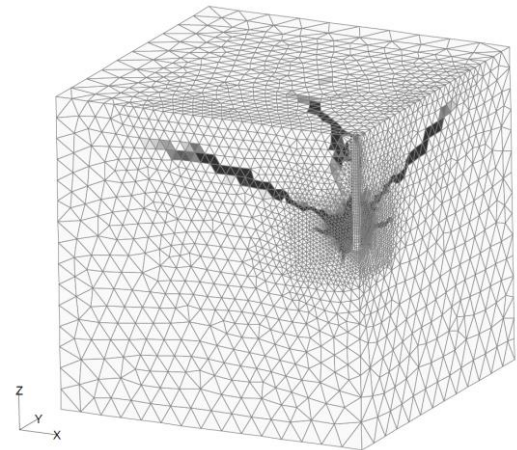
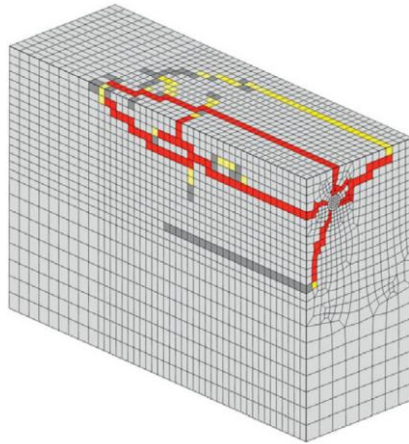
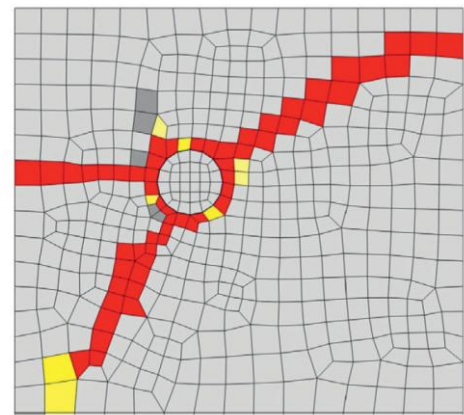
The main feature of the grid or mesh-based numerical model is by dividing a continuum domain into discrete small sub domains which is termed as discretization or meshing. A mesh (or grid) is developed by connecting the individual grid points (or nodes) together in a predefined manner with a topological map. Even though FE techniques already have a great success, however some of its techniques have certain inherent advantages and disadvantages, which exactly depend to a large extent on its particular application. Some problems related to the use of mesh are process of generating/regenerating an appropriate and effective mesh and difficulties to evaluate the reliability calculation of some mechanical behavior, such as shear, tensile, and flexural failure of concrete members. And among of these disadvantages, one notable weakness is that the FEM cannot figure the large deformation of failure member, so the real magnitude of failure cannot be identified. In the research papers of Etse (1998), Ozbolt *et al.* (2006), Periskic *et al.* (2007) and Ozbolt *et al.* (2014), they show the failure mode of anchor bolt structures analyzed by FEM (such examples as shown in Fig. 1-5) in the mesh-based numerical methods, particularly when working on large deformation problems.

### 1.3 Problem definition

It has been acknowledged that many researchers (Etse (1998), Ozbolt *et al.* (2006), Periskic *et al.* (2007) and Ozbolt *et al.* (2014)) have successfully analyzed the elastic-plastic behavior of anchorage structures under pull-out loads using a FEM. However, simulation of solid mechanics problem due to large displacement can cause in the application of FEM problems. Their difficulties and limitations can be investigated from the shown figures in their paper. When the material deforms, the large relative movement (large deformation) of the connecting nodes cannot be tracked accurately. Thus, the connectivity of arbitrarily distributed particles should be applied to provide a stable numerical solution. Smoothed Particle Hydrodynamics (SPH) as the particle based technique can be a superior to the FEM to solve the limitation in the mesh based technique. During the process of computation, the SPH method does not require a pre-defined mesh to render any particle connectivities. The state of a system is represented by a set of discrete particles, without a fixed connectivity; hence, such methods are inherently well-suited for the analysis of moving discontinuities and large deformations such as the breaking and fragmentation on structures. Besides, the SPH particles having material properties are allowed to move in light due to the internal interactions and external forces. The main advantage of SPH method is the absence of a computational grid or mesh since it is spatially discretized into Lagrangian moving particles. This allows the possibility of easily modeling deformation and fragmentation with a complex geometry or arbitrary movement where large deformations occur.



(a) Mesh generation of complex geometry

(b) Typical of crack patterns of small head anchor (Periskic *et al.*, 2007)(c) Predicted crack patterns of anchor bolt (Ozbolt *et al.*, 2014)(d) Crack patterns in the cross section (Ozbolt *et al.*, 2014)**Figure 1-5:** Computational meshes for the pul-out analysis using grid-based method

During the last few years, mesh-less methods has been widely and successfully applied to computation of solid mechanics problems. However, there is no researcher who study the anchor structure using mess-less methods, including SPH method. On the other hand, tensile response simulation of concrete structures using mesh-free techniques have been extensively presented such as in the study of Fukazawa and Sonoda (2011). This previous SPH analysis only considers the behavior of concrete and steel itself and ignore the effect of bond character in the interface zone. According to the bonding characteristics of concrete and anchor bolt, the bond character criterion is significantly important to evaluate accurate pull-out strength and failure mode of anchor bolt concrete/mortar under pull-out loads.



## 1.4 Objective of the research

From the study overview and problem statement as explained in the preceding subtopics, the specific targets of this research are outlined as follows:

- a) To investigate the behavior of anchor bolt structures under pull-out loads in aspects of failure through an experimental work.
- b) To develop an analysis procedure using the SPH method and implement a proper constitutive model that can effectively simulate the failure mode of anchor bolt in concrete under pull-out loads.
- c) To implement the bond character model between mortar concrete and anchor bolt and investigate its effect to the pull-out loading capacity and failure mode.
- d) To get a deviation between the numerical and experimental model of anchor bolt by with and without considering the bond character. It will be useful to validate the numerical model when it will be applied in the analysis and design of anchor bolt.

## 1.5 Scope and limitations of research

Some parameters affecting the strength of anchor bolt is such as the mechanical behavior of materials, anchor depth and diameter of anchor. Moreover, the adhesion factor (bond) between concrete and anchor bolt also plays an important role on the pullout strength, and it still has not been studied entirely. Thus, an attempt has been made in the current study by developing a simple and reliable bond character model, with regards to assessing the response of anchor bolt structures due to pull-out loads in term of failure mode and reaction force. The numerical capabilities were extensively verified against experimental result.

This research is limited to the static pull-out load because it is the most applicable to civil engineering structures. In addition, the investigation and the computation schemes focus on the failure behavior of anchor bolt structures. The aim of this research is to focus on concrete/mortar failure simulation and also the yielding and failure of steel anchor.

## **1.6 Organization of the thesis**

This dissertation presents and discusses the results of a numerical and experimental investigation of the failure mode and ultimate strength on the anchors embedded in concrete under pull-out loading. A literature review of the design formulas to predict the ultimate pullout capacity of anchors is provided in Chapter I. In this chapter a various different applications of anchor bolts are also reviewed. It is shown that the pullout failure is governed by the propagation of a single and discrete crack. This simplification resulted inaccurate result and may cause a premature failure. Furthermore, no provisions or investigations are available to evaluate bonding character of anchors embedded in the concrete matrix. It can be concluded that a better understanding of the effect of initial compressive strength of concrete and tensile fields on the load-carrying capacity of anchors is needed.

The experimental part of this study is described in Chapter II. The shallow depth of anchors and normal strength of mortar is conducted to investigate the failure mechanisms of the anchors. Load displacement curves, ultimate load-carrying capacity and crack paths are presented and discussed. Finally, the experimental results compare to the various design standards. In Chapter III, the SPH method and numerical calculation setting are presented. A basic formulation and calculation procedure of SPH are expressed. Constitutive model consists of von Mises and Drucker-Prager are also described in this chapter. The boundary problem in SPH method tried to be solved by applying dummy particles. The result shows that the distribution of the dummy particles around the boundary area is very useful to solve mechanical problems under the free surface condition.

In Chapter IV, numerical insights of the progressive pullout of anchors embedded in an unstressed concrete matrix are described. The low dynamic load is applied to the structures

and a perfect bonding between the concrete and anchor bolt is assumed. Constitutive model applied in this analysis consist of von Mises for the bolt and Drucker-Prager for the concrete. The effects of depth of anchor on the ultimate load carrying capacity and on the load displacement behavior are evaluated in terms of the failure mode analysis using the SPH method. It is also concluded that the SPH method adequately describes the large deformation of anchor failures.

The bonding character of numerical model is developed in Chapter V, since a combination failure between bond failure and cone failure is generally found in anchor structures. In order to solve the phenomenon, a modified constitutive model is constructed and applied to simulate the effects of the bonding zone on developing cracks around the contact surface between anchor bolt and concrete. All models analyzed in Chapter IV are reinvestigated by applying the bonding character. Then, the numerical analysis results between without and with considering bonding character, obtained in Chapter IV and in this chapter respectively are compared and reviewed.

In Chapter VI, numerical analysis of experimental model is conducted in with and without considering bonding character. Obtained results of the experimental program examined in Chapter II are compared to the numerical predictions gained in this chapter. Limits and differences between the experiments and the two analysis methods are discussed. Besides, these results are also compared to the standard design to verify the numerical analysis. The perfect bonding assumption explained in Chapter IV should be modified considering the bonding character between concrete and anchor bolt. Even though the loading capacity of numerical analysis results is in accordance with the design standards, however, it is still higher than the experimental result, consequently a certain correction factor should be used when the numerical analysis will be applied to the design and analysis of structure. Finally, in general, it can be concluded that there is a good correspond between experimental and numerical analysis.

In Chapter VII, a series of conclusions of each chapter are redrawn together with some recommendations for the future research are proposed.

## 1.7 References

- ACI Committee 318, Building code requirements for structural concrete (ACI 318M-11) and commentary (318M-11), *American Concrete Institute* (2011).
- ACI Committee 349, Code requirements for nuclear safety related concrete structures (ACI 349-01), *American Concrete Institute* (2001).
- Anonim: [https://www.osha.gov/doc/engineering/2012\\_r\\_04.html](https://www.osha.gov/doc/engineering/2012_r_04.html), accessed on 31 October 2014.
- Cook, R.A. and Konz, R.C.: Factors influencing bond strength of adhesive anchors, *ACI Structural Journal*, Vol. 98, No. 1, pp. 76-86 (2001).
- Eligehausen, R., Mallee, R., and Silva, J. F.: Anchorage in Concrete Construction, First edition, *Ernst & Sohn*, Berlin (2006a).
- Eligehausen, R., Cook, R. A., and Appl, J.: Behavior and design of adhesive bonded anchors, *ACI Structural Journal*, Vol. 103, No. 6, pp. 822-831 (2006b).
- Etse, G.: Finite element analysis of failure response behavior of anchor bolts in concrete, *Nuclear Engineering and Design*, Vol. 179, pp. 245-252 (1998).
- Fuchs, W., Eligehausen, R., and Breen, J. E.: Concrete Capacity Design (CCD) approach for fastening to concrete, *ACI Structural Journal*, Vol. 92, No. 1, pp. 73-94 (1995).
- Fujikake, K. et. al.: Chemically bonded anchors subjected to rapid pullout loading, *ACI Materials Journal*, Vol. 100, No. 3, pp. 246-252 (2003).
- Fukazawa, J. and Sonoda, Y.: Analysis accuracy of impact failure response of reinforced concrete beam using ASPH method, *Journal of Structural Engineering, Japan Society of Civil Engineers*, Vol. 57A, pp. 1205-1212 (2011).
- Hoehler, M.S., Mahrenholtz, P. and Eligehausen, R.: Behavior of anchors in concrete at seismic-relevant loading rates, *ACI Structural Journal*, Vol. 108, No. 2, pp. 238-247 (2011).
- Huer, T. and Eligehausen, R.: Splitting failure mode of bonded anchors, *Proceedings of FraMCoS-6 Catania, Italy* (2007).

- Jang, J.B. and Suh, Y.P.: The experimental investigation of crack's influence on the concrete breakout strength of a cast-in-place anchor, *Nuclear and Engineering Design*, Vol. 236, pp. 948-953 (2006).
- JSCE: Standard specifications for concrete structures-2007, Design, JSCE Guidelines for Concrete No. 15, *Japan Society of Civil Engineers (JSCE)* (2010).
- Munemoto, S. and Sonoda, Y.: An analytical study about dynamic failure mechanism of anchor bolts embedded in concrete, *Proceeding of Advances in Discontinuous Numerical Methods and Applications in Geomechanics and Geoengineering*, CRC Press (2012)
- NCHRP: Transfer, development, and splice length for strand/reinforcement in high-strength concrete (NCHRP Report 603), *National Cooperative Highway Research Program*, Washington (2008).
- Ozbolt, J., Eligehausen, R. and Reinhardt, H.W.: Size effect on the concrete cone pull-out load, *International Journal of Fracture*, Vol. 95, pp. 391-404 (1999).
- Ozbolt, J., Orsanic, F. and Balabanic, G.: Modeling pull-out resistance of corroded reinforcement in concrete: Coupled three-dimensional finite element model, *Cement & Concrete Composites*, Vol. 46, pp. 41-55 (2014).
- Ozbolt, J., Rah, K.K. and Mestrovic, D.: Influence of loading rate on concrete cone failure, *International Journal of Fracture*, Vol. 139, pp. 239-252 (2006).
- Periskic, G., Ozbolt, J. and Eligehausen, R.: 3D Finite Element analysis of stud anchors with large head and embedment depth, *Proceedings of FraMCoS-6 Catania*, Italy (2007).
- Primavera, E.J., Pinelli, J.P. and Kalajian, E.H.: Tensile behavior of cast-in-place and undercut anchors in high-strength concrete, *ACI Structural Journal*, Vol. 94, No. 5, pp. 583-592 (1997).
- Schokker, A.J.: The sustainability concrete guide, *U.S. Green Concrete Council*, USA (2010).
- Solomos, G. and Berra, M.: Testing of anchorage in concrete under dynamic tensile loading, *Materials and Structures*, Vol. 39, pp. 695-706 (2006).
- Yang, K.H., and Ashour, A. F.: Mechanism analysis for concrete breakout capacity of single anchors in tension, *ACI Structural Journal*, Vol. 105, No. 5, pp. 609-616 (2009).

## CHAPTER II

### EXPERIMENTAL TESTS

#### 2.1 Introduction

The objective of this chapter is to describe in details about the pull-out behavior and the failure mode of the anchorage in mortar concrete. Preparation of samples were conducted at the Concrete Laboratory, and tests of anchor bolt under pull-out load were performed at the Structural and Earthquake laboratory, Kyushu University. This chapter will include all important data which are required to construct a computational model of the anchor bolt structure in the next following chapter. A detailed characterization of the results found through experimental program is provided for comparison and validation of the proposed computational model.

In this experiment, the mortar block which only uses the fine aggregate has been chosen to eliminate the effect of aggregate on the crack propagation under tensile stress. The experimental work has shown that the anchor bolt under the pull-out load realizing a peak reaction force followed by cracking and concrete cone failure mode of the mortar block. To investigate further failure mode of the mortar block, further pull-out load has been imposed onto the specimen until the concrete cone was perfectly detached. The final angle of cone slope and cone failure area of the mortar block will be presented in the following sub-topics, where its common failure modes are most important for further analysis and comparison to the results of the numerical simulation.

## 2.2 Materials, mix proportion, anchor bolt depth

### 2.2.1 Preparation of materials.

Materials used for making mortar concrete in this research were ordinary Portland cement, normal fine aggregate (sea sand) and water. Ordinary Portland cement with bulk density ( $\gamma_c$ ) 3.16 g/cm<sup>3</sup> and blaine fineness or specific surface area (SSA) 3,390 cm<sup>2</sup>/g was used. The material data of fine aggregate, sea sand (washed) are SSD density ( $\gamma_s$ )= 2.58 g/cm<sup>3</sup> and fineness modulus (FM) = 2.77.

The threaded bolt with diameter 16 mm is used for bolt anchor in this research. Some mechanical property data of the bolt are needed to evaluate the anchor structure by numerical model. Therefore, tensile test will be conducted to find the current mechanical properties of bolt, namely yield strength, yield strain, ultimate strength and ultimate fracture strain.

### 2.2.2 Mix proportioning design of mortar.

In this experimental test, we use mortar in order to eliminate the effect of coarse aggregate to the development of cracking propagation. In addition, it is assumed that the strength of cement mortars with certain mix proportion reaches 32 MPa for cube samples or 29 MPa ( $f_c \approx 0.89 f_{cc}$ ) for cylinder samples after curing duration of 7 days. The proportion of materials are calculated (refer to ASTM C109-07, 2007) that the proportion of sand to cement is 2.75:1 (by mass) and water cement ratio (WCR) = 0.485. The porosity of mortar is assumed similar as normal concrete that is around 4.5%. Calculation of material needed for 1 m<sup>3</sup> mortar is shown in Table 2-1.

**Table 2-1:** Mortar mix proportion and expected compressive strength<sup>\*)</sup>

Water-cement ratio	Cement (kg)	Water (kg)	Fine Aggregate (kg)	Expected Compression Strength, 7 days (MPa)
0.485	508.88	246.81	1,399.41	29

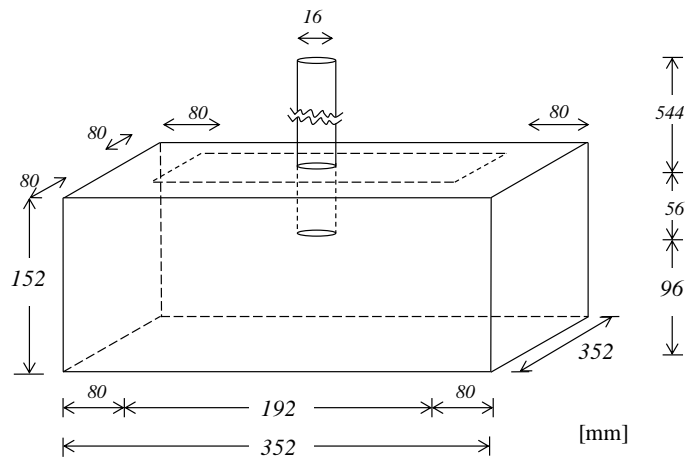
<sup>\*)</sup> Materials needed for 1 m<sup>3</sup> mixing, refer to ASTM C-109-07, 2007

### 2.2.3 Anchor bolt depth and sample size of mortar block.

The model size should be decided and then prepare the sample models of concrete anchor bolt model. The size of samples refers to established experimental result by other researchers and compare them to the computational model results. For the first step, we consider the samples that it will break due to concrete failure only (cone failure mode). So, by assuming a perfect bonding between concrete and steel anchor, the cone failure mode should be found.

Based on the some literatures (Solomos and Berra, 2006; Eligehausen *et al.*, 2006b; Fujikake *et al.*, 2003; Jang and Suh, 2006; Hoehler, 2011), the cone failure of anchor bolt can be found when the ratio between the depth (h) and diameter (d) of anchor (h/d) maximum equal to 5. However, to eliminate other unpredictable factors affecting the cone failure that may cause failure in shallow depth, we will conduct an experiment with a depth-diameter ratio equal to 3.5. This depth is chosen and considered with an assumption that the failure mode of anchor bolt is the cone failure mode. The depth of mortar is approximately 3 times of the depth of anchor. The concrete cover depth (the depth of concrete under the anchor bolt) is chosen thicker than the anchor depth which is 2 times of anchor depth, it is aimed to prevent an early cracking or spalling. Regarding the support distance, the ASTM standard (ASTM E488-96) stated that the distance between the support is no less than 4 times of the anchor depth. So that, we design with the distance of support as standard requirement. The detail size of anchor model can be seen in Fig. 2-1.



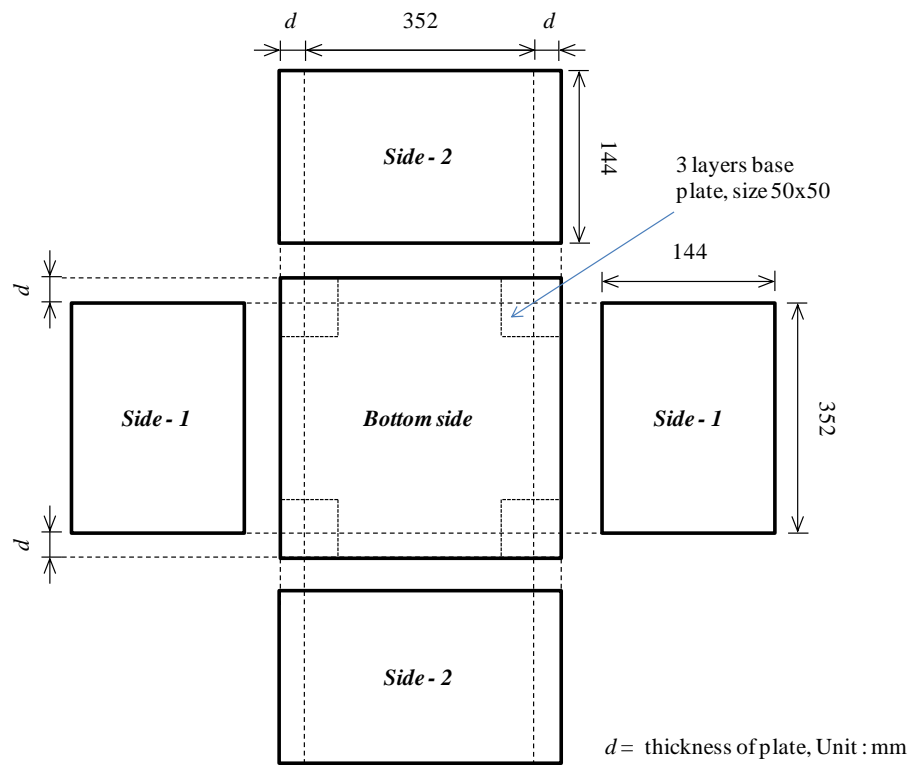


**Figure 2-1:** The size of anchor bolt specimen

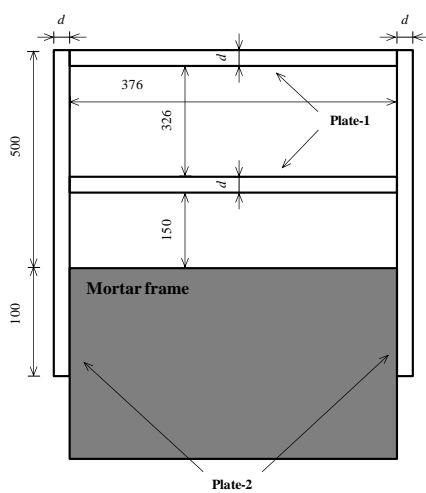
## 2.3 Experimental set up, equipment and procedures

### 2.3.1 Wooden moulds preparation

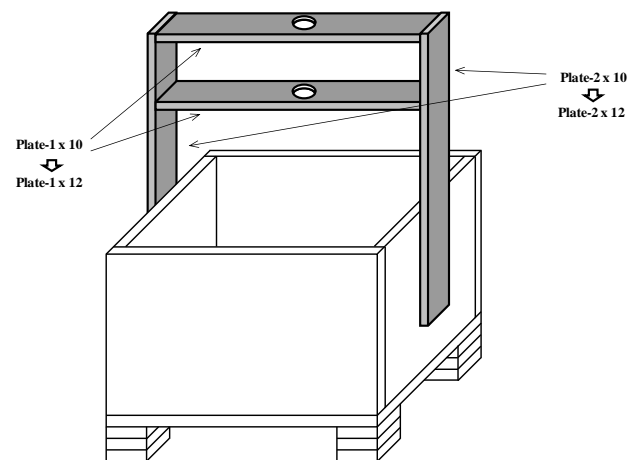
The wooden moulds were prepared to cast the five samples with all same size of mortar concrete block samples to maintain the fixed embedment depths. The inner surfaces of mould were used the watertight and slippery plastic surface for easier demoulding. The left and right of wooden mould was mounted upright and nailed wooden boards. And also two pieces board were flat nailed at the top and the middle position. The drill holes for 16mm diameter anchors were made in the flat wooden board to hold the steel anchor using 20mm drill bit. All of wooden mold elements are assembled with screw-nail to assure the adequacy of mould strength and no changing size when it is used. The component of wooden mould and final wooden mould structure is shown in Fig. 2.2.



(a) The wooden plates for assembling the moulds



(b) Attached of strain gauges



(c) Tensile test of anchor bolt

**Figure 2-2:** The wooden moulds preparation

### 2.3.2 Testing of mechanical properties of steel anchor bolt

The tensile test of steel anchor will be conducted to find its mechanical properties, namely yield strength, yield strain, ultimate strength and ultimate fracture strain. Figure 2-3 shows the procedure of tensile test of anchor bolt. Before conducting tensile test, a strain gauge attached to the smoothed surface of anchor bolt. The purpose of attaching the strain gauge is to measure the strain of the bolt when tensile load is applied on it, and finally the mechanical properties of anchor bolt can be properly identified. A stiff machine with a 100 ton maximum capacity is the main equipment for tensile test of anchor bolt.



(a) Attached of strain gauges



(b) Tensile test of anchor bolt

**Figure 2-3:** Laboratory works of tensile test of anchor bolt

### 2.3.3 Testing of mechanical properties of mortar

Several tests will be conducted to find the mechanical properties of mortar concrete, namely compression test, split tensile test, and density. The measurement of compressive strength of mortar concrete was conducted in accordance with JIS A 1108, and the mean of

results obtained with some identical specimens was reported. Double face of sample smoothed by grinding was used before testing. A stiff machine with a 3000 kN capacity will be used to perform this test on 100mm x 200mm cylinder specimens. The displacement of each specimen was measured using a compressometer during the compressive strength test for determining the modulus of elasticity. The measurement of modulus elasticity of mortar in accordance with JIS A 1127, and the mean of several results obtained will be reported.

The split tensile test will be conducted in accordance with JIS A 1113, and the average of split tensile strength will be obtained from several test data. A stiff machine with a 3000 kN capacity will be used to perform this test on 100x135mm cylinder specimens. Figure 2-4 shows the compression and split tensile test of mortar concrete.



(a) Compression test of mortar



(b) Split tensile test of mortar

**Figure 2-4:** Compression and split tensile test of mortar

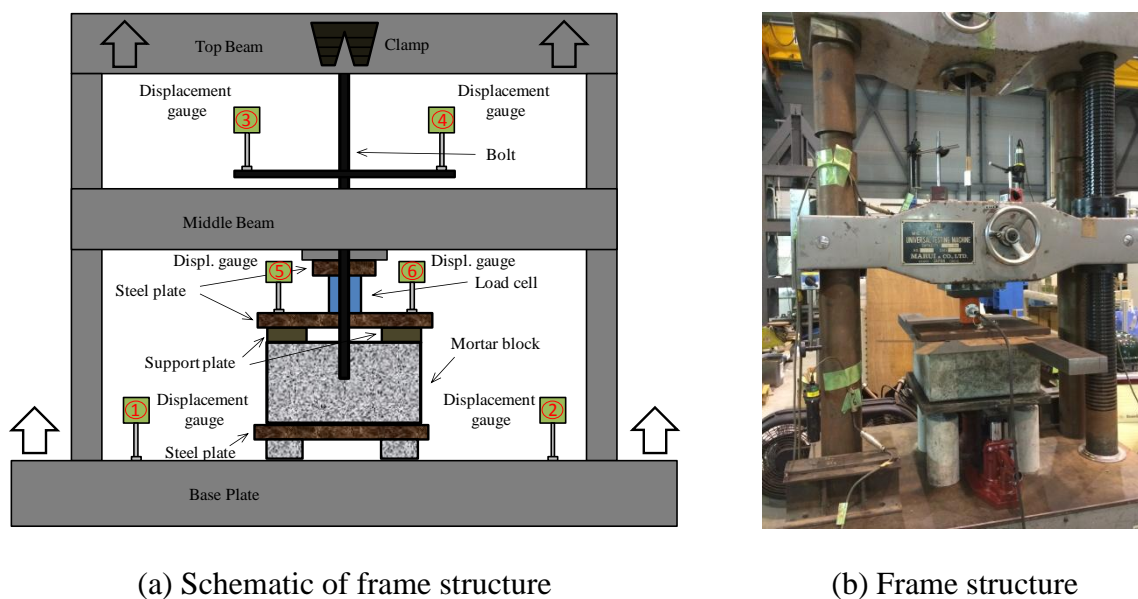
### 2.3.4 Testing of pull-out load test

A stiff machine with a 100 ton maximum capacity is the main equipment for anchor bolt test. A portal frame and a number of dial gauge will be used in this experimental program. There are two beams and base plate in this frame. The base plate and upper beam can move

up-down together, while the middle beam is still in the constantly position. The foundation that consists of concrete cylinder and steel plate put on the base plate. Procedure for testing of the anchor bolt test under pull-out load is:

- 1) Arrange a certain distance between the base plate, middle beam, and top beam.
- 2) Put some concrete cylinders and a steel plate on the top as a foundation. Also put two hydraulic jacks in the middle with the same level with the concrete cylinder.
- 3) The mortar block together with support plate, steel plate and load cell are placed on the steel plate, and then arrange the position of the middle beam until the anchor bolt can be screwed with the extended steel rod. Fixed the anchor to the top of the beam.
- 4) To get the displacement of anchor bolt, the mortar block sample was moved a few centimeters to up using hydraulic jack until touching and getting a fixed condition to the bottom side of the middle beam.
- 5) Placed some the dial gauge (displacement gauge) to measure the displacement of the frame and anchor bolt. The bottom dial gauges (no 1 and 2) are positioned to measure the displacement of base plate to the middle of beam, while the top dial gauges (no 3 and 4) are used to measure the gross of displacement of anchor bolt. On the other hand, the middle dial gauges (no 5 and 6) are used to measure the displacement of upper surface of concrete specimen.
- 6) The pull-out load is gradually applied to the structure of mortar block until failure.

An illustration of the structure for testing the anchor bolt under pull-out load can be seen in Fig. 2-5.



(a) Schematic of frame structure

(b) Frame structure

**Figure 2-5:** The structure of test equipment for pull-out test of anchor bolt

## 2.4 Mixing and casting

Mixing procedure for the mortar is as follows. The cement and aggregate were first poured into the mixing pan and then mixer started. Thirty second later, then the water was added to the mix. The mortar was then mixed for another two minute. While stopping for around 30 second, the mix is mixed by hand to prevent the cement agglomeration. A visual inspection on the consistency of fresh mortar was done to ensure that the aggregates had been evenly mixed with the paste.

Other consistency testing by flow table test was done to ensure the paste is good workability. The flow table test is conducted by pounding the mortar on the standard steel table for 15 times in 15 second. The slump examined by table test is expressed by percentage comparison between the increasing diameter of mortar after pounding and initial diameter. The average slump of three mortar test is 26.1%.

In general, each size of 100x200 mm cylinder for compression test, 100x135 mm cylinder for split tensile/ Brazilian test and 352x352x144 mm mortar block were cast for a batch of mortar concrete. Each five cylinder samples were used for compressive strength test and split tensile/ Brazilian test, and 5 mortar block samples for anchor bolt test. The cylinders



were cast in two layers, and whereby each layer was rammed by hand rodding for 8 times as the standard procedure and consolidated by vibration table for 15 second. A similar procedure was also applied for compacting the mortar block. The mixing and casting process of mortar concrete can be seen in Fig 2-6.



(a) Mixing process



(b) Flow table test



(c) Compaction process of mortar block



(d) Casting samples

**Figure 2-6:** The mixing and casting process

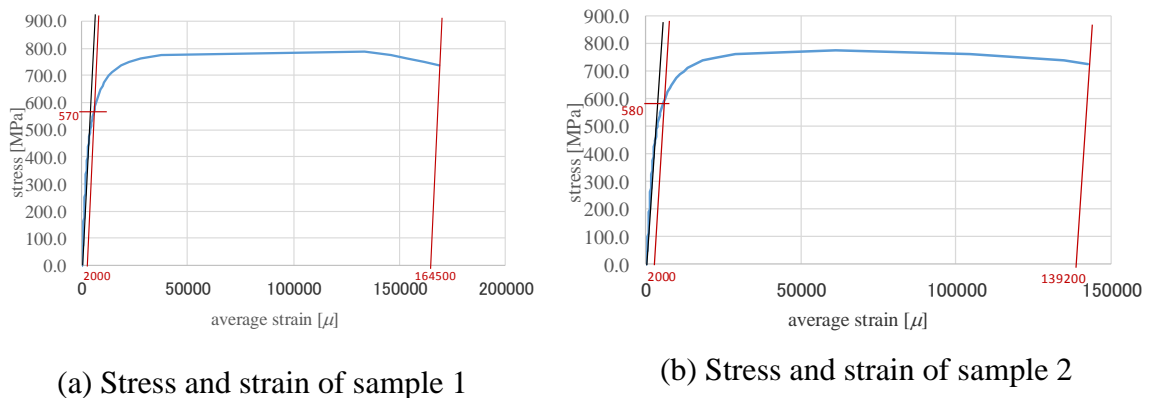
After casting, the samples were cured to a moist room at 20°C and 90 percent relative humidity for 24 hours. The weight of specimen was measured after being demolded and the volume of the specimen was obtained by averaging the diameter and height in three positions

of the specimen. After being demolded the specimens were covered by plastic bags and store in wet condition for curing at 20°C until a certain age for testing. Finally, the samples were mechanical tested after 14 and 35 days.

## 2.5 Experimental results

### 2.5.1 Tensile strength of anchor bolt

The number of tensile test samples of anchor bolt is two samples. By averaging these two samples of tensile test, the mechanical properties of anchor bolt were found, that is 575 MPa, 0.0054, 780 MPa, 0.152, and 161 GPa for yield strength, yield strain, ultimate strength, ultimate fracture strain, and modulus elasticity respectively. The stress-strain graph of tensile test of the anchor can be seen in Fig. 2-7.



(a) Stress and strain of sample 1

(b) Stress and strain of sample 2

**Figure 2-7:** Tensile test of anchor bolt

### 2.5.2 Compressive strength and modulus elasticity of mortar.

The measurement of compressive strength of mortar concrete was conducted after 14 days in accordance with JIS A 1108, and the mean of five results obtained with five identical specimens was reported. A stiff machine with a 3000 kN capacity was used to perform compressive test and split tensile test on cylinder specimens. The displacement of each



specimen was measured using a compressometer during the compressive strength test for determining the modulus of elasticity. The measurement of modulus elasticity of mortar in accordance with JIS A 1127, and the mean of five results obtained was reported. The compressive strength and modulus of elasticity of mortar for 14 days age test is 41.93 MPa and 25 GPa, respectively.

To briefly evaluate the strength of anchor bolt, the similar age between the compressive strength and anchor bolt test should be used. To fulfill this requirement, we used the compressive test sample by coring the mortar block after the anchor pullout test finish. The procedure of preparing samples and measuring of compressive strength of mortar concrete by core drill was conducted in accordance with JIS A 1107. Ten samples were tested and obtained for 35 days age, and the mean of compressive strength is, namely 48.18 MPa and 27 GPa for compressive strength and modulus elasticity, respectively. Figure 2-8 shows the core drill procedure and compression test of mortar concrete.



(a) Core drill of mortar sample



(b) Compression test of mortar concrete

**Figure 2-8:** The compression test of mortar concrete

### 2.5.3 Tensile strength of mortar.

The split tensile test was conducted in accordance with JIS A 1113, and the average of split tensile strength was obtained from five sample tests. Five samples were tested on 35 days age and the mean of split tensile strength is 3.31 MPa. By weighting and measuring the size, the density of mortar can be obtained, that is 2.22 kg/m<sup>3</sup>. The weighting procedure and split tensile test of mortar concrete are shown in Fig. 2-9. While, the complete data on mechanical properties of mortar can be found in Table 2-2.



(a) Weighting of sample



(b) Split tensile test of mortar concrete

**Figure 2-9:** The split tensile test of mortar concrete

**Table 2-2:** Mechanical properties of mortar

14 days age			35 days age				
Sample	Compr. Strength	Mod. Elasticity	Sample	Compr. Strength	Mod. Elasticity	Sample	Split Tensile Strength
	[Mpa]	[Mpa]		[Mpa]	[Mpa]		[Mpa]
1	46.35	27201.66	A1	52.39	27823.72	1	3.28
2	36.29	23465.70	A2	50.55	27277.62	2	3.02
3	37.45	24264.18	B1	48.76	27316.57	3	3.08
4	48.93	27387.01	B2	51.98	27859.42	4	3.44
5	40.62	23718.67	C1	48.04	27929.49	5	3.72
			C2	44.64	26606.64		
			D1	48.93	27189.32		
			D2	50.32	27729.82		
			E1	41.22	25456.45		
			E2	44.96	25504.97		
<b>Average</b>	<b>41.93</b>	<b>25207.44</b>		<b>48.18</b>	<b>27069.40</b>		<b>3.31</b>

## 2.5.4 Anchor bolt structures under pull-out load test

### 2.5.4.1 Reaction force and displacement

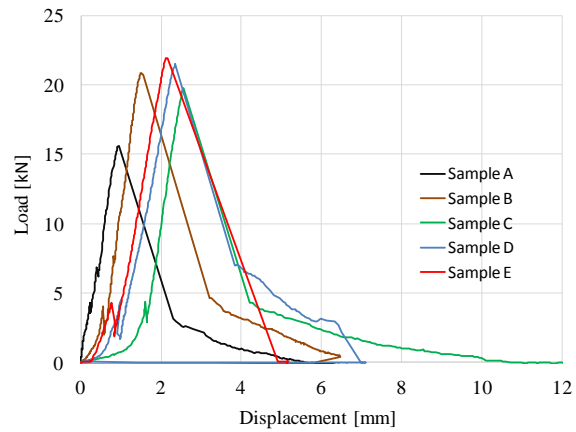
After conducting the pull-out test to the anchor bolt structure, several data can be gained, such as the reaction force, displacement and failure mode. Figure 2-10 depicts the graph showing correlation between load and displacement of the anchor bolt. The displacement of anchor bolt was examined by dial gauge no 3 and 4. It can be seen that sample A and B tested in 14 days relatively have a lower load bearing capacity as well as their displacement than sample C, D and E evaluated in 35 days. All of the graphs show a similar trend that there is a slight drop of the reaction force at the early stage when the load apply around 3 kN. It is supposed due to a small crack developed, so the structure loses a loading capacity. However, after this first crack the structure looks more stiff and can support the load until the maximum capacity. The average of the maximum load capacity has been 18.23 kN for 14 days age test and 20.87 kN for 35 days age test, so there is an increasing the loading capacity around 16%. It is also noted that the increasing rate of load-displacement is similar for all samples, also similarity can be recognized on the decreasing rate. All of samples show a significant displacement before final loading capacity were reached, except sample E showing a direct failure after peak load is attained. This long displacement towards final loading is presumed by tension softening effect.

### 2.5.4.2 Failure mode, cone failure area and concrete cone surface stress

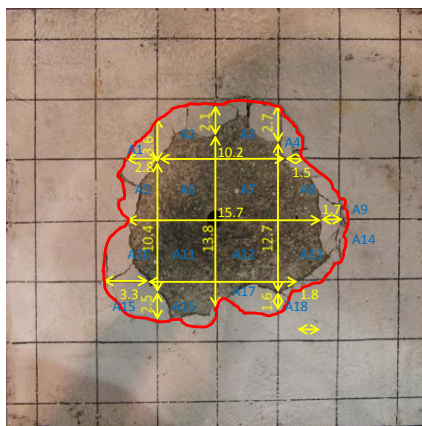
This experimental program uses a shallow depth of anchor bolt, with ratio depth to diameter of anchor equal 3.5. By applying this depth, the cone failure is expected and will be found in all samples. After examining the pull-out test applied to the anchor bolt structure, it can be notified that all samples have failures with the cone failure type, even they have a combination failure between cone failure and bond failure (see Fig. 2-12).

Figure 2-11 shows the cone failure surface which is examined from the top. The area of cone failure surface can be divided by inner and outside area. The outside area is the total area

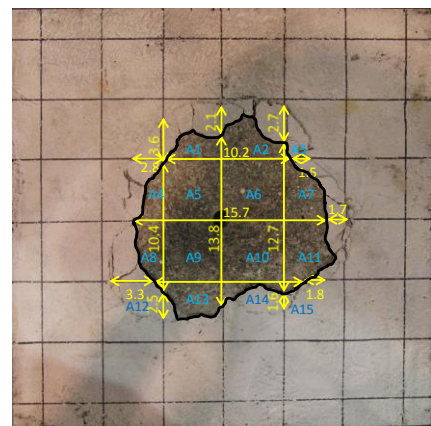
of cone failure before breaking, while the inner area is the conical form of concrete attaching to the pulled anchor bolt. The outside line is shown in Fig. 2-11(a) with a red line, while the inner line can be seen in Fig. 2-11(b) which is defined by a black line.



**Figure 2-10:** Load-displacement of anchor bolt under Pull-out load test



(a) Sample E - outside line

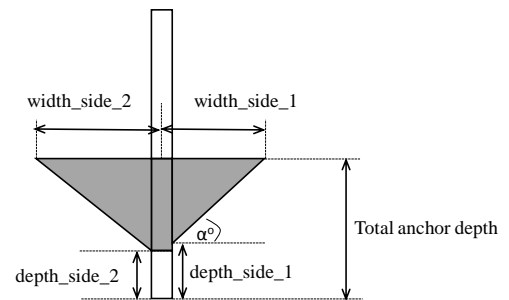


(b) Sample E - inner line

**Figure 2-11:** Cracking line on the concrete surface after pull-out load test



(a) Failure of Sample E



(b) Detail of failure sizes

**Figure 2-12:** The side view of anchor failure and detail of failure sizes

**Table 2-3:** The detail of failure sizes of the inner side area of anchor bolt cone failure

Sample	Failure type	Bond failure depth [cm]						Concrete depth [cm]	Width [cm]					Cone slope	
		total	side-1	side-2	side-3	side-4	Average		side-1	side-2	side-3	side-4	Average	tangent	$\alpha$ (°)
A	cone and bond	5.5	2.8	2.8	2.9	3.2	2.9	2.6	7.8	6.5	5.9	6.7	6.7	0.383	21.0
B	cone and bond	5.5	1.9	2.7	2.8	2.5	2.5	3.0	4.7	7.3	9.6	6.9	7.1	0.425	23.0
C	cone and bond	5.7	3.1	3.4	3.8	3.5	3.5	2.3	6.4	6.5	9.5	7.2	7.4	0.304	16.9
D	fail														
E	cone and bond	5.5	2.6	2.3	2.2	2.0	2.3	3.2	6.9	7.2	7.4	9.5	7.8	0.416	22.6
Average		5.6					2.8	2.8					7.3		20.9

**Table 2-4:** The detail of failure sizes of the outside area of anchor bolt cone failure

Sample	Failure type	Bond failure depth [cm]						Concrete depth [cm]	Width [cm]					Cone slope	
		total	side-1	side-2	side-3	side-4	Average		side-1	side-2	side-3	side-4	Average	tangent	$\alpha$ (°)
A	cone and bond	5.5	2.8	2.8	2.9	3.2	2.9	2.6	7.5	8.0	7.5	6.7	7.4	0.347	19.1
B	cone and bond	5.5	1.9	2.7	2.8	2.5	2.5	3.0	10.0	10.7	9.6	9.7	10.0	0.303	16.8
C	cone and bond	5.7	3.1	3.4	3.8	3.5	3.5	2.3	9.3	6.0	9.5	7.2	8.0	0.281	15.7
D	fail														
E	cone and bond	5.5	2.6	2.3	2.2	2.0	2.3	3.2	9.3	7.2	7.2	10.2	8.5	0.381	20.8
Average		5.6					2.8	2.8					8.5		18.1

A side view of the combination between cone failure and bond failure of anchor bolt after the pull-out loading test can be seen in Fig. 2-12. This figure clearly shows how the bonding failure occurs at the end of anchor bolt, whereas the cone failure occurs in the near to concrete surface. Figure 2-12(a) shows the sample of side view of anchor bolt cone failure, while the illustration of detail size of this failure can be seen in Fig. 2-12(b). Furthermore, the measuring size for each side and the degree of cone slope ( $\alpha$ ) can be observed in Table 2-3 and Table 2-4, that are inner side area and outside area, respectively. The degree of cone slope found by experiment is significantly lower than the design standard assumed, that is around  $15^\circ \sim 23^\circ$  for experiment compare to  $35^\circ \sim 45^\circ$  for design standard.

**Table 2-5:** The stress of concrete cone surface by experimental

Sample	Area [cm <sup>2</sup> ]		Max load [kN]	Cone stress based on experimental test [MPa]		note <sup>*)</sup>
	inner line	outside line		inner area	outside area	
Sample A (14 days)	121.07	170.06	15.60	1.29	0.92	
Sample B (14 days)	135.52	286.12	20.86	1.54	0.73	
<b>Average</b>	<b>128.29</b>	<b>228.09</b>	<b>18.23</b>	<b>1.41</b>	<b>0.82</b>	
Sample C (35 days)	128.52	192.15	19.80	1.54	1.03	
Sample D (35 days)	285.95	546.67	21.53	0.75	0.39	fail
Sample E (35 days)	162.40	256.30	21.93	1.35	0.86	
<b>Average</b>	<b>145.46</b>	<b>224.22</b>	<b>20.87</b>	<b>1.45</b>	<b>0.94</b>	

To determine the stress of the concrete cone surface, the area of the concrete cone surface should be calculated. The size of each cracking side refers to the grid with the size 5 cm. The total inner and outside area of cone failure surface can be seen in Table 2-5. By assuming that the stress of concrete is uniform on the cone failure surface thoroughly, the cone stress can be determined by the maximum loading capacity and the concrete cone surface area. The result of cone stress of experimental test is shown in Table 2-5, that is 0.94 MPa and 1.45 MPa for outside area and inner area respectively.

## 2.6 Comparison between experimental result and standard design

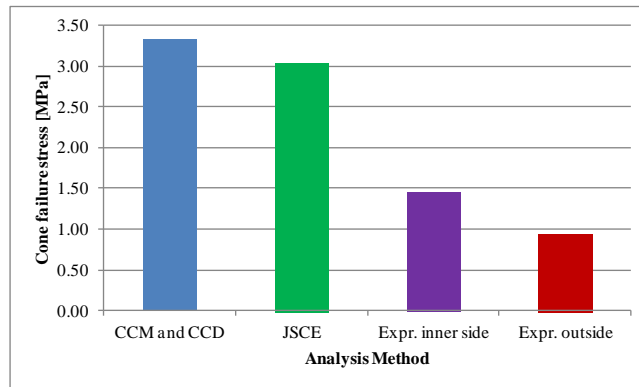
### 2.6.1 Comparison of cone stress.

There are several data that can be collected by the experimental program, namely the mechanical properties of steel anchor and mortar, maximum loading capacity of anchor structure, and cone stress. On the other hand, some equations are already available to predict the cone stress of the anchor bolt structure, such as CCM (Eligehausen *et al.*, 2006a), CCD (ACI 349, 2001; Fuchs *et al.*, 1995) and Japanese standard (JSCE, 2010). To evaluate and validate the experimental result, we need to compare the experimental to the design standard, and in this case we only compare the tensile cone stress between the experiment result to the design standards. Table 2-6 and Fig. 2-13 show the comparison of cone stress between experimental result and design standard. The result reveals that the cone stress of the experimental result is extremely lower than the design standard, this is either in inner side area or outside area. It is predicted due to the cracking of samples of the experimental result spread widely with a lower cone slope and resulting wider cone area than the design standard. Moreover, the failure mode also affects the cone stress since the design standards which is assumed the cone failure mode have a higher stress than the experimental results having a combination failure mode, cone and bond failure. Refer to Fig. 2-13, it can be recognized that the cone stress of the outside area around two-third of the inner side area. It is also should be noted that the stress of experimental result less than half of the standard, either CCM and CCD or JSCE standard. The average of cone stress is 0.94, 1.45, 3.04 and 3.33 MPa for the

outside area, inner side area of experimental results, JSCE, and CCM and CCD standard, respectively.

**Table 2-6:** Comparison of tensile cone failure stress between experimental and standard design

Sample	Maximum Compr. Stress [Mpa]	Cone failure stress				note
		prediction by CCM and CCD [Mpa]	prediction by JSCE [Mpa]	experiment result [Mpa]		
				inner side crack [Mpa]	outside crack [Mpa]	
A1	52.39	3.47	3.22	-	-	
A2	50.55	3.41	3.14	-	-	
B1	48.76	3.35	3.07	-	-	
B2	51.98	3.46	3.20	-	-	
C1	48.04	3.33	3.04	1.54	1.03	
C2	44.64	3.21	2.89	1.54	1.03	
D1	48.93	3.36	3.08	0.75	0.39	fail
D2	50.32	3.40	3.13	0.75	0.39	fail
E1	41.22	3.08	2.74	1.35	0.86	
E2	44.96	3.22	2.91	1.35	0.86	
<b>Average</b>	<b>48.18</b>	<b>3.33</b>	<b>3.04</b>	<b>1.45</b>	<b>0.94</b>	



**Figure 2-13:** The comparison of cone failure stress between experimental and standard design

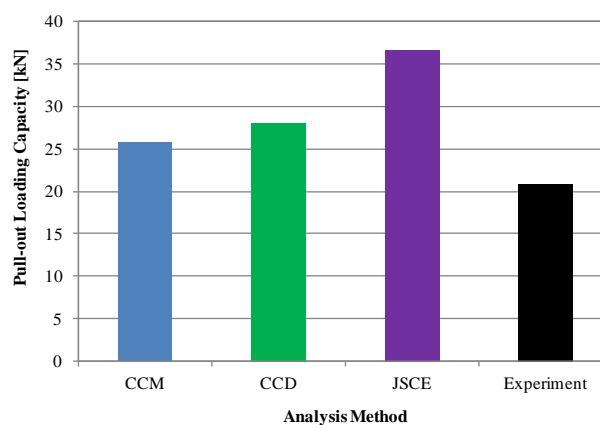
### 2.6.2 Comparison of maximum pull-out loading capacity.

Pull-out loading capacity is one of the most important matter as well as one of crucial problem regarding the anchor bolt design. Many methods have been proposed to find a reliable design, either by experimental program or numerical approach. However, it still needs to evaluate due to many factors affecting the pull-out loading capacity of anchor bolt, such as mechanical properties of concrete and steel anchor, depth-diameter ratio of anchor, loading

type, size effect, and many more. In this experiment, the pull-out loading capacity of normal strength mortar which is found by experimental program will be compared to the standard design. However, in this case only three well known standard design method will be considered, that is CCM method, CCD method and Japanese method. To design a single anchor, some parameters are needed, such as compressive strength of concrete, diameter of anchor, depth of anchor.

**Table 2-7:** Comparison of pull-out loading capacity between experimental and standard design

Sample	Maximum Compr. Stress [Mpa]	Depth of anchor (h) [mm]	Diameter of anchor (d) [mm]	Pull-out Loading Capacity			Experimental result [N]	note
				prediction by CCM [N]	prediction by CCD [N]	prediction by JSCE [N]		
				C1	48.04	57		
C2	44.64	57	16	26,687.87	28,751.29	37,698.46		
D1	48.93		16				21,530.00	fail
D2	50.32		16					
E1	41.22	55	16	24,067.55	26,186.87	33,548.49	21,930.00	
E2	44.96	55	16	25,137.74	27,351.30	35,552.11		
<b>Average</b>	<b>46.35</b>			<b>25,895.29</b>	<b>28,029.56</b>	<b>36,598.22</b>	<b>20,865.00</b>	



**Figure 2-14:** The comparison of pull-out loading capacity between experimental and standard design

The mechanical properties of concrete and steel anchor have been already gained as well as the depth and diameter of anchor have been designed, so it has enabled to compare between experimental and design standard. The detail comparison result of the pull-out loading capacity of anchor bolt under static pull-out loading is presented in Table 2-7, and Fig.



2-14 also clearly shows this comparison. The result expresses that the loading capacity of experimental significantly lower than the design standard, even almost a half of JSCE standard. It is also can be noticed that the JSCE has the highest resistance (36.60 kN) than other standards, then followed by CCD method (28.03 kN) and CCM method (25.90 kN), respectively. While the experimental result has a load resistance equal to 20.87 kN. The design standards have a higher loading resistance than experimental result because the crack pattern is assumed a single crack and the cracks propagate from end of anchor to the concrete surface. It is absolutely assumed cone failure only without bonding failure. On the other hand, the experimental result clearly shows that the failure is a combination between cone failure and bond failure, so that the cone failure part is a shallow depth and the angle of cone slope ( $\alpha=15^\circ \sim 23^\circ$ ) is smaller than design standard ( $\alpha=35^\circ \sim 45^\circ$ ).

## 2.7 Conclusion

An experimental investigation into the behavior of anchor bolt structures under pull-out loads has been described. The failure mode, reaction force, and concrete cone stress of the anchor bolt structure have been discussed precisely in this chapter. Finally, a comparison between the experimental results and design standard has been presented. Based on the experimental results, the following conclusions were drawn:

- 1) The experiment resulted the combination failure mode, cone failure and bond failure, of anchor bolt under pull-out loading test. Furthermore, the degree of cone slope ( $\alpha$ ) for the inner side area and outside area is significantly lower than the design standard assumed, that is around  $15^\circ \sim 23^\circ$  for experiment compare to  $35^\circ \sim 45^\circ$  for design standard.
- 2) The cone stress of the experimental result is extremely lower than the design standard, this is either in inner side area or outside area. It is even less than half of the standard, either CCM and CCD or JSCE standard. This phenomena are predicted due to the cracking of samples of the experimental result spread widely with a lower

cone slope and resulting wider cone area than the design standard. It is also should be noted that the stress of experimental result less than half of the standard, either CCM and CCD or JSCE standard. The average of cone stress is 0.94, 1.45, 3.04 and 3.33 MPa for the outside area, inner side area of experimental results, JSCE, and CCM and CCD standard, respectively.

- 3) The loading capacity of experimental result is significantly lower than the design standard, even almost a half of JSCE standard. It may due to in the design standard the crack pattern is assumed a single crack and the cracks propagate from end of the anchor to the mortar concrete surface. Moreover, in the design standard it is absolutely assumed that the failure mode is cone failure only without considering bond failure. While, the experimental result clearly shows that the failure is a combination between cone failure and bond failure, so that the cone failure part is a shallow depth and the angle of cone slope is smaller than design standard.

## 2.8 References

- ACI Committee 349, Code requirements for nuclear safety related concrete structures (ACI 349-01), *American Concrete Institute* (2001).
- ASTM C-109-07: Standard Test Method for Compressive Strength of Hydraulic Cement Mortars, *ASTM International* (2007).
- ASTM E488-96: Standard test methods for strength of anchors in concrete elements, *ASTM International* (1996).
- Eligehausen, R., Mallee, R., Silva, J. F.: Anchorage in Concrete Construction, First edition, *Ernst & Sohn*, Berlin (2006a).
- Eligehausen, R., Cook, R. A. and Appl, J.: Behavior and design of adhesive bonded anchors, *ACI Structural Journal*, Vol. 103, No. 6, pp. 822-831 (2006b).
- Fuchs, W., Eligehausen, R., and Breen, J. E.: Concrete Capacity Design (CCD) approach for fastening to concrete, *ACI Structural Journal*, Vol. 92, No. 1, pp. 73-94 (1995).

- Fujikake, K., *et al.*: Chemically bonded anchors subjected to rapid pullout loading, *ACI Materials Journal*, Vol. 100, No. 3, pp. 246-252 (2003).
- Hoehler, M.S., Mahrenholtz, P. and Eligehausen, R.: Behavior of anchors in concrete at seismic-relevant loading rates, *ACI Structural Journal*, Vol. 108, No. 2, pp. 238-247 (2011).
- Jang, J.B. and Suh, Y.P.: The experimental investigation of crack's influence on the concrete breakout strength of a cast-in-place anchor, *Nuclear and Engineering Design*, Vol. 236, pp. 948-953 (2006).
- JIS A 1107: Method of sampling and testing for compressive strength of drilled cores of concrete, *Japan Society of Civil Engineer*.
- JIS A 1108: Method of test for compressive strength of concrete, *Japan Society of Civil Engineer*.
- JIS A 1113: Method of test for splitting tensile strength of concrete, *Japan Society of Civil Engineer*.
- JIS A 1127: Methods of test for dynamic modulus of elasticity, rigidity and Poisson's ratio of concrete, *Japan Society of Civil Engineer*.
- JSCE: Standard specifications for concrete structures-2007, Design, JSCE Guidelines for Concrete No. 15, *Japan Society of Civil Engineers (JSCE)* (2010).
- Solomos, G. and Berra, M.: Testing of anchorage in concrete under dynamic tensile loading, *Materials and Structures*, Vol. 39, pp. 695-706 (2006).

## CHAPTER III

### SPH METHOD AND NUMERICAL CALCULATION SETTING

#### 3.1 Introduction

The overviews of some typical mesh-free based computational methods are briefly reviewed in this chapter. The numerical calculation scheme of SPH method and its continuum governing equation will be presented in the following sub-topics. Then, applications of the SPH method using existing constitutive model onto a pull-out load analysis of anchor bolt in concrete are presented.

#### 3.2 Review of mesh-free method

Development of mesh-free method originally have been started since 1970s by introducing the moving least squares (MLS) approximation as a parallel path of constructing for particle approximations. Then, following by a diffuse element method (DEM) that used MLS interpolant in combining with Galerkin method to formulate a mesh-free computational formulation has been introduced by Nayroles *et al.* (1992). Based on DEM, Belytschko *et al.* (1994) modified the DEM and proposed the element-free Galerkin (EFG) method. Currently the EFG is one of the most popular meshfree methods for solving many solid mechanics problems.

The mesh-free methods were then advancing developed by comprising the generalized finite difference method (GFDM) which is introduced by Perrone and Kao (1975) to handle with the nodes that are arranged arbitrarily in the interest domain, to which the researcher made the earliest contributions. Mesh-free methods also include the hp-clouds method introduced by Duarte and Oden (1996), and the Meshless Local Petrov-Galerkin (MLPG) method has been introduced by Atluri and Zhu (1998). The characteristic of MLPG, it requires only local background mesh and does not need a global background mesh for integration.

Smoothed Particle Hydrodynamics (SPH) method is one of the earliest mesh-free and particle methods. SPH originally intended for modeling astrophysical phenomena is proposed by Lucy (1977) and Gingold and Monaghan (1977). Recently this method has been widely extended for many applications to solve problems of solid as well as fluid mechanics. Because of the distinct advantages of the particle method, the SPH method was widely adopted as one of the efficient computational techniques to solve applied mechanics problems.

The advantages of the mesh-free particle methods may be summarized as follows (Li and Liu, 2002):

- 1) They can easily handle very large deformations, since the connectivity among nodes is generated as part of the computation and can change with time;
- 2) The methodology can be linked more easily with a CAD database than finite elements, since it is not necessary to generate an element mesh;
- 3) The method can easily handle damage of the components, such as fracture, which should prove very useful in modelings of material failure;
- 4) Accuracy can be controlled more easily, since in areas where more refinement is needed, nodes can be added quite easily (h-adaptivity);
- 5) The method can incorporate an enrichment of fine scale solutions of features, such as discontinuities as a function of current stress states, into the coarse scale; and
- 6) Mesh-free discretization can provide accurate representation of geometric objects.

### 3.3 Smoothed particle hydrodynamics (SPH) method

This thesis focuses on the SPH method that originally for modeling astrophysical phenomena in 3D open space and particular polytropes. SPH is a “truly” mesh-free particle method uses the integral representation for field function approximation. However, recently it is widely applied for continuum scale applications due to the collective movement of astrophysical particles is similar to the movement of a liquid or gas flow, and can be calculated by the governing equations of the classical Newtonian hydrodynamics. The methodology and its applications were further developed in several excellent review papers and book, including those by Monaghan (1988, 1992, 2005), Wingate and Miller (1993), Randles and Libersky (2000), and Liu and Liu (2003). Even though this method has been introduced in 1970’s, however the development and application of SPH rapidly increased after 1990s due to their advantages. In the early applications on astrophysical, the SPH method was based on the Monte Carlo theorem and random sampling. In order to produce the rational explanation of this method, Gingold and Monaghan (1982) employed the kernel approximation, which can also serve as a smoothing interpolation field. Therefore, the foundation of SPH is the interpolation theory itself. The conservation equations of the continuum dynamics can be transformed into integral equations by using an interpolation function that gives the ‘kernel estimate’ of the field variables at a point. Computationally, information is known only at discrete points, so that the integrals are evaluated as sums over the neighboring particles. The underlying grid is not needed because that function is evaluated using their values at the discrete neighboring points (particles) and an interpolation kernel.

SPH technique is used in this study to investigate the structural response of the anchor bolt in concrete under pull-out loads. In the SPH method, the material is divided into a set of discrete elements denoted as particles. These particles have a spatial distance or smoothing length ( $h$ ), over which their properties are smoothed by a *kernel function*. By summing the relevant properties of all particles within the range of the kernel, the mechanical quantity of any particle can be obtained. The superscript  $A$  and  $B$  are used in this thesis to denote the

target particle  $A$  and neighboring particle  $B$ , respectively. For example, to calculate field variable of particle  $A$  in the domain integral  $\Omega$ , the integral of this particle is shown below,

$$f(x^A) = \int_{\Omega} f(x^B) \delta^{AB}(x^A - x^B, h) dv^B \quad 3.1$$

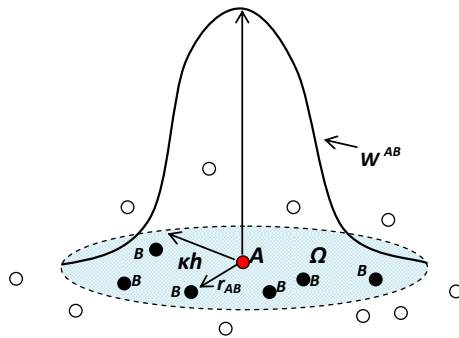
$\delta^{AB}(x^A - x^B)$  is the Dirac Delta function expressed as

$$\delta^{AB}(x^A - x^B) = \begin{cases} 1 & x^A = x^B \\ 0 & x^A \neq x^B \end{cases} \quad 3.2$$

Obviously, Eq. 3.1 is rigorous and exact. If the Dirac delta function is substituted by a smoothing kernel function  $W^{AB}$ , approximation of  $f(x^A)$  on the volume of integral  $\Omega$ , can be obtained

$$f(x^A) = \int_{\Omega} f(x^B) W^{AB}(x^A - x^B, h) dv^B \quad 3.3$$

where  $f(x^A)$  and  $f(x^B)$  are functions of target particle  $A$  and neighboring particle  $B$ , respectively. The particle  $A$  is weighted by kernel function  $W^{AB}(x^A - x^B, h)$  and integral computation in Eq. 3.3 is approximated by the summation of all neighboring particle  $B$  in the support domain  $kh$ .



**Figure 3-1:** Particle approximation in in a three-dimensional problem domain  $\Omega$

Figure 3-1 shows the particle approximations in a three-dimensional problem domain  $\Omega$ . The smoothing function,  $W^{AB}$  is used to approximate the field variables at particle  $A$  using averaged summations over particles  $B$  within the support domain  $kh$ . The three-dimensional illustration in Fig. 3-1 shows the target domain consists of particles as discretized of a body, where each particle is associated with certain field properties. These particles can be employed for integration, interpolation, and differentiation, even also for representing the material as mass particles. The volume of a sub-domain is lumped on the corresponding particle. Therefore, each particle is associated with a fixed lumped volume. If a volume,  $dv$  is associated with particle  $B$  to present the concept of particle mass  $m$ ,

$$dv^B = \frac{m^B}{\rho^B} \quad 3.4$$

By assuming the kernel function has a compact supporting radius of  $kh$ , an approximation form of Eq. 3.3 by the discretized particles becomes;

$$f(x^A) = \sum_{B=1}^N \frac{m^B}{\rho^B} f(x^B) W^{AB}(x^A - x^B, h) \quad 3.5$$

where, the summation is over all the particles (with a total number of  $N$ , including particle  $A$ ) within the supporting domain  $\Omega$  of the given particle  $A$ . Those influenced particles are the neighboring particles of particle  $A$  within the support domain  $kh$ . It is clearly shown that particle  $B$  has mass  $m^B$ , density  $\rho^B$ , position  $x^B$ , and initial velocity  $v^B$  and other properties.

Finally, the function of particle  $A$  is calculated by using the first-order partial differentiation of kernel functions to solve the Eq. 3.5. The first-order differentiation is only applied to smoothing kernel function as shown in Eq. 3.6.

$$\nabla \cdot f(x^A) = \sum_{B=1}^N \frac{m^B}{\rho^B} f(x^B) \cdot \nabla W^{AB}(x^A - x^B, h) \quad 3.6$$



where,  $\nabla W^{AB}(x^A - x^B, h)$  represents the spatial derivative of the function  $W^{AB}(x^A - x^B, h)$ .

The smoothing kernel functions or smoothing functions plays a very important role in SPH as they determine the shape and dimension of the support domain of particles, effective support domain, consistency and accuracy of the approximation, and efficiency of the computation. The methods for function approximation are classified into three categories: 1) integral representation; 2) series representation, and; 3) differential representation. Generally, the kernel should satisfy the following requirements:

- 1) Delta function property when  $h \rightarrow 0$ ,  $\lim_{h \rightarrow 0} W^{AB}(x^A - x^B, h) = \delta^{AB}(x^A - x^B)$
- 2) Normalized condition,  $\int W^{AB}(x^A - x^B, h) dx^B = 1$
- 3) Compact condition,  $W^{AB}(x^A - x^B, h) > 0$  when  $x^B$  inside the support domain, otherwise  $W^{AB}(x^A - x^B, h) = 0$
- 4) Monotonically decreasing function property with the distance  $r$ ,  $r = |x^A - x^B|$
- 5) Symmetric property, the smoothing function should be an even function
- 6) Smoothing property, the smoothing function should be sufficiently smooth

The first condition promises the convergence and this property makes sure that as the smoothing length tends to zero. The second condition ensures that the integral of smoothing function over the support domain to be unity for the normal arrangement of particles. The third condition allows the approximation to be generated only within a local representation. Besides, this property states that the smoothing function should be non-negative in the support domain, since negative value may cause a serious consequences in some unphysical parameters, such as negative density and energy. The fourth one arises from the theory of the physics, which means that the force exerted by one particle on the other decreases with the distance between them. A nearer particle should have a bigger influence on the particle consideration. The fifth property means that particles should have an equal effect if the given particles have same distance but in different positions. The last property aims to obtain better approximation accuracy by requiring that the kernel function must be differentiable at least in its first order (Liu and Liu, 2010). The continuity derivative of a kernel function will prevent

great fluctuation in the force felt by the particle providing the particle disorder is not too extreme. This is given by the method, that is the “smoothed” particle hydrodynamics.

Basically, any function satisfying the above requirements can be employed as the kernel function of the SPH. Based on literatures, the following lists some of the smoothing function that the most commonly used by many researchers and practitioners.

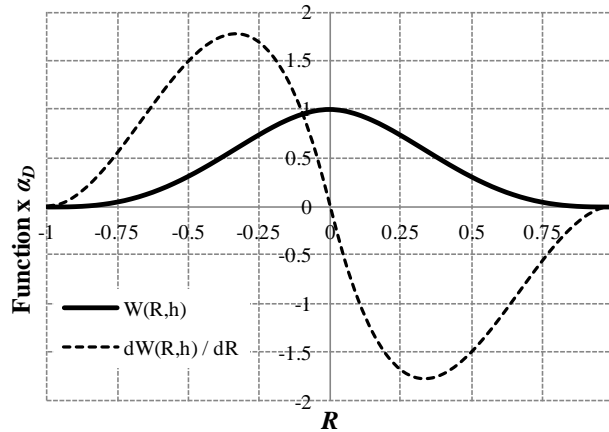
Figure 3-2 shows the bell-shaped function which is first utilized by Lucy (1977), the smoothing function in the first SPH paper. The smoothing function of bell-shaped is as follows.

$$W(R, h) = \alpha_D \begin{cases} (1+3R)(1-R)^3 & R \leq 1 \\ 0 & R > 1 \end{cases} \quad 3.7$$

$R$  is the relative distance between particle  $A$  and particle  $B$ ,

$$R = \frac{r}{h} = \frac{|x^A - x^B|}{h} \quad 3.8$$

where  $r$  is the distance between two particles.  $\alpha_D$  is a factor, namely  $5/4h$ ,  $5/\pi h^2$ ,  $105/16\pi h^3$  in one-, two- and three-dimensional space, respectively, so that the condition of unity can be satisfied for all the three dimensions.  $h$  is smoothing length defining the influence area of smoothing function  $W^{AB}$ .

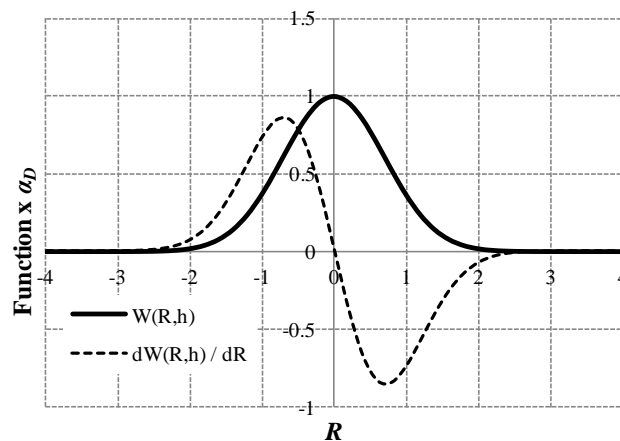


**Figure 3-2:** The smoothing function and its derivative  $W'$  of Bell-shaped function

Gingold and Monaghan (1977) in their original paper simulated the non-spherical stars using Gaussian smoothing function (Fig. 3-3) due to its stability and accuracy, especially for disordered particles. However, the function is not really compact and computationally more expensive since it never goes to zero theoretically, unless  $R$  approaches to infinity. It can take a longer distance for the kernel to approach zero and could produce a larger bandwidth in the discrete system matrix.

$$W(R, h) = \alpha_D e^{-R^2} \tag{3.9}$$

where,  $\alpha_D$  is  $1/\pi^{1/2}h$ ,  $1/\pi h^2$ ,  $1/\pi^{3/2}h^3$ , respectively in one-, two- and three-dimensional space, for the unity requirement.



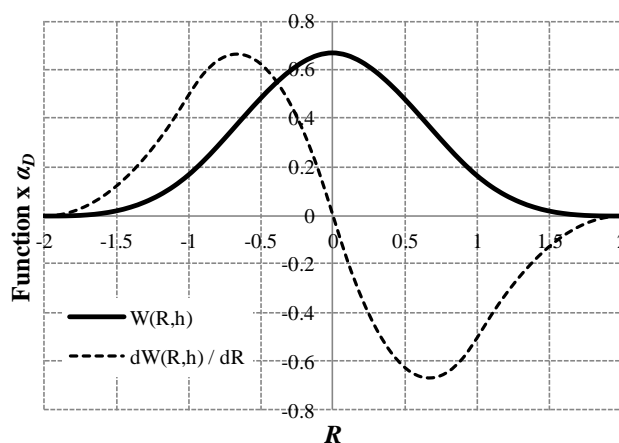
**Figure 3-3:** The smoothing and its first  $W'$  of Gaussian function

To get the narrower compact support and efficiency in computation of Gaussian kernel function, Monaghan and Lattanzio (1985) proposed the smoothing function based on the cubic spline functions known as B-spline function. The graphic of B-spline function can be seen in Fig. 3-4, whereas the function is as follows,

$$W(R,h) = \alpha_D \begin{cases} \frac{2}{3} - R^2 + \frac{1}{2}R^3 & 0 \leq R < 1 \\ \frac{1}{6}(2-R)^3 & 1 \leq R < 2 \\ 0 & R \geq 2 \end{cases} \quad 3.10$$

where,  $\alpha_D$  is  $1/h$ ,  $5/7\pi h^2$ ,  $3/2\pi h^3$ , respectively in one-, two- and three-dimensional space, for the unity requirement.

The B-spline function has been the most widely used smoothing function in the SPH literatures. However, the second derivative of the cubic spline is a piecewise linear function, and accordingly, the stability properties can be inferior to those of smoother kernels. After comparing to other kernel functions, finally this study uses B-spline function to get the stable condition of the calculation.

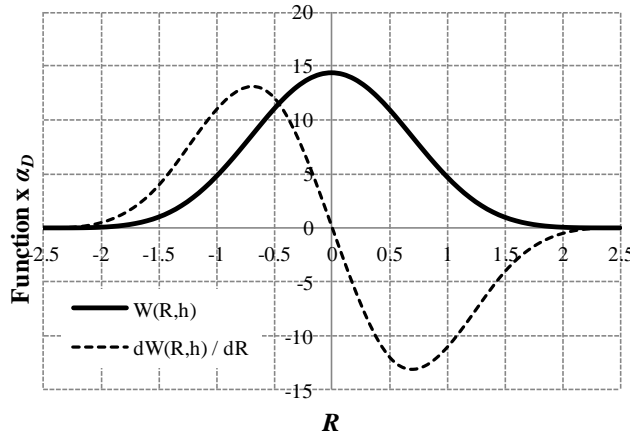


**Figure 3-4:** The smoothing function and its first derivative  $W'$  of B-(cubic) spline function

Morris (1994, 1996) proposed a higher order (quartic and quintic) splines (Fig. 3-5 and Fig. 3-6) that are more closely approximating the Gaussian and more stable. The equation of quartic spline can be obtained as below,

$$W(R, h) = \alpha_D \begin{cases} (R + 2.5)^4 - 5(R + 1.5)^4 + 10(R + 0.5)^4 & 0 \leq R < 0.5 \\ (2.5 - R)^4 - 5(1.5 - R)^4 & 0.5 \leq R < 1.5 \\ (2.5 - R)^4 & 1.5 \leq R < 2.5 \\ 0 & R > 2.5 \end{cases} \quad 3.11$$

where,  $\alpha_D$  is  $1/24h$  in one-dimensional space.

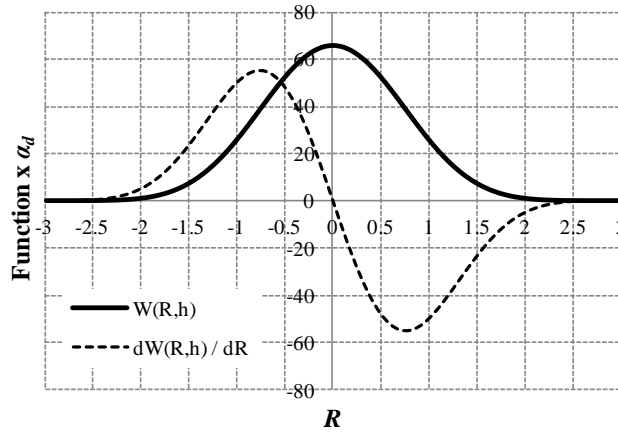


**Figure 3-5:** The smoothing function and its first derivative  $W'$  of quartic function

Whereas the quintic spline equation is as follows,

$$W(R, h) = \alpha_D \begin{cases} (3 - R)^5 - 6(2 - R)^5 + 15(1 - R)^5 & 0 \leq R < 1 \\ (3 - R)^5 - 6(2 - R)^5 & 1 \leq R < 2 \\ (3 - R)^5 & 2 \leq R < 3 \\ 0 & R > 3 \end{cases} \quad 3.12$$

where,  $\alpha_D$  is  $120/h$ ,  $7/478\pi h^2$ ,  $3/359\pi h^3$  in one-, two- and three-dimensional space, respectively.



**Figure 3-6:** The smoothing function and its first derivative  $W'$  of quintic function

### 3.4 Conservation equations and its approximation forms

Response of structures due to the external force often behaves like fluids, the force propagates through internal elements or particles. Analytically, the equation of motion is the key descriptors of the dominated material behavior. The governing conservation equations of continuum mechanics for hydrodynamics with material strength are:

$$\text{a) The continuity equation} \quad \frac{d\rho}{dt} = -\rho \cdot \frac{\partial v_i}{\partial x_i} \quad 3.13$$

$$\text{b) The momentum equation} \quad \frac{dv_i}{dt} = \frac{1}{\rho} \cdot \frac{\partial \sigma_{ij}}{\partial x_j} \quad 3.14$$

$$\text{c) The particle moving equation} \quad \frac{dx_i}{dt} = v_i \quad 3.15$$

The dependent variables of the above equations can be defined by the scalar density ( $\rho$ ), the velocity components ( $v_i$ ), and the stress tensor ( $\sigma_{ij}$ ), where the stress tensor can be decomposed into two symmetric tensors, the deviatoric stress tensor ( $\sigma'_{ij}$ ) and the hydrostatic or spherical stress tensor as shown below;

$$\sigma_{ij} = \sigma'_{ij} + \sigma_{mn} \delta_{ij} = \sigma'_{ij} + \frac{1}{3}(\sigma_{11} + \sigma_{22} + \sigma_{33}) = \sigma'_{ij} + \frac{1}{3}I_1 \quad 3.16$$

As commonly used in engineering assumption, the stresses are positive in tension and negatively in compression. On the other hand, to set the displacement value, only three conservation equations are used in this study, which are, the continuity equation, momentum equation and particle moving particle. The detailed explanation of these three conservation equations will be described in the following sub-chapters.

The independent variables are classified by the spatial coordinates ( $x_i$ ) and the time ( $t$ ). The total time derivative operator ( $d/dt$ ) is taken in the moving Lagrangian frame. The subscript  $i$  and  $j$  in the above equation are applied to symbolize the index notation.

The particle approximation based on the Navier-Stokes equations is the main feature in SPH method. Considering the derivative form of smoothing function, it yields to:

$$W^{AB} = W(x^A - x^B); \quad \frac{\partial W^{AB}}{\partial x^A} = \frac{\partial [W(x^A - x^B, h)]}{\partial x^A} \quad 3.17$$

### 3.4.1 Conservation of mass equation

The density approximation is very important for deriving calculation in the SPH method. The density basically determines the particle distribution and the smoothing length evolution. For the density approximation, there are two methods of approximation forms for the density approximation. The first one is the summation density form, which directly applies the SPH approximations to the density itself, that is based on Eq. 3.5,

$$\rho^A = \sum_{B=1}^N m^B W^{AB} \quad 3.18$$

The Eq. 3-18 simply states that the density of a particle can be approximated by the weighted average of the densities of the particles in the support domain. By using this equation, only particle coordinates and masses are required to approximate the density, and the Eq. 3.13 is automatically satisfied. However, the disadvantage comes up due to the lack of particles, for

example, when it applies near boundaries and near the material interfaces (if different materials composed). The simply corrective approach is by using the Shepard interpolation technique proposed by Shepard (1968) to revise Eq. 3.17 as,

$$\rho^A = \sum_{B=1}^N m^B (W^{AB})_S ; \quad (W^{AB})_S = \frac{W^{AB}}{\sum_{B=1}^N \frac{m^B}{\rho^A} W^{AB}} \quad 3.19$$

This permits reproducing exactly consistent functions. The other one is the continuity density, which approximates the density according to the continuity equation and time-dependent form. The equation is written as below;

$$\frac{d\rho^A}{dt} = \sum_{B=1}^N m^B (v_i^A - v_i^B) \frac{\partial W^{AB}}{\partial x_i^A} \quad 3.20$$

For the continuity density approach, besides particle mass and positions, its velocity is also necessary in the calculation. This equation provides many advantages, that the use of the relative velocities in unsymmetrized form serves an approach to diminish particle inconsistency. Therefore, it can improve the approximation accuracy. When the calculation is applied to two or more different materials, and the ratio of their densities more than 2, the following formula is chosen according to Gray *et al.* (2001),

$$\frac{d\rho^A}{dt} = \rho^A \sum_{B=1}^N \frac{m^B}{\rho^B} (v_i^A - v_i^B) \frac{\partial W^{AB}}{\partial x_i^A} \quad 3.21$$

### 3.4.2 Conservation of momentum equation

In solid mechanics, the constitutive model, in general, permits the stress to be a function of strain and strain rate. The strain rate tensor  $\dot{\epsilon}_{ij}$  can be derived from the velocity as,



$$\dot{\varepsilon}_{ij}^A = \frac{1}{2} \left( \frac{\partial v_i}{\partial x_j} + \frac{\partial v_j}{\partial x_i} \right) \quad 3.22$$

In the SPH approximation, the Eq. 3.22 can be expressed based on particle approximation,

$$\dot{\varepsilon}_{ij}^A = \frac{1}{2} \sum_{B=1}^N \frac{m^B}{\rho^B} \left[ \left( v_i^B - v_i^A \right) \frac{\partial W^{AB}}{\partial x_j^A} + \left( v_j^B - v_j^A \right) \frac{\partial W^{AB}}{\partial x_i^A} \right] \quad 3.23$$

and the rotation rate tensor  $\dot{R}_{ij}^A$  can be written as,

$$\dot{R}_{ij}^A = \frac{1}{2} \sum_{B=1}^N \frac{m^B}{\rho^B} \left( \left( v_i^B - v_i^A \right) \frac{\partial W}{\partial x_j^A} - \left( v_j^B - v_j^A \right) \frac{\partial W}{\partial x_i^A} \right) \quad 3.24$$

The derivation of particle approximation of momentum equation is similar to the continuity density approach, and usually incorporates some transformations. Applying the SPH particle approximation concepts to the gradient on the RHS of the momentum equation in Eq. 3.14 yields following equation

$$\frac{dv_i^A}{dt} = \frac{1}{\rho} \sum_{B=1}^N \frac{m^B}{\rho^B} (\sigma_{ij}) \frac{\partial W^{AB}}{\partial x_j^A} \quad 3.25$$

By considering the following identity,

$$\begin{aligned} \sum_{B=1}^N \frac{m^B}{\rho^A \rho^B} (\sigma_{ij}^A) \frac{\partial W^{AB}}{\partial x_j^A} &= \frac{\sigma_{ij}^A}{\rho^A} \sum_{B=1}^N \frac{m^B}{\rho^B} \frac{\partial W^{AB}}{\partial x_j^A} \\ &= \frac{\sigma_{ij}^A}{\rho^A} [\nabla(1)] \\ &= 0 \end{aligned} \quad 3.26$$

The stress tensor  $\sigma_{ij}$  can be obtained based on the calculation of the elastic constitutive equation.

$$\sigma_{ij} = 2\mu\varepsilon_{ij} + \lambda\delta_{ij}\varepsilon_{kk} \quad 3.26(b)$$

Substitute Eq. 3.26 into 3.25, yield to

$$\frac{dv_i^A}{dt} = \sum_{B=1}^N m^B \left( \frac{\sigma_{ij}^A + \sigma_{ij}^B}{\rho^A \rho^B} \right) \frac{\partial W^{AB}}{\partial x_j^A} \quad 3.27$$

Consider the following identity

$$\frac{1}{\rho} \frac{\partial \sigma_{ij}}{\partial x_i} = \frac{\partial \left( \frac{\sigma_{ij}}{\rho} \right)}{\partial x_i} + \frac{\sigma_{ij}}{\rho^2} \frac{\partial \rho}{\partial x_i} \quad 3.28$$

and by applying the SPH particle approximation to the gradients, we can obtain,

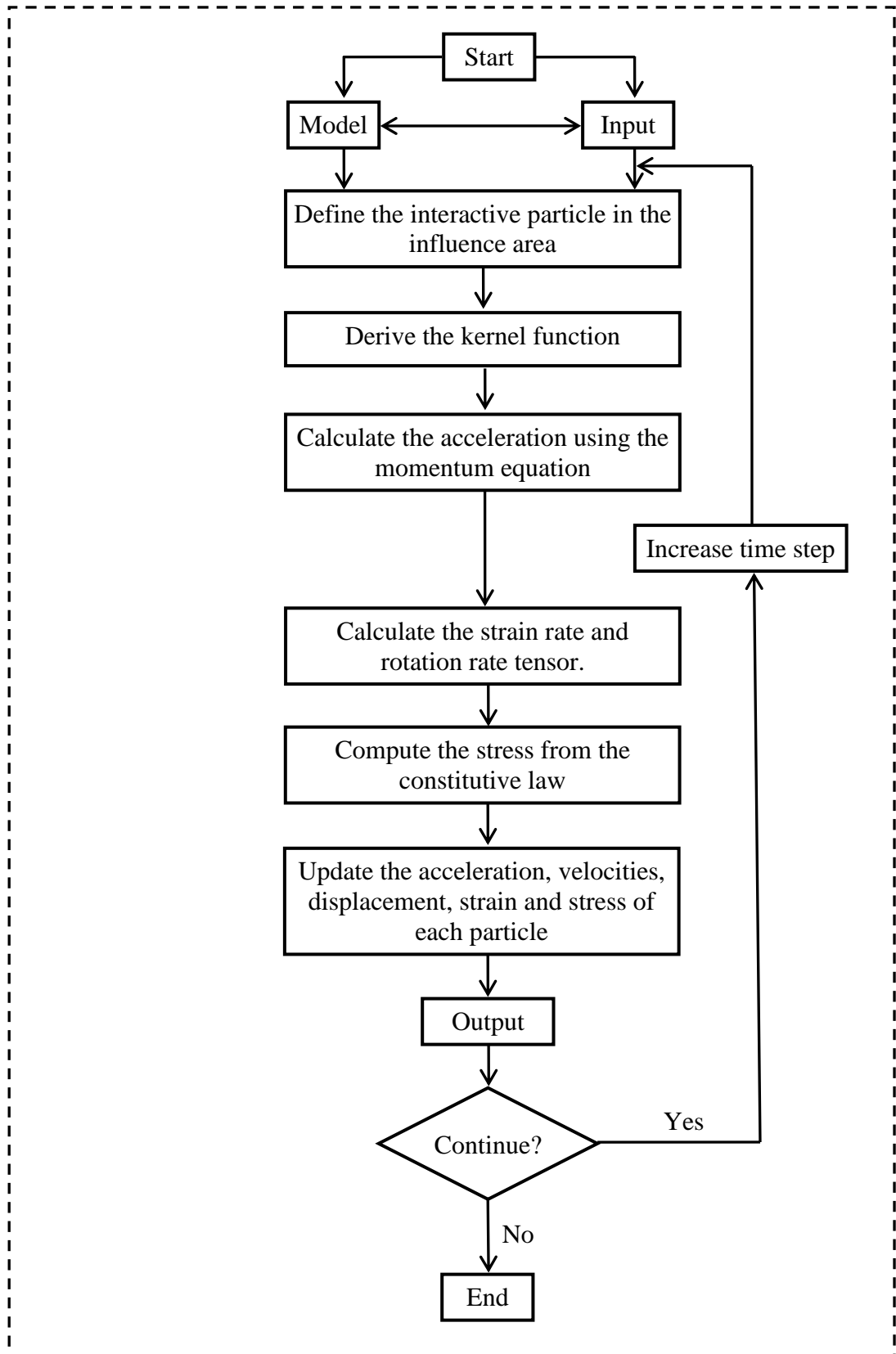
$$\begin{aligned} \frac{dv_i^A}{dt} &= \left( \sum_{B=1}^N \frac{m^B \sigma_{ij}^B}{(\rho^B)^2} \frac{\partial W^{AB}}{\partial x_j^A} + \frac{\sigma_{ij}^A}{(\rho^A)^2} \sum_{B=1}^N \frac{m^B}{\rho^B} \rho^B \frac{\partial W^{AB}}{\partial x_j^A} \right) \\ &= \sum_{B=1}^N m^B \left( \frac{\sigma_{ij}^A}{(\rho^A)^2} + \frac{\sigma_{ij}^B}{(\rho^B)^2} \right) \frac{\partial W^{AB}}{\partial x_j^A} \end{aligned} \quad 3.29$$

Monaghan (1992) stated that Eq. 3.29 had an advantage over Eq. 3.27 in that linear and angular momentums were conserved for its produced axisymmetric central force between pair particles.

### 3.5 Calculation scheme of SPH to the solid-state analysis

The calculation scheme of this study has been shown in Fig. 3-6 and described as follows:

- 1) The interactive particles in the influence area are defined prior updating the time increment. Where, only a fixed number of particles are within the support domain used in the particle approximations.
- 2) Calculate the derivative of the kernel function using first-order partial differential form in Eq. 3.6. The B (cubic)-spline kernel function (Eq. 3.10) is used in this analysis.
- 3) Compute the acceleration of particle *A* under the force thread using the momentum equation (Eq. 3.29). Then, update the acceleration, velocity and displacement of each particle.
- 4) Compute the strain rate tensor and rotation rate tensor as in Eq. 3.23 and 3.24, respectively.
- 5) Calculate the plasticity theory for yield criterion, the flow rule and the hardening rule of both materials, concrete/mortar and steel anchor bolt under the stress thread. Explanation of this calculation is described in the following section.
- 6) The strain and stress calculations are updated due to the time increment and applying the constitutive equation, respectively.

**Figure 3-7:** Calculation flow of the SPH method algorithm

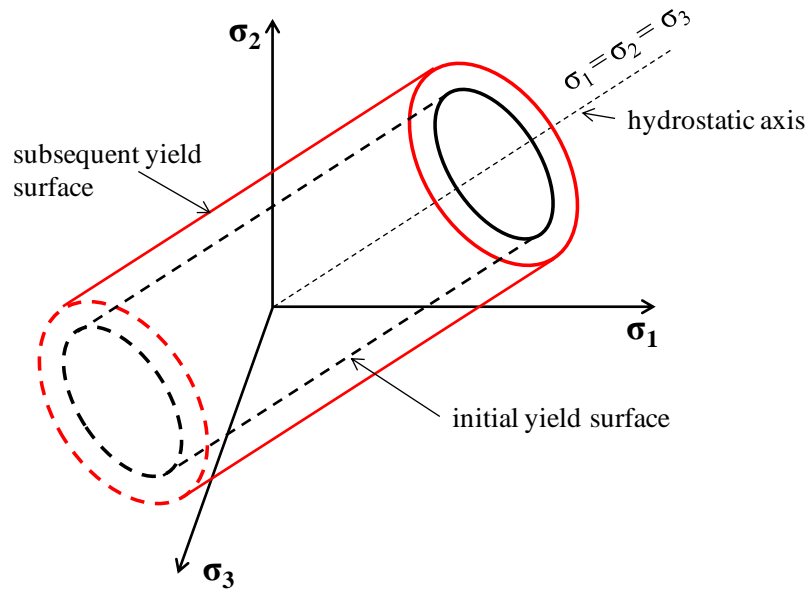
### 3.6 Constitutive model

In general the mechanical behavior of material can be described as a mathematical description by weaving the relation between the stress and strain tensor in a material point of the body. This mathematical description is well-known as a constitutive model. The constitutive model plays an important role in the numerical analysis to simulate the material behavior. The constitutive models are developed and based on the elasticity and plasticity theory. The linear elasticity theory, generating the linear elastic model is derived from the generalized Hooke's law. The linear elastic model is widely applied to the elastic materials by assuming the material in following conditions: continuous, homogeneous, isotropic and linear elastic. When these conditions are achieved, the model can be constructed by elastic Young's modulus ( $E$ ) and the Poisson's ratio ( $\nu$ ). Based on these parameters, more sophisticated models can be easily derived. In the numerical analysis, failure criteria are defined with stress invariants to simulate the strength of materials in various states, and they were developed by: 1-parameter criterion and 2-parameter criterion. Even though other researcher have attempted to extend the application of plasticity model until 3- to 5 parameters, however, only 1- and 2-parameter criterion will be considered in this analysis to describe deformational characteristics of materials in the ultimate stress state. That is von Mises criterion (1-parameter criterion) for steel anchor bolt and Drucker-Prager criterion (2-parameter criterion) for concrete.

#### 3.6.1 Elastic-plastic constitutive equation von Mises criteria

The von Mises yield criterion is formulated as follows. Yielding or plastic condition is assumed will take place when the second invariant of deviatoric stress tensor,  $J_2$  reaches a certain value. This criterion is calculated based on distortional energy theory or shearing-stress criteria, in which the yielding is occurred when distortional energy reaches a value that is equal to the distortional energy at yield in simple tension. The yield surfaces of VM in

principal stress coordinate demarcates a cylinder with radius  $\sqrt{\frac{2}{3}}\sigma_y$  around the hydrostatic axis as shown in the Fig. 3-9. Moreover, the effect of hydrostatic pressure on compression domain is neglected in this criterion and this phenomenon is quite reasonable especially for metal plasticity. In this chapter, the VM yield criterion is employed to simulate the steel anchor bolt failure on anchor bolt structure under pull-out load.



**Figure 3-8:** Graphic of VM cylinder with hardening criteria

In the VM model, there are two limited conditions and they can be expressed by the function as follows,

$$f_{VM}(J_2) = J_2 - k^2 < 0 \rightarrow \text{elastic} \quad 3.30(a)$$

$$f_{VM}(J_2) = J_2 - k^2 = 0 \rightarrow \text{plastic} \quad 3.30(b)$$

where  $k$  is the material constant and the second invariant of deviatoric stress,  $J_2$  can be derived as,

$$J_2 = \frac{1}{2} \sigma'_{ij} \sigma'_{ij} \quad 3.31(a)$$

and the deviatoric stress  $\sigma'_{ij}$ , can be written as the inverse of Eq. 3.16.

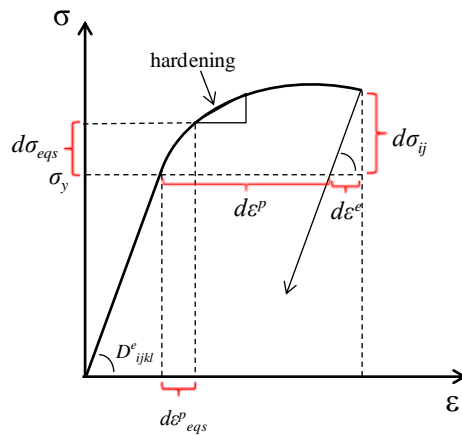
$$\sigma'_{ij} = \sigma_{ij} - \frac{1}{3} \sigma_{mm} \delta_{ij} \quad 3.31(b)$$

Details of steps of deriving the VM yield criteria based on incremental stress-strain are given below. By assuming that the total strain increment  $d\varepsilon_{ij}$  as in Fig. 3-10 can be divided into increments of elastic strain,  $d\varepsilon^e_{ij}$  and incremental of plastic strain,  $d\varepsilon^p_{ij}$  components to yield

$$d\varepsilon_{ij} = d\varepsilon^e_{ij} + d\varepsilon^p_{ij} \quad 3.32$$

Whereas the incremental of plastic strain is computed using flow rule associated with the yield criterion  $f$ ,

$$d\varepsilon^p_{ij} = \lambda_{vm} \frac{\partial f_{VM}}{\partial \sigma_{ij}} \quad 3.33$$



**Figure 3-9:** Uniaxial stress-strain curve

Figure 3-10 clearly shows that the equivalent plastic strains ( $d\varepsilon^p_{eqs}$ ) increase in accordance with the increasing of equivalent stress ( $d\sigma_{eqs}$ ). Considering the theory of plastic work and

work hardening, the equivalent plastic strain increment can be defined in terms of the plastic work per unit volume in the form

$$dW^P = \sigma_{eqs} d\varepsilon_{eqs}^P \quad 3.34$$

Refer to Fig. 3-10, the incremental stress of VM is incorporated with hardening rule, where the hardening coefficient parameter is defined by the ratio of the increment of equivalent stress ( $d\sigma_{eqs}$ ) to the increment of equivalent plastic strain ( $d\varepsilon_{eqs}^P$ ).

$$H' = \frac{d\sigma_{eqs}}{d\varepsilon_{eqs}^P} \quad 3.35$$

In general, the incremental stress can be expressed as

$$d\sigma_{ij} = D_{ijkl}^e d\varepsilon_{kl}^e \quad 3.36$$

Considering the incremental stress for the linear elastic path, substitute Eq. 3.32 and the incremental of elastic strain can be separated into

$$d\sigma_{ij} = D_{ijkl}^e d\varepsilon_{kl}^e = D_{ijkl}^e (d\varepsilon_{kl} - d\varepsilon_{kl}^P) \quad 3.37$$

and fourth-tensor of elastic stiffness can be represented by Lamè constant as,

$$D_{ijkl}^e = \lambda(\delta_{ij}\delta_{kl}) + \mu(\delta_{ik}\delta_{jl} + \delta_{il}\delta_{jk}) \quad 3.38$$

In plastic loading condition, both initial yield and subsequent stress states must satisfy the yield condition

$$f_{VM}(\sigma_{ij}, k(\varepsilon_{eqs}^P)) = 0 \quad 3.39$$



From Eq. 3.30(b), for yielding under a uniaxial state of stress incorporated with isotropic hardening, the function can be written as

$$f_{VM}(J_2, k(\varepsilon_{eqs}^p)) = J_2 - k^2(\varepsilon_{eqs}^p) = 0 \quad 3.40$$

In VM criterion, the yield surface expands uniformly with the expanding size is assigned by the value  $k^2$ , which depends upon plastic strain history. The constant value,  $k^2$  can be expressed as in Eq. 3.41 by defining  $\sigma_y = \sigma_{eqs}$  when the yielding occurred.

$$k^2 = \frac{1}{3}\sigma_{eqs}^2 \quad 3.41$$

Substitute Eq. 3.41 into Eq. 3.40, the function becomes

$$f_{VM}(J_2, \varepsilon_{eqs}^p) = J_2 - \frac{1}{3}\sigma_{eqs}^2 = 0 \quad 3.42$$

then it is differentiated as,

$$\frac{\partial f_{VM}}{\partial \sigma_{eqs}} = \left( \frac{\partial f_{VM}}{\partial J_2} \right) \left( \frac{\partial J_2}{\partial \sigma_{eqs}} \right) = \frac{2}{3}\sigma_{eqs} \quad 3.43$$

By noting that  $\varepsilon_{ij}^p = \varepsilon_{eqs}^p$  when reaches the yield condition, Eq. 3.33 can be changed by

$$d\varepsilon_{eqs}^p = \lambda_{vm} \frac{\partial f_{VM}}{\partial \sigma_{eqs}} \quad 3.44$$

Recall the yield condition in Eq. 3.39, the plastic flow is governed by the consistency condition, implying that

$$df = \frac{\partial f_{VM}}{\partial \sigma_{ij}} d\sigma_{ij} + \frac{\partial f_{VM}}{\partial \varepsilon_{eqs}^p} d\varepsilon_{eqs}^p = 0 \quad 3.45$$

Then, Eq. 3.45 can be expressed by

$$\frac{\partial f_{VM}}{\partial \sigma_{ij}} d\sigma_{ij} = - \frac{\partial f_{VM}}{\partial \varepsilon_{eqs}^p} d\varepsilon_{eqs}^p \quad 3.46(a)$$

From Eq. 3.46(a), insert the incremental of equivalent plastic strain in Eq. 3.44, the derivation in Eq. 3.43 and hardening in Eq. 3.35 into it, to obtain

$$\frac{\partial f_{VM}}{\partial \sigma_{ij}} d\sigma_{ij} = - \frac{\partial f_{VM}}{\partial \sigma_{eqs}} \left( \frac{d\sigma_{eqs}}{d\varepsilon_{eqs}^p} \right) \lambda_{vm} \frac{\partial f_{VM}}{\partial \sigma_{eqs}} = - \left( \frac{2}{3} \sigma_{eqs} \right) H' \lambda_{vm} \left( \frac{2}{3} \sigma_{eqs} \right) = - \frac{4}{9} H' \lambda_{vm} \sigma_{eqs}^2 \quad 3.46(b)$$

Now, consider the stiffness matrix and substitute Eq. 3.32 into incremental of total strain, yield

$$D_{ijkl}^e d\varepsilon_{kl} = D_{ijkl}^e (d\varepsilon_{kl}^e + d\varepsilon_{kl}^p) = D_{ijkl}^e d\varepsilon_{kl}^e + D_{ijkl}^e d\varepsilon_{kl}^p \quad 3.47$$

and substitute Eq. 3.37 and 3.33 into 3.47, to get

$$D_{ijkl}^e d\varepsilon_{kl} = d\sigma_{ij} + D_{ijkl}^e \lambda_{vm} \frac{\partial f_{VM}}{\partial \sigma_{kl}} \quad 3.48$$

Then, multiply Eq. 3.48 to the  $(\partial f_{VM} / \partial \sigma_{ij})$  to form

$$\frac{\partial f_{VM}}{\partial \sigma_{ij}} D_{ijkl}^e d\varepsilon_{kl} = \frac{\partial f_{VM}}{\partial \sigma_{ij}} d\sigma_{ij} + \lambda_{vm} \frac{\partial f_{VM}}{\partial \sigma_{ij}} D_{ijkl}^e \frac{\partial f_{VM}}{\partial \sigma_{kl}} \quad 3.49$$

Substitute 3.46(a) into Eq. 3.49, and also substitute Eq. 3.44 and get

$$\frac{\partial f_{VM}}{\partial \sigma_{ij}} D_{ijkl}^e d\varepsilon_{kl} = -\lambda_{vm} \frac{\partial f_{VM}}{\partial \varepsilon_{eqs}^p} \frac{\partial f_{VM}}{\partial \sigma_{ij}} + \lambda_{vm} \frac{\partial f}{\partial \sigma_{ij}} D_{ijkl}^e \frac{\partial f_{VM}}{\partial \sigma_{kl}} \quad 3.50$$

Setting Eq. 3.50 and change the index notation appropriately in order to get the plastic multiplier form  $\lambda_{vm}$

$$\lambda_{vm} = \frac{\frac{\partial f_{VM}}{\partial \sigma_{ij}} D_{ijkl}^e d\varepsilon_{kl}}{-\frac{\partial f_{VM}}{\partial \varepsilon_{eqs}^p} \frac{\partial f_{VM}}{\partial \sigma_{ij}} + \frac{\partial f_{VM}}{\partial \sigma_{ab}} D_{abcd}^e \frac{\partial f_{VM}}{\partial \sigma_{cd}}} \quad 3.51$$

Then, recall the form of stress increment in Eq. 3.37. Substitute Eq. 3.33 and Eq. 3.51 into it, then we can get the stress increment as below

$$d\sigma_{ij} = D_{ijkl}^e d\varepsilon_{kl} - D_{ijkl}^e \left( \frac{\frac{\partial f_{VM}}{\partial \sigma_{ij}} D_{ijkl}^e d\varepsilon_{kl}}{-\frac{\partial f_{VM}}{\partial \varepsilon_{eqs}^p} \frac{\partial f_{VM}}{\partial \sigma_{ij}} + \frac{\partial f_{VM}}{\partial \sigma_{ab}} D_{abcd}^e \frac{\partial f_{VM}}{\partial \sigma_{cd}}} \right) \frac{\partial f_{VM}}{\partial \sigma_{ij}} \quad 3.52$$

Rearrange Eq. 3.52 and substitute 3.46(b) into it and change the index notation to obtain

$$d\sigma_{ij} = \left[ D_{ijkl}^e - \frac{D_{ijrs}^e \frac{\partial f_{VM}}{\partial \sigma_{rs}} D_{mnkl}^e \frac{\partial f_{VM}}{\partial \sigma_{mn}}}{\frac{4}{9} H' \sigma_{eqs}^2 + \frac{\partial f_{VM}}{\partial \sigma_{ab}} D_{abcd}^e \frac{\partial f_{VM}}{\partial \sigma_{cd}}} \right] d\varepsilon_{kl} \quad 3.53$$

Substitute Eq. A.7 and A.19 [refer Appendix 1] into Eq. 3.53 to simplify the derivation

$$d\sigma_{ij} = \left[ D_{ijkl}^e - \frac{\overbrace{D_{ijrs}^e \sigma'_{rs}}^{2\mu\sigma'_{ij}} \overbrace{D_{mnkl}^e \sigma'_{mn}}^{2\mu\sigma'_{kl}}}{\frac{4}{9} H' \sigma_{eqs}^2 + \underbrace{\sigma'_{ab} D_{abcd}^e \sigma'_{cd}}_{2\mu\sigma'_{ab}}} \right] d\varepsilon_{kl} \quad 3.54$$

Then we can write

$$d\sigma_{ij} = \left[ D_{ijkl}^e - \frac{2\mu\sigma'_{ij} 2\mu\sigma'_{kl}}{\frac{4}{9}H'\sigma_{eqs}^2 + 2\mu\sigma'_{ab}\sigma'_{ab}} \right] \delta_{ik} \delta_{jl} d\epsilon_{kl} \quad 3.55$$

Finally, solve Eq. 3.55 by using the notation in Eq. A.11, thus, the incremental of stress for VM that used in this study can be simplified as below

$$d\sigma_{ij} = \left[ D_{ijkl}^e - \frac{4\mu^2\sigma'_{ij} \mu\sigma'_{kl}}{\frac{4}{9}H'\sigma_{eqs}^2 + 2\mu\frac{\sigma'_{ab}\sigma'_{ab}}{\frac{2}{3}\sigma_{eqs}^2}} \right] \delta_{ik} \delta_{jl} d\epsilon_{kl} = \left[ D_{ijkl}^e - \underbrace{\frac{\mu^2\sigma'_{ij} \sigma'_{kl}}{\frac{1}{9}H'\sigma_{eqs}^2 + \mu\frac{1}{3}\sigma_{eqs}^2}}_{[D]^p} \right] \delta_{ik} \delta_{jl} d\epsilon_{kl} \quad 3.56$$

and the matrix form of  $[D]^p$  can be formed by

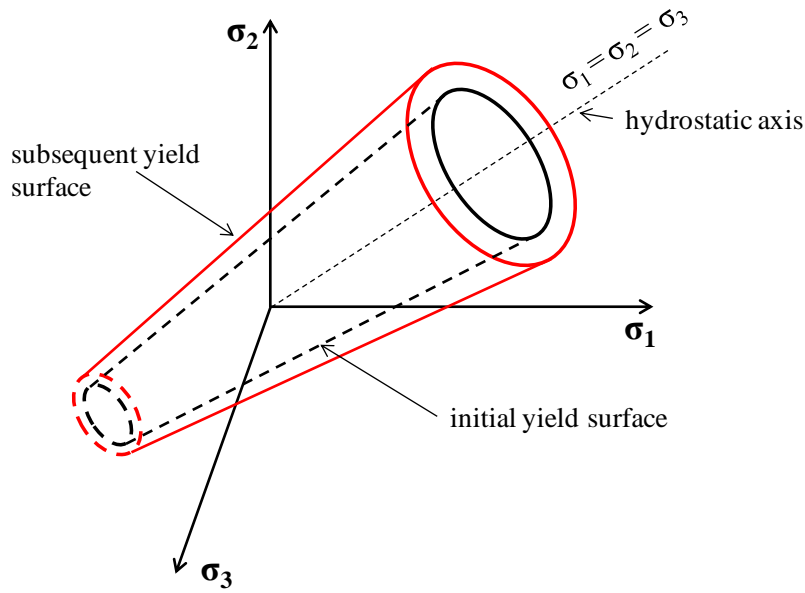
$$[D]^p = \frac{9\mu^2}{\sigma_{eqs}^2(H'+3\mu)} \begin{bmatrix} \sigma_{11}^{\prime 2} & \sigma_{11}^{\prime 2} \sigma_{22}^{\prime 2} & \sigma_{11}^{\prime 2} \sigma_{33}^{\prime 2} & \sigma_{11}^{\prime 2} \sigma_{12}^{\prime 2} & \sigma_{11}^{\prime 2} \sigma_{23}^{\prime 2} & \sigma_{11}^{\prime 2} \sigma_{31}^{\prime 2} \\ & \sigma_{22}^{\prime 2} & \sigma_{22}^{\prime 2} \sigma_{33}^{\prime 2} & \sigma_{22}^{\prime 2} \sigma_{12}^{\prime 2} & \sigma_{22}^{\prime 2} \sigma_{23}^{\prime 2} & \sigma_{22}^{\prime 2} \sigma_{31}^{\prime 2} \\ & & \sigma_{33}^{\prime 2} & \sigma_{33}^{\prime 2} \sigma_{12}^{\prime 2} & \sigma_{33}^{\prime 2} \sigma_{23}^{\prime 2} & \sigma_{33}^{\prime 2} \sigma_{31}^{\prime 2} \\ & & & \sigma_{12}^{\prime 2} & \sigma_{12}^{\prime 2} \sigma_{23}^{\prime 2} & \sigma_{12}^{\prime 2} \sigma_{31}^{\prime 2} \\ & & & & \sigma_{23}^{\prime 2} & \sigma_{23}^{\prime 2} \sigma_{31}^{\prime 2} \\ & & & & & \sigma_{31}^{\prime 2} \end{bmatrix} \quad 3.57$$

Symmetry

### 3.6.2 Elastic-plastic constitutive equation Drucker Prager criteria

Concrete is one of brittle materials having a high loading capacity in compression, and on the contrary in tension. It has not only differ in strength, but also in fracture behavior. The differences of mechanical properties and fracture behavior of concrete under compression and tension load induced the concrete may not appropriate to analyze by using one-parameter criteria, the von Mises yield criterion. In this analysis, two-parameter criteria (Drucker-Prager yield criterion) will be employed to investigate the fracture behavior of concrete. In a two-parameter criteria the yielding of concrete under hydrostatic pressure in compression zone and fracture property in tension zone are combined, or in the other words the Drucker-Prager

criteria is basically the VM yield criterion which is extended by including the effect of hydrostatic pressure on the shearing resistance of the material. Figure 3-11 shows the graphic representation of linear DP yield surfaces in the principal stress space. The figure presents a phenomena of the pressure dependent flow due to the internal friction, which is a typical feature of brittle materials.



**Figure 3-10:** Graphic of DP cylinder with hardening criteria

In the DP model, there are two limited conditions and they can be expressed by the function as follows

$$f_{DP}(J_2, I_1) = \sqrt{J_2} + I_1\alpha - k < 0 \rightarrow \text{elastic} \quad 3.58(a)$$

$$f_{DP}(J_2, I_1) = \sqrt{J_2} + I_1\alpha - k = 0 \rightarrow \text{plastic} \quad 3.58(b)$$

The stress point is on the yield surface if Eq. 3.58(b) is always satisfying, and hence the variation in  $f$  is zero. That is,

$$df_{DP} = 0 \quad 3.59 (a)$$

The variation in  $f$  to be as follows

$$df_{DP} = \frac{\partial f_{DP}}{\partial \sigma_{ij}} d\sigma_{ij} = 0 \quad 3.59(b)$$

Considering the second invariant of deviatoric stress,  $J_2$  in Eq. 3.31(a) and  $I_1 = \sigma_{ij}\delta_{ij}$ , the function in Eq. 3.59 can be derived to be;

$$\frac{\partial f_{DP}}{\partial \sigma_{ij}} = \left( \frac{\partial f_{DP}}{\partial \sqrt{J_2}} \frac{\partial \sqrt{J_2}}{\partial \sigma_{ij}} \right) + \left( \frac{\partial f_{DP}}{\partial I_1} \frac{\partial I_1}{\partial \sigma_{ij}} \right) = \left( \frac{1 \cdot J_2^{-1/2}}{2} \sigma'_{ij} \right) + (\alpha \cdot \delta_{ij}) = \frac{\sigma'_{ij}}{2\sqrt{J_2}} + \alpha \delta_{ij} \quad 3.60$$

Calculation of plastic strain incremental using flow rule associated with yield criterion  $f_{DP}$  has been stated in Eq. 3.33. Then the result of substitution Eq. 3.60 into Eq. 3.33 is as follows,

$$d\varepsilon_{ij}^p = \lambda_{dp} \frac{\partial f_{DP}}{\partial \sigma_{ij}} = \lambda_{dp} \left( \frac{\sigma'_{ij}}{2\sqrt{J_2}} + \alpha \delta_{ij} \right) \quad 3.61$$

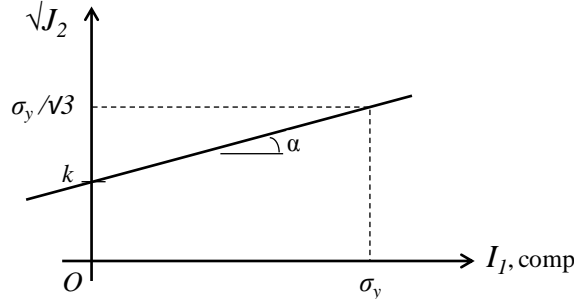
where  $\lambda_{dp}$  is a plastic multiplier of the Drucker-Prager model. According to Eq. 3.32, the total strain increment  $d\varepsilon_{ij}$  can be divided into elastic and plastic strain components, so the general incremental stress relationships can be written as,

$$d\sigma_{ij} = D_{ijkl}^e (d\varepsilon_{kl} - d\varepsilon_{kl}^p) \quad 3.62$$

and fourth-order tensor of elastic stiffness can be represented by Lamè constant as,

$$D_{ijkl}^e = \lambda(\delta_{ij}\delta_{kl}) + \mu(\delta_{ik}\delta_{jl} + \delta_{il}\delta_{jk}) \quad 3.63$$

When material yielding under a uniaxial state of stress,  $\sigma_y$  ( $\sigma_y > 0$ ),  $f = 0$  and thus  $k$  can be expressed as,



**Figure 3-11:** Calculation of the parameter  $k$  using  $J_2 - I_1$  plot

$$k = \left[ \alpha + \frac{1}{\sqrt{3}} \right] \sigma_y \quad 3.64$$

Substitute Eq. 3.64 into Eq. 3.58, the effective stress  $\sigma_{eqs} = \sigma_y$  can be defined as,

$$\sqrt{J_2} + I_1 \alpha = \left[ \alpha + \frac{1}{\sqrt{3}} \right] \sigma_{eqs} \quad 3.65 (a)$$

$$\sigma_{eqs} = \frac{\sqrt{J_2} + I_1 \alpha}{\left[ \alpha + \frac{1}{\sqrt{3}} \right]} \quad 3.65 (b)$$

$$\sigma_{eqs} \left[ \alpha + \frac{1}{\sqrt{3}} \right] = \sqrt{J_2} + I_1 \alpha \quad 3.65 (c)$$

Now calculate the effective plastic strain  $d\varepsilon_p$  by plastic work

$$dW^p = \sigma_{ij} d\varepsilon_{ij}^p = \sigma_{eqs} d\varepsilon_p \quad 3.66$$

Substitute Eq. 3.61 into Eq. 3.66 gives,

$$\sigma_{ij} \lambda_{dp} \left( \frac{\sigma'_{ij}}{2\sqrt{J_2}} + \alpha \delta_{ij} \right) = \sigma_{eqs} d\varepsilon_p \quad 3.67$$

Expand Eq. 3.67 and use notation as Eq. A.21 in Appendix 1 to yield,

$$\lambda_{dp} \left( \frac{\overbrace{\sigma_{ij} \sigma'_{ij}}^{2J_2}}{2\sqrt{J_2}} + \alpha \overbrace{\sigma_{ij} \delta_{ij}}^{\sigma_{ii}=I_1} \right) = \sigma_{eqs} d\varepsilon_p \quad 3.68$$

$$\lambda_{dp} \left( \frac{\sqrt{J_2}}{2\sqrt{J_2}} + I_1 \alpha \right) = \sigma_{eqs} d\varepsilon_p \quad \text{or} \quad \lambda_{dp} (\sqrt{J_2} + I_1 \alpha) = \sigma_{eqs} d\varepsilon_p \quad 3.69$$

Substitute Eq. 3.65 (c) into Eq. 3.69 gives,

$$\lambda_{dp} \sigma_{eqs} \left[ \alpha + \frac{1}{\sqrt{3}} \right] = \sigma_{eqs} d\varepsilon_p \quad 3.70$$

As a result,

$$d\varepsilon_p = \lambda_{dp} \left[ \alpha + \frac{1}{\sqrt{3}} \right] \quad 3.71$$

Let consider Eq. 3.61 to get the form of plastic multiplier  $\lambda_{dp}$  by squaring this equation,

$$d\varepsilon_{ij}^p d\varepsilon_{ij}^p = \lambda_{dp}^2 \left( \frac{\sigma'_{ij}}{2\sqrt{J_2}} + \alpha \delta_{ij} \right) \left( \frac{\sigma'_{ij}}{2\sqrt{J_2}} + \alpha \delta_{ij} \right) \quad 3.72$$

By noting that

$$\sigma'_{ij} \cdot \delta_{ij} = \sigma_{ii} = 0, \delta_{ij} \cdot \delta_{ij} = 3 \quad 3.73$$

and consider a notation in Eq. A.21 [Appendix 1]. Eq. 3.72 can be expanded and solved as,



$$d\varepsilon_{ij}^p d\varepsilon_{ij}^p = \lambda_{dp}^2 \left( \frac{\overbrace{\sigma'_{ij} \sigma'_{ij}}^{2J_2}}{4\sqrt{J_2}\sqrt{J_2}} + \alpha \frac{\overbrace{\sigma'_{ij} \delta_{ij}}^0}{2\sqrt{J_2}} + \alpha \frac{\overbrace{\sigma'_{ij} \delta_{ij}}^0}{2\sqrt{J_2}} + \alpha^2 \delta_{ij} \delta_{ij} \right) \quad 3.74(a)$$

$$= \lambda_{dp}^2 \left( \frac{2J_2}{4J_2} + \alpha^2 3 \right) = \lambda_{dp}^2 \left( \frac{1}{2} + 3\alpha^2 \right) \quad 3.74(b)$$

Hence,

$$\lambda_{dp} = \sqrt{\frac{d\varepsilon_{ij}^p d\varepsilon_{ij}^p}{\left(\frac{1}{2} + 3\alpha^2\right)}} \quad 3.75$$

Substitute Eq. 3.75 into Eq. 3.71 in order to get  $d\varepsilon_p$

$$d\varepsilon_p = \sqrt{\frac{d\varepsilon_{ij}^p d\varepsilon_{ij}^p}{\left(\frac{1}{2} + 3\alpha^2\right)}} \left[ \alpha + \frac{1}{\sqrt{3}} \right] \quad 3.76$$

In plastic loading condition, both initial yield and subsequent stress states must satisfy the yield condition  $f_{DP}(\sigma_{ij}, \varepsilon_{ij}^p, k(\varepsilon_p)) = 0$ , where a yield criterion of DP is a function of stress  $\sigma_{ij}$ , plastic strain  $\varepsilon_{ij}^p$  and  $k(\varepsilon_p)$ . Consequently, plastic flow is governed by the consistency condition, implying that,

$$df_{DP} = \frac{\partial f_{DP}}{\partial \sigma_{ij}} d\sigma_{ij} + \frac{\partial f_{DP}}{\partial \varepsilon_{ij}^p} d\varepsilon_{ij}^p + \frac{\partial f_{DP}}{\partial k(\varepsilon_p)} dk(d\varepsilon_p) = 0 \quad 3.77$$

Then, substitute Eq. 3.61, Eq. 3.62 and Eq. 3.76 into Eq. 3.77, we can get the consistency condition as;

$$\frac{\partial f_{DP}}{\partial \sigma_{ij}} \left[ D_{ijkl}^e [d\varepsilon_{kl} - \left( \lambda_{dp} \frac{\partial f_{DP}}{\partial \sigma_{ij}} \right)] + \frac{\partial f_{DP}}{\partial \varepsilon_{ij}^p} \left( \lambda_{dp} \frac{\partial f_{DP}}{\partial \sigma_{ij}} \right) + \frac{\partial f_{DP}}{\partial \varepsilon_p} \left( \sqrt{\frac{d\varepsilon_{ij}^p d\varepsilon_{ij}^p}{\left( \frac{1}{2} + 3\alpha^2 \right)}} \left[ \alpha + \frac{1}{\sqrt{3}} \right] \right) \right] = 0 \quad 3.78$$

Substitute Eq. 3.75 into Eq. 3.78 and change the index notation appropriately, it yields to

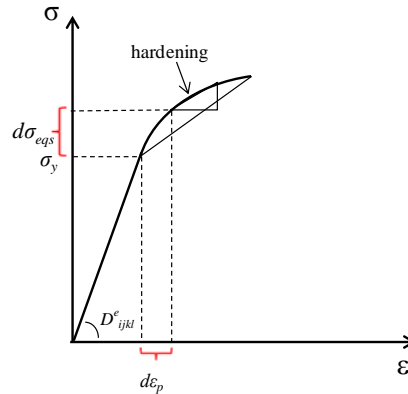
$$\frac{\partial f_{DP}}{\partial \sigma_{ij}} D_{ijkl}^e d\varepsilon_{kl} - \lambda_{dp} \frac{\partial f_{DP}}{\partial \sigma_{ab}} D_{abmn}^e \frac{\partial f_{DP}}{\partial \sigma_{mn}} + \lambda_{dp} \frac{\partial f_{DP}}{\partial \varepsilon_{ij}^p} \left( \frac{\partial f_{DP}}{\partial \sigma_{ij}} \right) + \lambda_{dp} \frac{\partial f_{DP}}{\partial \varepsilon_p} \left[ \alpha + \frac{1}{\sqrt{3}} \right] = 0 \quad 3.79$$

Setting Eq. 3.79 in order to get form of plastic multiplier  $\lambda_{dp}$

$$\frac{\partial f_{DP}}{\partial \sigma_{ij}} D_{ijkl}^e d\varepsilon_{kl} = \lambda_{dp} \left( \frac{\partial f_{DP}}{\partial \sigma_{ab}} D_{abmn}^e \frac{\partial f_{DP}}{\partial \sigma_{mn}} - \frac{\partial f_{DP}}{\partial \varepsilon_{ab}^p} \frac{\partial f_{DP}}{\partial \sigma_{ab}} - \frac{\partial f_{DP}}{\partial \varepsilon_p} \left[ \alpha + \frac{1}{\sqrt{3}} \right] \right) \quad 3.80$$

$$\lambda_{dp} = \frac{\frac{\partial f_{DP}}{\partial \sigma_{ij}} D_{ijkl}^e d\varepsilon_{kl}}{\frac{\partial f_{DP}}{\partial \sigma_{ab}} D_{abmn}^e \frac{\partial f_{DP}}{\partial \sigma_{mn}} - \frac{\partial f_{DP}}{\partial \varepsilon_{ab}^p} \frac{\partial f_{DP}}{\partial \sigma_{ab}} - \frac{\partial f_{DP}}{\partial \varepsilon_p} \left[ \alpha + \frac{1}{\sqrt{3}} \right]} \quad 3.81$$

For a general form of plastic multiplier  $\lambda_{dp}$ , Eq. 3.81 can be used. Now let consider the hardening effect to the DP constitutive equation. Figure 3-13 shows the increasing of equivalent plastic strain also increases the equivalent stress.



**Figure 3-12:** Typical uniaxial stress-strain curve

Then, the hardening modulus which is the ratio between the equivalent of stress to equivalent plastic strain can be expressed as,

$$H = \frac{\partial \sigma_{eqs}}{\partial \varepsilon_p} \quad 3.82$$

During plastic loading, the general form of the DP function can be written as,

$$f(J_2, I_1, \varepsilon_p) = J_2 + I_1 \alpha - k^2 = J_2 + I_1 \alpha - \left[ \alpha^2 + \frac{1}{3} \right] \sigma_{eqs}^2 \quad 3.83$$

The DP function in Eq. 3.83 can be derived to  $\sigma_{eqs}$ ,

$$\frac{\partial f_{DP}}{\partial \sigma_{eqs}} = - \left[ 2\alpha^2 + \frac{2}{3} \right] \sigma_{eqs} \quad 3.84$$

and the derivation term of DP function to the incremental plastic strain  $d\varepsilon_p$  can be written as in Eq. 3.85 if we change the hardening modulus  $H$  from the Eq. 3.82,

$$\frac{\partial f_{DP}}{\partial \varepsilon_p} = \frac{\partial f_{DP}}{\partial \sigma_{eqs}} \left( \frac{\partial \sigma_{eqs}}{\partial \varepsilon_p} \right) = \frac{\partial f_{DP}}{\partial \sigma_{eqs}} (H) \quad 3.85$$

Then, substitute Eq. 3.84 into Eq. 3.85, gives

$$\frac{\partial f_{DP}}{\partial \varepsilon_p} = - \left[ 2\alpha^2 + \frac{2}{3} \right] \sigma_{eq} (H) \quad 3.86$$

In Eq. 3.58 and Eq. 3.83, the function does not depend on  $\varepsilon_{ij}^p$ . Therefore, when deriving the DP model, the term of  $\partial f / \partial \varepsilon_{ij}$  can be eliminated in the general form of plastic multiplier as shown in Eq. 3.81. Let substituting Eq. 3.60, Eq. 3.63, and Eq. 3.86 into Eq. 3.81 to solve it and obtain

$$\lambda_{dp} = \frac{\left( \frac{\sigma'_{ij}}{2\sqrt{J_2}} + \alpha\delta_{ij} \right) (\lambda(\delta_{ij}\delta_{kl}) + \mu(\delta_{ik}\delta_{jl} + \delta_{il}\delta_{jk})) d\varepsilon_{kl}}{\left( \frac{\sigma'_{ab}}{2\sqrt{J_2}} + \alpha\delta_{ab} \right) (\lambda(\delta_{ab}\delta_{mn}) + \mu(\delta_{am}\delta_{bn} + \delta_{an}\delta_{bm})) \left( \frac{\sigma'_{mn}}{2\sqrt{J_2}} + \alpha\delta_{mn} \right) + \left[ 2\alpha^2 + \frac{2}{3} \right] \sigma_{eqs}(H) \left[ \alpha + \frac{1}{\sqrt{3}} \right]} \quad 3.87$$

By using the notation in Eq. 3.73, we can solve Eq. 3.87. The detail of deriving the equation was elaborated in Eq. A.23 and Eq. A.24 [Appendix 1] and finally it was solved as,

$$\lambda_{dp} = \left[ \frac{\frac{\mu\sigma'_{kl}}{\sqrt{J_2}} + \alpha(3\lambda + 2\mu)\delta_{kl}}{3\alpha^2(3\lambda + 2\mu) + \mu + \left[ 2\alpha^2 + \frac{2}{3} \right] \sigma_{eqs}(H) \left[ \alpha + \frac{1}{\sqrt{3}} \right]} \right] d\varepsilon_{kl} \quad 3.88$$

Then, recall Eq. 3.62 and substitute Eq. 3.61 into it.

$$d\sigma_{ij} = D_{ijkl}^e (d\varepsilon_{kl} - d\varepsilon_{kl}^p) = \underbrace{D_{ijkl}^e d\varepsilon_{kl}}_{[D]^e} - \underbrace{D_{ijkl}^e \lambda_{dp} \frac{\partial f_{DP}}{\partial \sigma_{ij}}}_{[D]^p} \quad 3.89$$

Substitute again the derivation form in Eq. 3.60 and Eq. 3.88 into Eq. 3.89,

$$d\sigma_{ij} = D_{ijkl}^e d\varepsilon_{kl} - D_{ijkl}^e \underbrace{\left[ \frac{\frac{\mu\sigma'_{kl}}{\sqrt{J_2}} + \alpha(3\lambda + 2\mu)\delta_{kl}}{3\alpha^2(3\lambda + 2\mu) + \mu + \left[ 2\alpha^2 + \frac{2}{3} \right] \sigma_{eqs}(H) \left[ \alpha + \frac{1}{\sqrt{3}} \right]} \right] \left( \frac{\sigma'_{ij}}{2\sqrt{J_2}} + \alpha\delta_{ij} \right) d\varepsilon_{kl}}_{[D]^p} \quad 3.90$$

Substitute  $D_{ijkl}^e$  in Eq. 3.63 for expanding  $[D]^p$  in Eq. 3.90 and modify the index notation,

$$[D]^p = \left[ \lambda(\delta_{ij}\delta_{kl}) + \mu(\delta_{ik}\delta_{jl} + \delta_{il}\delta_{jk}) \right] \left( \frac{\sigma'_{kl}}{2\sqrt{J_2}} + \alpha\delta_{kl} \right) \left[ \frac{\frac{\mu\sigma'_{mn}}{\sqrt{J_2}} + \alpha(3\lambda + 2\mu)\delta_{mn} d\varepsilon_{mn}}{3\alpha^2(3\lambda + 2\mu) + \mu + \left[ 2\alpha^2 + \frac{2}{3} \right] \sigma_{eqs}(H) \left[ \alpha + \frac{1}{\sqrt{3}} \right]} \right] \quad 3.91(a)$$

Further derivation of Eq. 3.91 (a) can be found in Eq. A.27(a) to A.27(e) [Appendix 1]. By modifying the index notation, finally the  $[D]^p$  is,

$$[D]^p = \left[ \frac{\left[ \frac{\mu\sigma'_{kl}}{\sqrt{J_2}} + \alpha(3\lambda + 2\mu)\delta_{kl} \right] \left[ \frac{\mu\sigma'_{mn}}{\sqrt{J_2}} + \alpha(3\lambda + 2\mu)\delta_{mn} \right]}{3\alpha^2(3\lambda + 2\mu) + \mu + \left[ 2\alpha^2 + \frac{2}{3} \right] \sigma_{eqs}(H) \left[ \alpha + \frac{1}{\sqrt{3}} \right]} \right] \delta_{mk} \delta_{nl} d\varepsilon_{kl} \quad 3.91(b)$$

Substitute  $[D]^p$  in Eq. 3.91(b) to Eq. 3.89 for expanding of  $d\sigma_{ij}$ , the constitutive equation of DP can be expressed as,

$$d\sigma_{ij} = \underbrace{D_{ijkl}^e}_{[D]^e} d\varepsilon_{kl} - \underbrace{\left[ \frac{\left[ \frac{\mu\sigma'_{kl}}{\sqrt{J_2}} + \alpha(3\lambda + 2\mu)\delta_{kl} \right] \left[ \frac{\mu\sigma'_{mn}}{\sqrt{J_2}} + \alpha(3\lambda + 2\mu)\delta_{mn} \right]}{3\alpha^2(3\lambda + 2\mu) + \mu + \left[ 2\alpha^2 + \frac{2}{3} \right] \sigma_{eqs}(H) \left[ \alpha + \frac{1}{\sqrt{3}} \right]} \right]}_{[D]^p} \delta_{mk} \delta_{nl} d\varepsilon_{kl} \quad 3.92$$

and the plastic stiffness matrix form of  $[D]^p$  for DP model can be expressed as below

$$[D]^p = \begin{bmatrix} \frac{(H^\# + H^* \sigma'_{11})^2}{H_3} & \frac{(H^\# + H^* \sigma'_{11})(H^\# + H^* \sigma'_{22})}{H_3} & \frac{(H^\# + H^* \sigma'_{11})(H^\# + H^* \sigma'_{33})}{H_3} & \frac{(H^\# + H^* \sigma'_{11})(H^* \sigma'_{12})}{H_3} & \frac{(H^\# + H^* \sigma'_{11})(H^* \sigma'_{13})}{H_3} & \frac{(H^\# + H^* \sigma'_{11})(H^* \sigma'_{23})}{H_3} \\ \frac{(H^\# + H^* \sigma'_{22})^2}{H_3} & \frac{(H^\# + H^* \sigma'_{22})(H^\# + H^* \sigma'_{33})}{H_3} & \frac{(H^\# + H^* \sigma'_{22})(H^* \sigma'_{12})}{H_3} & \frac{(H^\# + H^* \sigma'_{22})(H^* \sigma'_{13})}{H_3} & \frac{(H^\# + H^* \sigma'_{22})(H^* \sigma'_{23})}{H_3} & \\ \frac{(H^\# + H^* \sigma'_{33})^2}{H_3} & \frac{(H^\# + H^* \sigma'_{33})(H^* \sigma'_{12})}{H_3} & \frac{(H^\# + H^* \sigma'_{33})(H^* \sigma'_{13})}{H_3} & \frac{(H^\# + H^* \sigma'_{33})(H^* \sigma'_{23})}{H_3} & & \\ \frac{(H^* \sigma'_{12})^2}{H_3} & \frac{(H^* \sigma'_{12})(H^* \sigma'_{13})}{H_3} & \frac{(H^* \sigma'_{12})(H^* \sigma'_{23})}{H_3} & & & \\ \frac{(H^* \sigma'_{13})^2}{H_3} & \frac{(H^* \sigma'_{13})(H^* \sigma'_{23})}{H_3} & & & & \\ \frac{(H^* \sigma'_{23})^2}{H_3} & & & & & & \end{bmatrix} \quad 3.93(a)$$

symmetry

where,

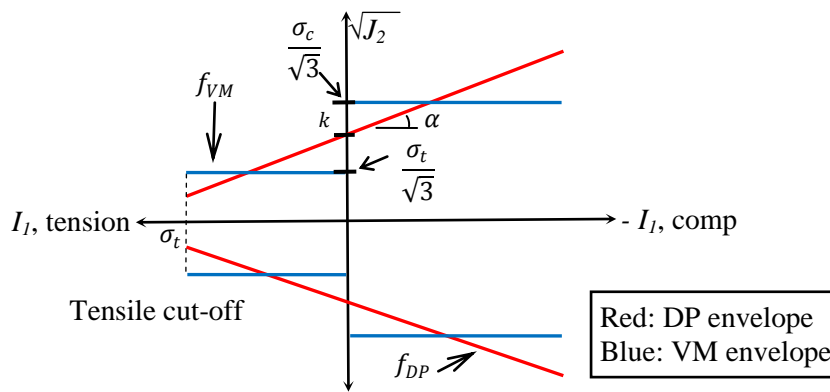
$$H^\# = \alpha[3\lambda + 2\mu]\delta_{ij} \quad 3.93(b)$$

$$H^* = \frac{\mu}{\sqrt{J_2}} \quad 3.93(c)$$

$$H_3 = 3\alpha^2(3\lambda + 2\mu) + \mu + \left[2\alpha^2 + \frac{2}{3}\right] \sigma_{eqs}(H) \left[\alpha + \frac{1}{\sqrt{3}}\right] \quad 3.93(d)$$

### 3.7 Combination of von Mises (VM) and Drucker-Prager (DP) failure criterion

The elastic-plastic constitutive equation of pressure independent (VM) and pressure dependent (DP) criterion models have been explained in the previous sub-topic. Then, in this sub-topic the effect of mean stress on shear failure criteria is described. Figure 3-14 shows the combination of failure envelopes of pressure dependent (DP) criterion and pressure independent (VM) criterion model.



**Figure 3-13:** Envelope for DP and VM models

In above figure (Fig. 3-14), x-axis represents the first invariant of stress tensor ( $I_1$ ) as shown in Eq. 3.94. While, y-axis represents the second invariant of the deviatoric stress tensor ( $\sqrt{J_2}$ ).

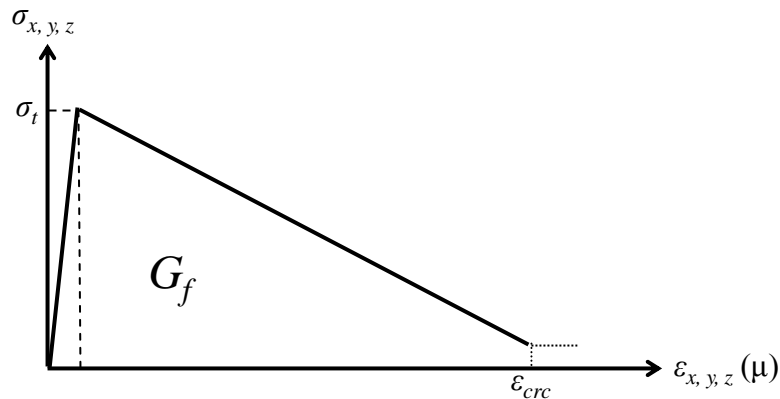
$$I_1 = \sigma_{11} + \sigma_{22} + \sigma_{33} = \sigma_{ij} \delta_{ij} \quad 3.94$$

where the two-parameter of this model, slope of failure line,  $\alpha$  and intercept of the failure line,  $k$  can be defined as;

$$\alpha = \frac{(\sigma_c - \sigma_t)}{\sqrt{3}(\sigma_c + \sigma_t)} \quad \text{and} \quad k = \left[ \alpha + \frac{1}{\sqrt{3}} \right] \sigma_t \quad 3.95$$

### 3.8 Tensile softening – elastic degradation

The tensile fracture of concrete is common prominent features on anchor structure failure mode occurred under pull-out load. As known that the tensile cracking degrades the stiffness of concrete material. Therefore, the local material orthotropy caused by tensile failure of concrete is deeply considered in this thesis. The plasticity and damage are directly defined after exceeding the tensile strength,  $\sigma_t$  using the linear softening path. Figure 3-14 shows the stiffness degradation of the concrete materials under tensile stress that can be identified by linear tension-softening path. In addition, the ultimate strain  $\varepsilon_{crc}$  (crack, end point of softening path) is assumed. The adequate value of ultimate strain is chosen in order to prevent particle size dependency using the relation between fracture energy,  $G_f$  and particle size,  $d^p$ . The determination of ultimate strain can be obtained in the Appendix 2.

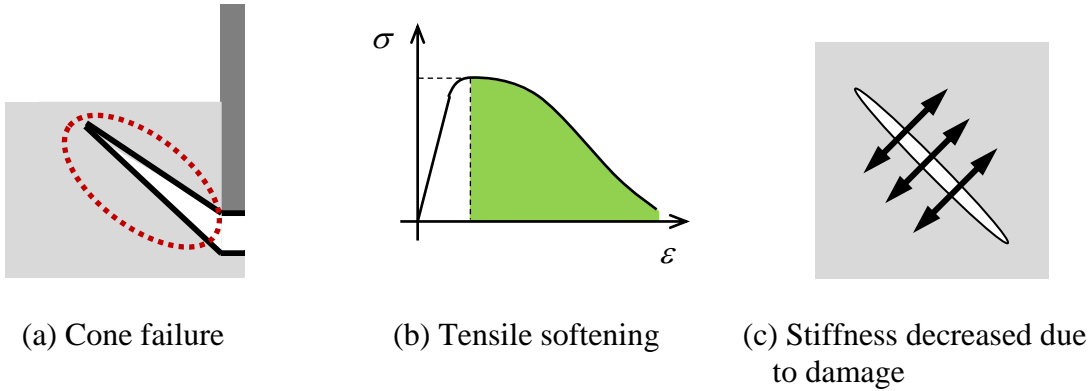


**Figure 3-14:** Linear tensile strain-softening and fracture energy,  $G_f$

In order to express the cone failure of concrete, tension softening model is applied to our numerical analysis. A cracking of the material is assumed to arise in the direction normal to the principal tensile strain. And the stiffness decrease due to the cracking of the material. To prevent excessive local tensile failure, tensile softening model is adopted. The illustration of the condition can be seen in Fig. 3-15 that are: (a) Cone failure of concrete resulted by pull-out load of anchor bolt; (b) stress-strain relationship commencing the tensile softening of concrete after the maximum tensile stress is exceeded; and (c) the decreasing of stiffness due



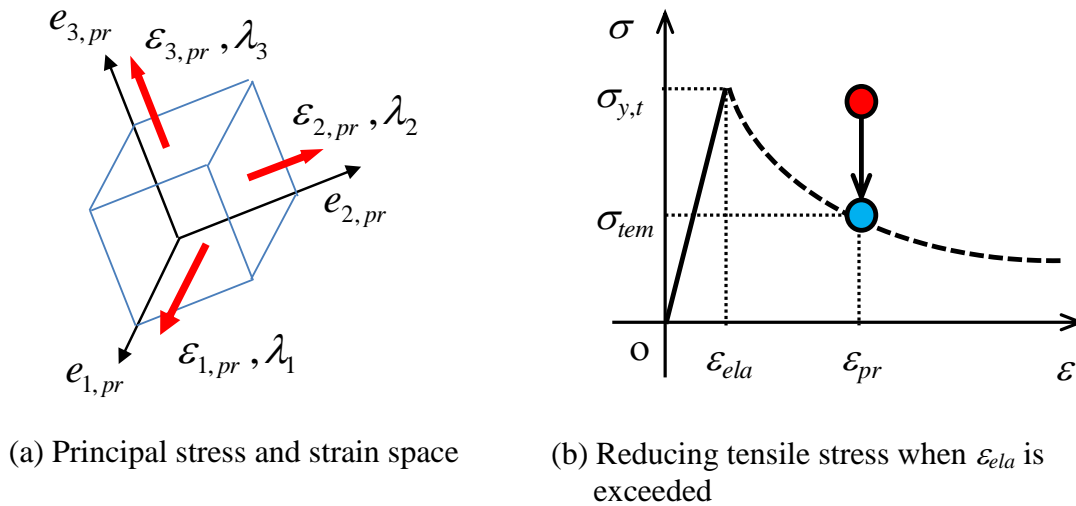
to the cracking damage with the direction of stress considered is perpendicular to the cracking path.



**Figure 3-15:** Numerical method of cone failure

The analysis flow of tensile softening and damage level is explained as follows.

- 1) Principal value and the directions of stress and strain are calculated. In principal space, the principal strain and unit vector are  $\varepsilon_{i,pr}$  and  $e_{i,pr}$  respectively (Fig. 3-16 (a)).



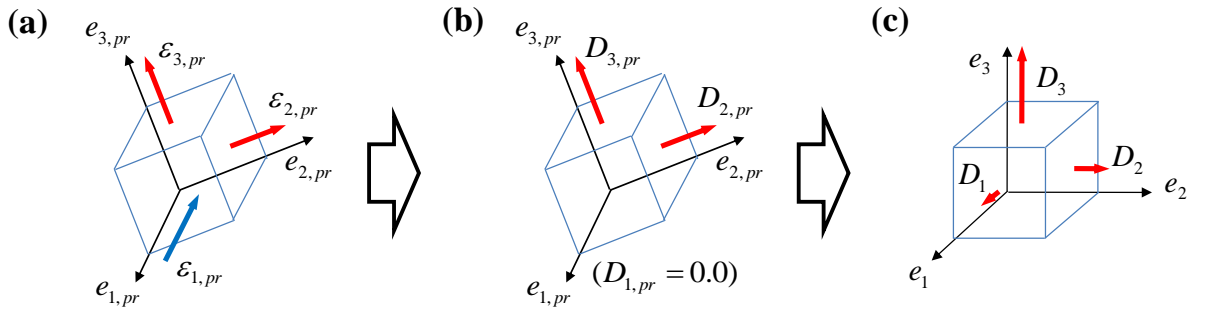
**Figure 3-16:** Principal stress and strain calculation

- 2) If the principal strain exceeds the strain correspond to the elastic tensile strength ( $\varepsilon_{ela}$ ), the softening of principal stress is reduced by softening parameter ( $\lambda_i$ ) as shown in Eq. 3.96.

$$\sigma_{tem} = \sigma_{y,t} \times \lambda_i \begin{cases} \lambda_i = (1 - 4\sqrt{(\varepsilon_{pr} - \varepsilon_{ela}) / \varepsilon_u}) & (\varepsilon_{pr} - \varepsilon_{ela}) < \varepsilon_u \\ \lambda_i = 0.0001 & (\varepsilon_{pr} - \varepsilon_{ela}) \geq \varepsilon_u \end{cases} \quad 3.96$$

where,  $\sigma_{y,t}$  is the tensile strength of concrete,  $\varepsilon_{ela}$  is the strain at the elastic tensile strength and  $\varepsilon_u$  is the ultimate strain in tension which is defined by failure energy of concrete and particle length. The term which is multiplied by  $\sigma_{y,t}$  in Eq. 3.96 express reducing slope of tensile stress (see Fig. 3-16 (b)).

- 3) Estimated the damage level in principal stress, then transformed into the global space.



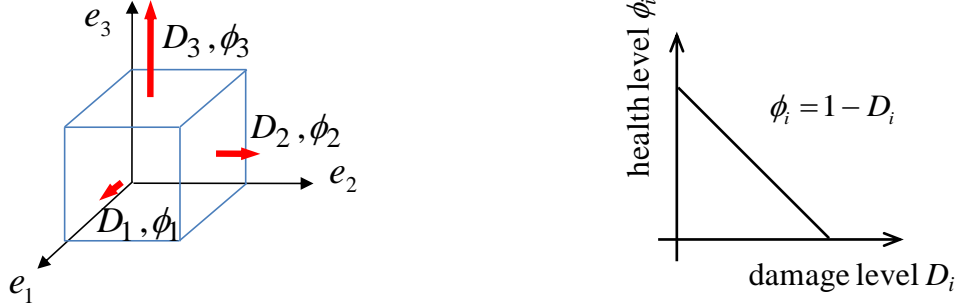
**Figure 3-17:** The chronology of calculation for damage parameter

The damage level in principal space ( $D_{i,pr}$ ) can be estimated and modified in global space ( $D_i$ ) as shown in Fig. 3-17 and also computed by Eq. 3.97 and 3.98. The damage is only considered for the tensile strain, otherwise assumed zero.

$$D_{i,pr} = \frac{\varepsilon_{i,pr}}{\varepsilon_u} \quad \text{with } (0 \leq D_{i,pr} \leq 1) \quad 3.97$$

$$D_i = \sum_{i=1}^3 |D_{i,pr} \varepsilon_{i,pr}| \quad 3.98$$

- 4) Calculated the health level ( $\phi_i$ ) in global space. The health level of material is demonstrated in Fig. 3-18.



(a) Damage level in global space

(b) Linear graph of damage-health level

**Figure 3-18:** Damage-health level of material

Finally, in order to calculate the damage parameter, the stiffness are corrected by the integrity tensor of damage level ( $\varphi_{ij}$ ).

$$\varphi_{ij} = \sqrt{(1 - D_i)(1 - D_j)} \quad 3.99$$

Then, the damage formulations according to Eq. 3.99 are reproduced to the initial fourth-order isotropic elastic matrix to form the orthotropic constitutive equation.

$$\sigma_{ij} = \varphi_{ij} [D_{ijkl}^e] \varepsilon_{kl} \quad 3.100$$

Finally, their damage stiffness matrix can be formed as shown in Eq. 3.101.

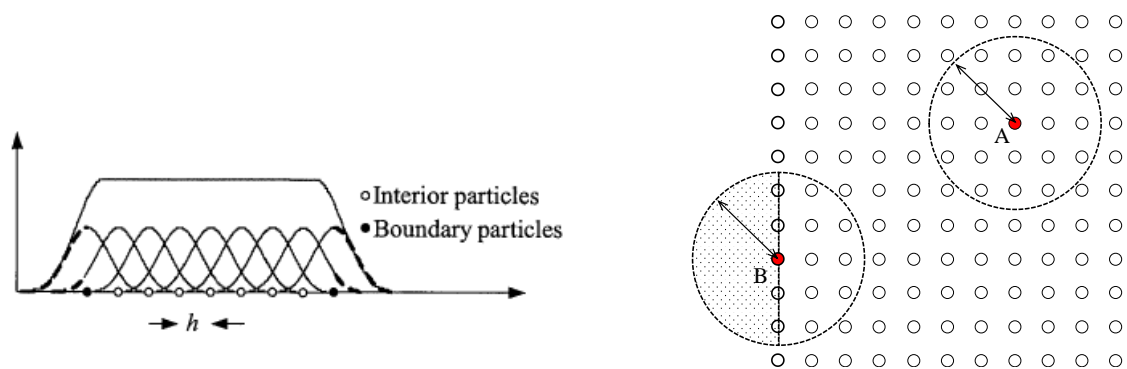
$$[D]^e = \begin{bmatrix} (\lambda + 2\mu) \times \varphi_{11} & \lambda \times \varphi_{12} & \lambda \times \varphi_{13} & 0 & 0 & 0 \\ & (\lambda + 2\mu) \times \varphi_{22} & \lambda \times \varphi_{23} & 0 & 0 & 0 \\ & & (\lambda + 2\mu) \times \varphi_{33} & 0 & 0 & 0 \\ & & & 2\mu \times \varphi_{12} & 0 & 0 \\ \text{Symmetry} & & & & 2\mu \times \varphi_{23} & 0 \\ & & & & & 2\mu \times \varphi_{31} \end{bmatrix} \quad 3.101$$

### 3.9 Boundary condition problem on SPH

#### 3.9.1 Boundary condition on the free surface

Since the SPH method based on particle as discrete element and calculation of certain particle by summing over all the particles within the supporting domain of the given particle, and the summation of particles within the support domain is calculated for approximation of the field variable. Therefore, the number of particles which are arranged inner the support domain is important to ensure the accuracy of analysis. The problem of particle deficiency is hampered near or on the boundary, which results from the integral that is truncated by the boundary. For these particles, only particles inside the boundary contribute to the summation of the particle interaction, and no contribution from outside since there are no particles beyond the boundary. It resulted one-side contribution and it does not give a good solution due to the velocity to be zero, see Fig. 3-19(a).

Figure 3-19(b) shows a disadvantage of the SPH method about the arrangement of particle as above described. As shown in this figure, the particle A has sufficient numbers of particles within support domain to calculate SPH approximation. By contrast, particle B on the boundary cannot get enough number of particles due to the lack of particles at outer side of the surface. So, the SPH method requires a special treatment for free surface condition. In this study, the dummy particles are adopted to solve this problem.

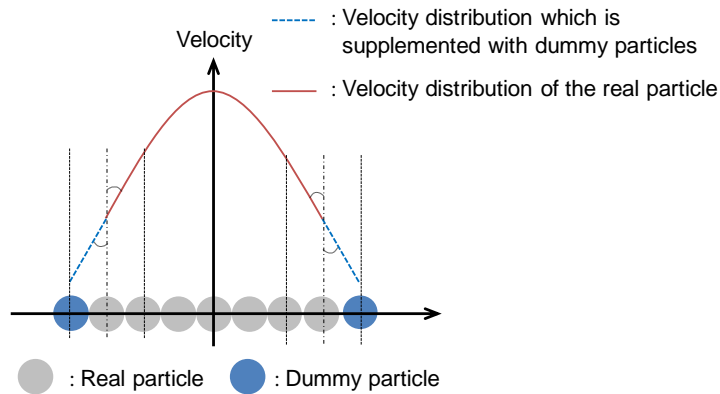


(a) Problem of particle deficiency on boundary (Liu and Liu, 2003) (b) The deficient condition of particle to be used for SPH approximation

**Figure 3-19:** SPH kernel and particle approximation for interior and boundary particles.

### 3.9.2 Dummy particles and its effect to the numerical stability

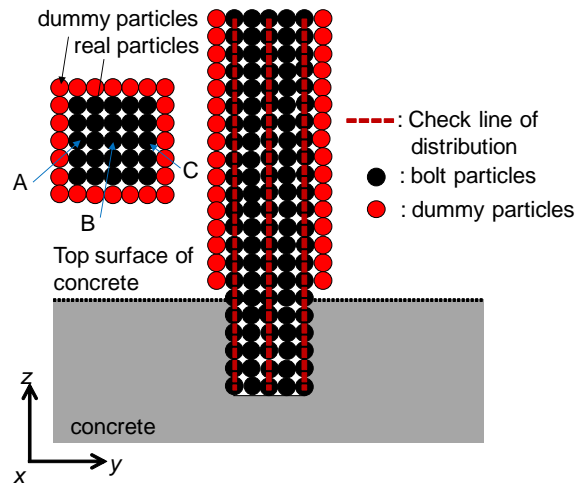
In this study, the dummy particles are used to treat a problem regarding the boundary conditions. The dummy particles are arranged around the surface of steel anchor bolt in one layer. They are placed symmetrically on the outside of the boundary. These dummy particles have the same material properties as the corresponding real particles. Calculation of velocity is one step in the SPH method, so it is assumed that there is a linear correlation of velocity (by interpolation) between a dummy particle and the closest real particle to calculate the velocity of dummy particles (Fig. 3-20).



**Figure 3-20:** Dummy particle on the outside of the boundary

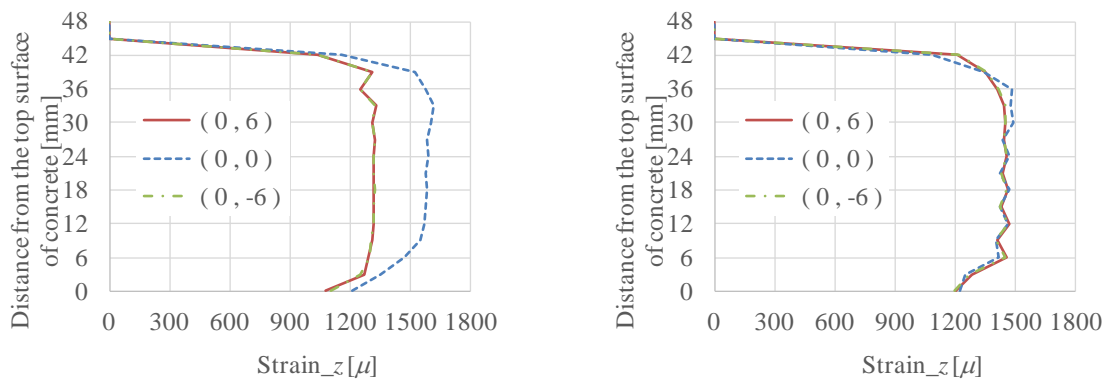
To grasp the effect of dummy particles on the strain distributions, two kinds of pullout simulations of steel bolt with or without dummy particles are carried out as shown in Fig. 3-21. The influence of dummy particles was investigated to evaluate the stress and strain of the anchor bolt, and analysis of result was focused on the stress and strain distribution. An investigation was conducted in the cross section of  $x = 0$  (center line) to create a contour plot of the stress and strain distribution. Since the problem of particle deficiency exists on the boundary, the particles of bolt at around the surfaces do not satisfy in the unity condition. It is due to lack of particles used in particle approximation of SPH method. In contrary, particles at the center which have satisfied the unity condition do not need a dummy particle. Figure 3-21 shows the three vertical lines of particle position in the bolt axis direction of structures with

and without dummy particles. High depth embedment anchor model ( $h/d=10$ ), with the diameter of the bolt 12 mm was used for the detailed analysis. Thus, the considered three line particles are  $(0, -6)$ ,  $(0, 0)$ ,  $(0, 6)$  in x-y coordinate, the strain distributions are compared by three kinds of observed points in Fig. 3-21 (points A, B and C).



**Figure 3-21:** Initial position of dummy particles

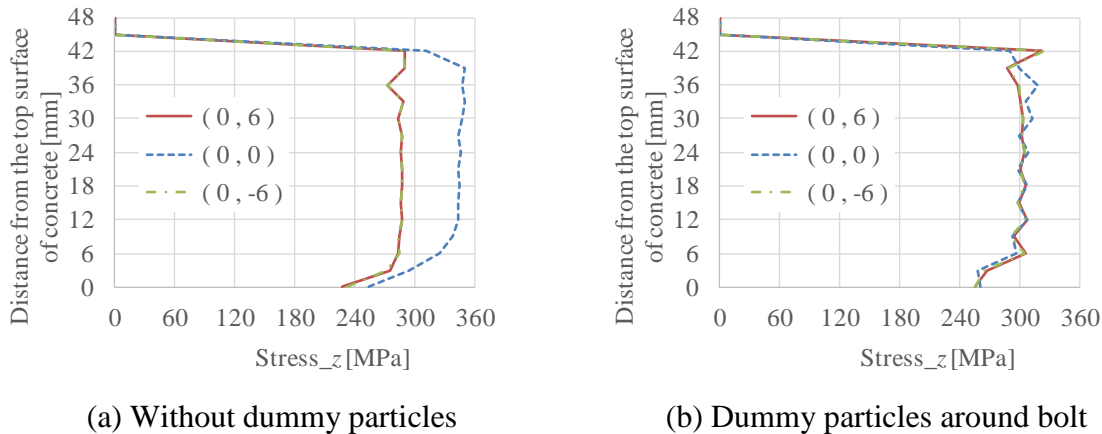
The example of the dummy particle effect to solve the particle deficiency problem is explained as follows. For the time increment = 4000 ms or the displacement = 0.2 mm, it resulted the stress and strain distribution (focused in z-direction only) for structures with and without dummy particles corresponding to the vertical distance from the upper surface of the concrete (see Fig. 3-22 and Fig. 3-23).



(a) Without dummy particles

(b) Dummy particles around bolt

**Figure 3-22:** Strain in z-direction



**Figure 3-23:** Stress in z-direction

Based on Fig. 3-22 and Fig. 3-23, it can be seen that by placing a dummy particle around the surface of anchor bolt, there is an apparent improvement. In particular, the differences of stress and strain between the center and surface are very small. Thus, it is recognized that distributing the dummy particles around the surface of anchor bolt is very useful to solve mechanical problems under the free surface condition. Furthermore, distributing the dummy particles at around the peripheral surface of the anchor bolt is very useful to solve the particle deficiency at the boundary of the anchor bolt. Considering the effect of vertical position of particles to the stress and strain, it can be notified that the top three layers of particles indicate a drop in the stress and strain value. It is predicted that the constant velocity of loading was applied to this layer. Moreover, the anchor particles that close to the concrete surface also exhibit a reduced stress and strain. It is reasonable since the particle at the support domain fully contributed on calculating a target particle of anchor particle.

### 3.10 Conclusion

This chapter precisely explains about the numerical calculation setting and presents a solution of the particle deficiency problem around the boundary area in the SPH method. A

basic formulation and calculation procedure of SPH are expressed. Constitutive model consists of von Mises and Drucker-Prager are also described in this chapter. Dummy particles apply to solve the boundary problem on the anchor bolt since it is a slender rod and only a few particles constructed on its cross section, so it may result inaccurate result and difficult to justify the failure mode of the anchor bolt. The result shows that the distribution of the dummy particles around the boundary area is very useful to solve mechanical problems under the free surface condition.

### 3.11 References

- Atluri, S.N. and Zhu, T.L.: A new meshless local Petrov-Galerkin (MLPG) approach to nonlinear problems in computer modeling and simulation, *Computational Modeling and Simulation in Engineering*, Vol. 3, No. 3, pp. 187-196 (1998).
- Belytschko, T., Lu, Y.Y. and Gu, L.: Element-free Galerkin Methods, *International Journal for Numerical Methods in Engineering*, Vol. 37, pp. 229-256 (1994).
- Duarte, C. A. and Oden, J. T.: H-p clouds - an h-p meshless method, *Numerical Methods for Partial Differential Equations*, Vol. 12, pp. 673-705 (1996).
- Gingold, R. A. and Monaghan, J. J.: Smoothed particle hydrodynamics: theory and application to non-spherical stars, *Monthly Notices of the Royal Astronomical Society*, Vol. 181, pp. 375-389 (1977).
- Gingold, R. A. and Monaghan, J. J.: Kernel estimates as a basis for general particle methods in hydrodynamics, *Journal of Computational Physics*, Vol. 46, pp. 429-453 (1982).
- Gray, J. P., Monaghan, J. J., and Swift, R. P.: SPH elastic dynamics, *Computer Methods in Applied Mechanics and Engineering*, Vol. 190, pp. 6641-6662 (2001).
- JSCE: Standard specifications for concrete structures-2007, Design, JSCE Guidelines for Concrete No. 15, *Japan Society of Civil Engineers (JSCE)* (2010).
- Li, S. and Liu, W.K.: Meshfree and particle methods and their applications, *Applied Mechanics and Reviews*, Vol. 55, No. 1, pp. 1-34 (2002).



- Liu, G. R. and Liu, M. B.: Smoothed Particle Hydrodynamics: A meshfree particle method, *World Scientific Publishing Co. Pte. Ltd.* (2003).
- Liu, M. B. and Liu, G. R.: Smoothed Particle Hydrodynamics (SPH): an overview and recent developments, *Archives of Computational Methods in Engineering*, Vol. 17, No. 1 (2010).
- Lucy, L. B.: A numerical approach to the testing of the fission hypothesis, *Astronomical Journal*, Vol. 82, No. 12, pp. 1013-1024 (1977).
- Monaghan, J. J. and Lattanzio, J. C.: A refined particle method for astrophysical problems, *Astronomy and Astrophysics*, Vol. 149, pp. 135-143 (1985).
- Monaghan, J. J.: An introduction to SPH, *Computer Physics Communications*, Vol. 48, pp. 89-96 (1988).
- Monaghan, J. J.: Smoothed particle hydrodynamics, *Annual review of astronomy and astrophysics*, Vol. 30, pp. 543-574 (1992).
- Monaghan, J. J.: Smoothed particle hydrodynamics, *Reports on Progress in Physics*, Vol. 68, pp. 1703-1759 (2005).
- Morris, J. P.: A study of the stability properties of SPH, *Applied Mathematics Report and Preprints*, Monash University, (1994).
- Morris J. P.: Analysis of smoothed particle hydrodynamics with applications, Ph.D. thesis, Monash University, (1996).
- Nayroles, B., Touzot, G. and Pillon, V.: Generalizing the finite element method: Diffuse approximation and diffuse elements, *Computational Mechanics*, Vol. 10, pp. 307-318 (1992).
- Perrone, N. and Kao, R.: A general finite difference method for arbitrary meshes, *Computer & Structures*, Vol. 5, pp. 45-58 (1975).
- Randles, P. W. and Libersky, L. D.: Normalized SPH with stress points, *International Journal for Numerical Methods in Engineering*, Vol. 48, pp. 1445-1462 (2000).
- Shepard, D.: Two-dimensional interpolation function for irregularly spaced data, *Proc 23rd Nat Conf ACM*, pp. 517-524 (1968).

Wingate, C. A. and Miller, W. A.: Workshop on advances in smooth particle hydrodynamics, *Workshop Proceedings, Los Alamos National Lab, NM (United States), LA-UR--93-4375; CONF-9309337--1*, (1993).



## CHAPTER IV

### NUMERICAL ANALYSIS WITH PERFECT BOND OF ANCHOR AND CONCRETE

#### 4.1 Introduction

The embedded anchor bolt is used in many concrete structures such as bridge restrainer systems on the concrete pier. In general, failure mode of them under pull-out load are classified as the fracture of anchor bolt or the failure of concrete. Possible failure modes and design formulas of pull-out load are bolt, cone, and bond failures. The design strength is generally defined as the smallest load of these predicted failures. Actually, to prevent the brittle failure of concrete, embedment depth of the anchor bolt is decided more than certain times to the diameter of anchor in the design. However, it is difficult to presume the failure mode and in some cases embedment depth of anchor bolt is not sufficient due to the configuration of reinforcing bars in concrete. Therefore, to guarantee the safety of concrete structures with embedded anchor bolts is difficult and it is very important to construct an accurate evaluation method on the load bearing capacity of anchor bolt.

Many analytical studies on the mechanical problem of concrete structures using FEM have been already carried out, such as Etse (1998), Ozbolt *et al.* (2006), Periskic *et al.* (2007) and Ozbolt *et al.* (2014). However, it is still difficult to simulate the discontinuous phenomenon such as crack growth problem. Thus, Smoothed Particle Hydrodynamics (SPH) is applied in this study since it can evaluate discontinuous displacement field and it is expected to simulate the local failure phenomena such as cone failure or bond failure between anchor bolt and concrete due to their meshfree concept. In this chapter, pull-out load simulations of anchor bolt by SPH are conducted. In particular, the perfect bond between steel

anchor and concrete is assumed and the effect of embedment depth of anchor bolt on their failure mode and ultimate pull-out strength are investigated.

## **4.2 Numerical analysis of pull-out simulation models**

This has been generally known that the mortar/concrete is a brittle material. The tensile strength of mortar/concrete materials is much lower than the compression strength; hence, in many cases the failure of concrete structures is mainly caused by tensile failure. In this analysis, the elastic-plastic constitutive equation of pressure independent, the Von Mises criteria (VM) is assumed for steel anchor bolt, while to express the effect of confined pressure on the concrete strength, the Drucker-Prager (DP) yield criterion is applied on mortar/concrete material.

### **4.2.1 Tensile failure mechanism of anchor bolt with various anchor depth**

#### **4.2.1.1 Pull-out simulation models**

There are some parameters affecting the strength of anchor, one of the most giving a significant effect is the depth of anchor bolt in concrete. Therefore, in this chapter we try to apply an SPH method to analyze the strength of anchor bolt by considering variations of anchor bolt depths. To analyze the pull-out simulation model, the description of the model is as follows.

##### **(1) Mechanical model of concrete**

To express the effect of confined pressure on the concrete strength, the Drucker-Prager yield criterion was applied. In this analysis, it was assumed that the cone failure of concrete occurs by tensile failure in maximum principal stress direction. To prevent excessive local tensile failure, tensile softening model is adopted. The analysis flow of tensile softening is as follows.

- 1) Principal value and the directions of stress and strain are calculated.

- 2) If principal strain exceeds the strain correspond to the tensile strength, the softening of principal stress is calculated using Eq. 4.1.

$$\begin{cases} \sigma_{tem} = \sigma_{y,t} \times (1 - \sqrt[4]{(\varepsilon_{pr} - \varepsilon_{ela}) / \varepsilon_u}) & (\varepsilon_{pr} - \varepsilon_{ela}) < \varepsilon_u \\ \sigma_{tem} = \sigma_{y,t} \times 0.0001 & (\varepsilon_{pr} - \varepsilon_{ela}) \geq \varepsilon_u \end{cases} \quad 4.1$$

where,  $\sigma_{y,t}$  is the tensile strength of concrete,  $\varepsilon_{ela}$  is the strain at tensile strength and  $\varepsilon_u$  is the ultimate strain in tension which is defined by failure energy of concrete and particle length. The term which is multiplied by  $\sigma_{y,t}$  in Eq. 4.1 express reduced slope of tensile stress.

- 3) Modified principal stresses are transformed into stress component in the global coordinate system.

Herein, the reality is that there is no interaction through the crack, however SPH method has a potential to act each other across the crack because the particle within influence domain can affect due to their nonzero stresses. So, in this study, the threshold value of maximum principal strain  $\varepsilon_{max}$  is defined and all stress components of the particle cut-offed if the maximum principal strain reach to this threshold value. This numerical procedure has been explained in the sub Chapter 3.8.

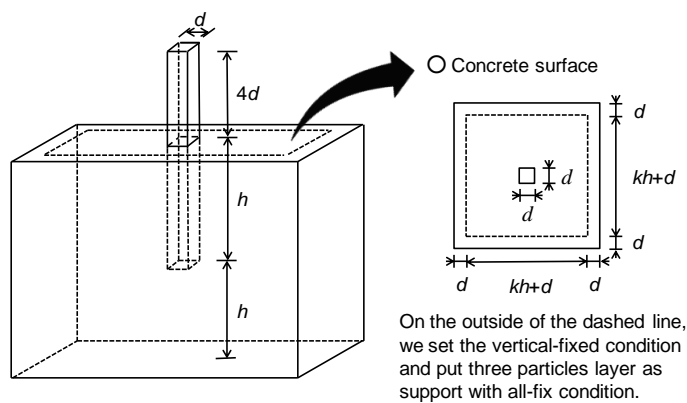
## (2) Mechanical model of anchor bolt

Yield condition of anchor bolt is evaluated by conventional Von Mises yield criteria and isotropic strain hardening is assumed. As to the fracture of anchor bolt, cut-off model is also adopted. In particular to prevent the interaction through the fracture surface, equivalent plastic strain limit is defined by their threshold value.

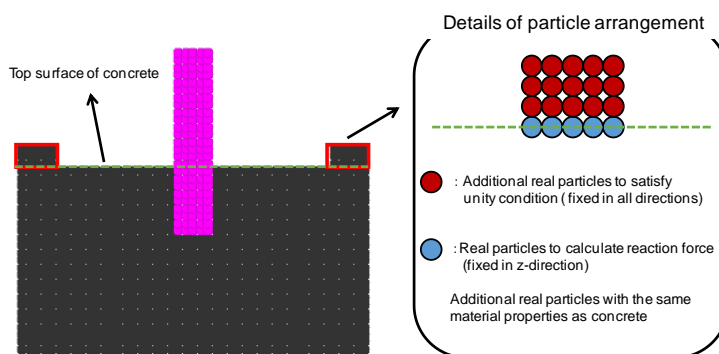
## (3) Analytical model

Figure 4-1 shows an analytical model in this study. The model comprises anchor bolt (a diameter size 12mm) with embedment depth  $h$  at the center of concrete block. The parameter  $k$  in this figure is the factor associated with the distance from the center to outside boundary

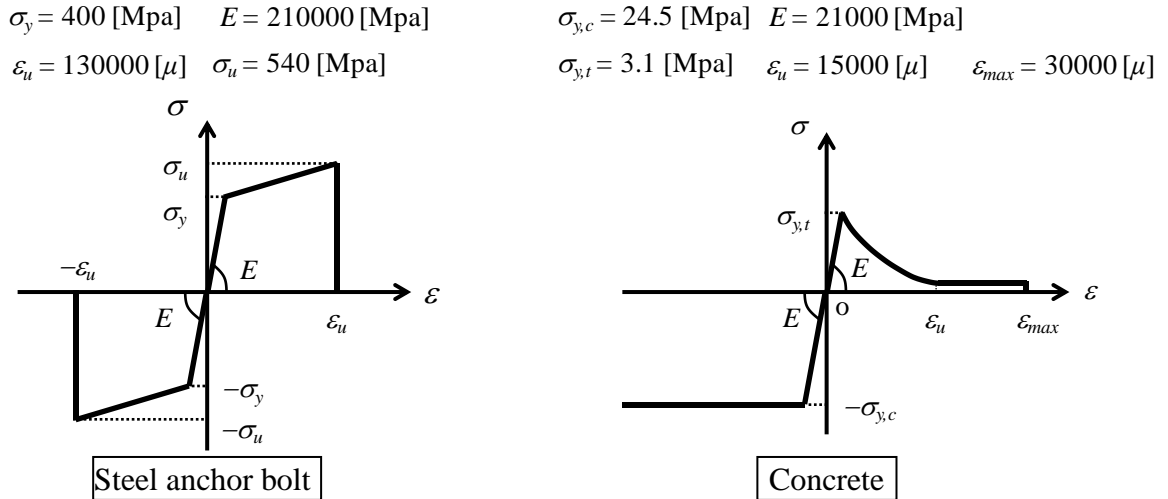
edge. The diameter size of each particle is 3 mm in this model. In addition, dummy particles such as Fig. 3-21 in the Chapter 3 are applied to the lateral sides of anchor bolt. Pull-out load is acted in the anchor bolt particles from the top layer to the third layer by 0.5 m/s constant velocity. As to the boundary condition of analytical models, vertical displacement restraints are applied in the four corners on upper surface shown in Fig. 4-1. Therefore the pull-out bearing force is calculated as the total reaction force on these four corners. Furthermore, to calculate accurate bearing force, dummy particles shown in Figure 4-2 are also applied. The adhesive condition between anchor bolt and concrete is assumed as a perfect bond condition in this analysis. Figure 4-3 shows a schematic view of the stress-strain curve of concrete and steel material and Table 4-1 shows applied material properties in this simulation.



**Figure 4-1:** Analytical model



**Figure 4-2:** Detail of particle arrangement as support



**Figure 4-3:** Stress-strain relation of concrete and steel

**Table 4-1:** Material properties of each material

	Concrete	Bolt
Density (kg / cm <sup>3</sup> )	2.35	7.9
Poisson's ratio	0.2	0.3

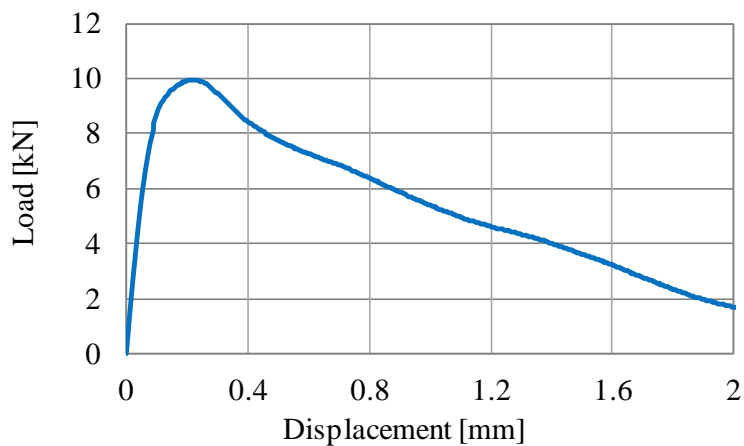
#### 4.2.1.2 Analysis result and discussion

In this chapter pull-out analyses are conducted in order to investigate the failure mode and pull-out strength. Five patterns of embedment depth with ratio of embedment depth to diameter of anchor,  $h/d = 2,4,6,8,10$  are used in this simulation.

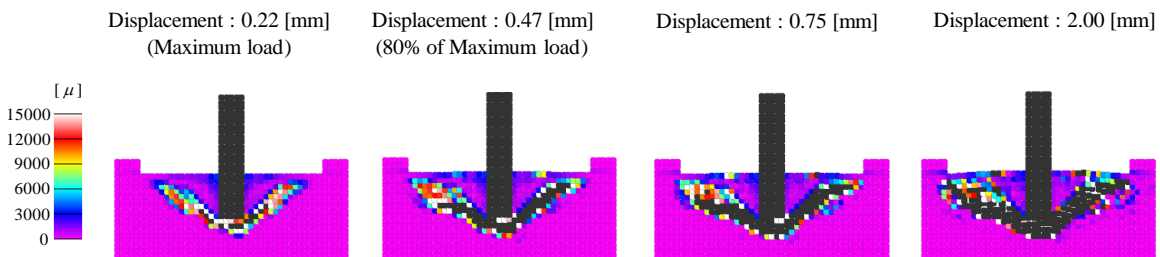
Figures 4-4~4-8 show the pull-out load and displacement relations and the distributions of a maximum principle strain of concrete, the equivalent plastic strain of anchor bolt are also shown in these figures. Furthermore, concrete particles in black color represent cut-off treatment due to the tensile failure of concrete. In this analysis, the behavior under constant speed pull-out load is calculated by time integration scheme, hence, oscillation of reaction force is shown. However, the smoothing procedure of the graphs is applied to find a reliable result.



In addition, Fig. 4-4 and Fig. 4-5 indicate that the bolt does not generate a plastic deformation, therefore, equivalent plastic strain of bolt is not observed. From these results, cone failure of concrete must develop from the bottom of bolt. When the cone failure is approximately generated, reaction force reaches to the maximum pull-out resistance, and followed by a gradual decline. This pull-out load decrease is due to the development of tensile failure of concrete. As shown in Fig. 4-4 and Fig. 4-5, it is presumed that cone failure is the most probable failure mode in shallow embedment depth cases.

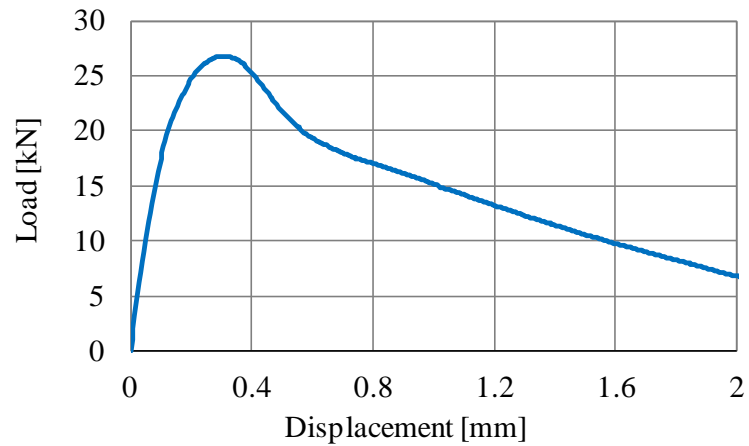


(a) relation of reaction force and displacement

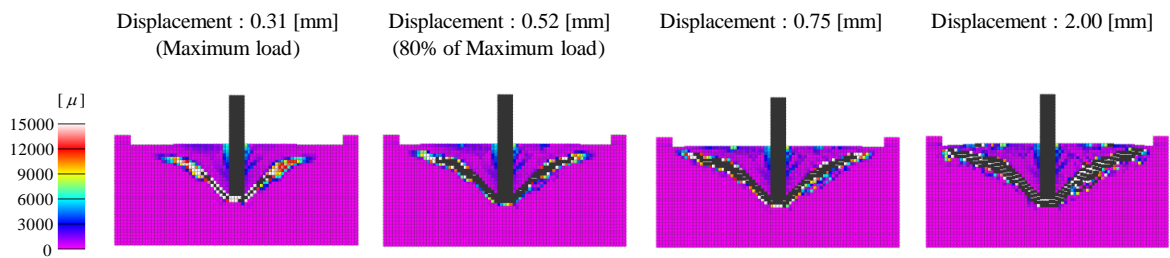


(b) maximum principal strain distribution of concrete

**Figure 4-4:** Pull-out analysis result of anchor bolt ( $h / d = 2$ )

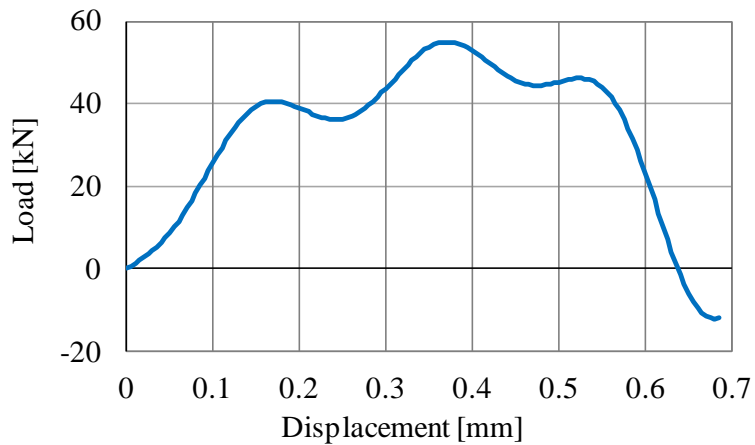


(a) relation of reaction force and displacement



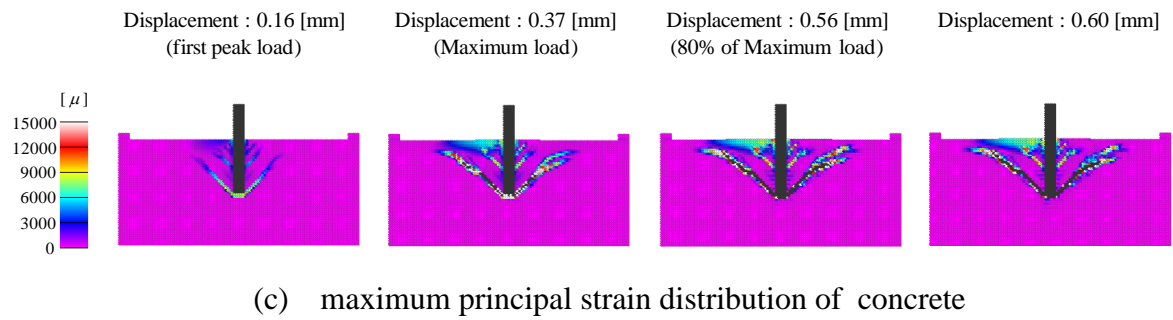
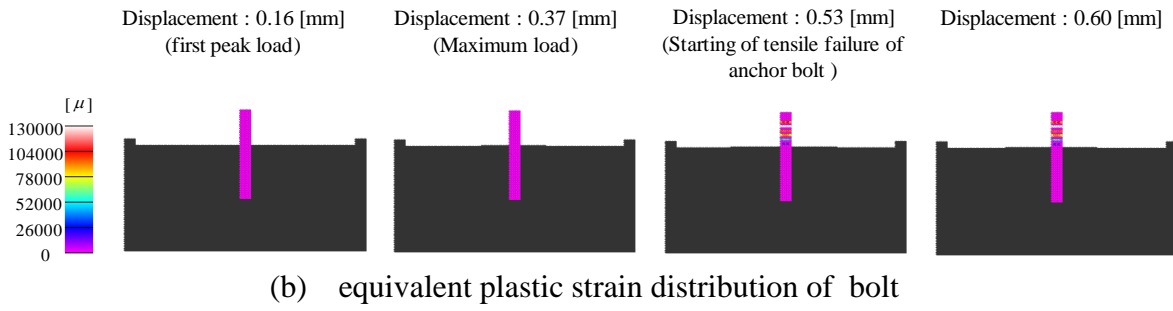
(b) maximum principal strain distribution of concrete

**Figure 4-5:** Pull-out analysis result of anchor bolt ( $h / d = 4$ )

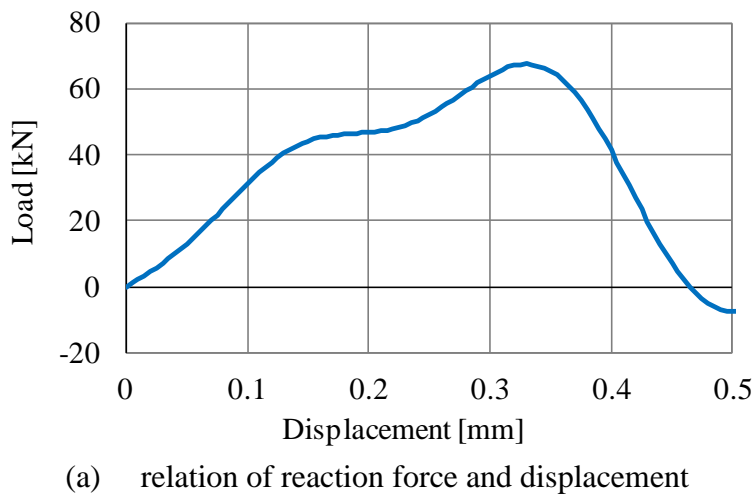


(a) relation of reaction force and displacement

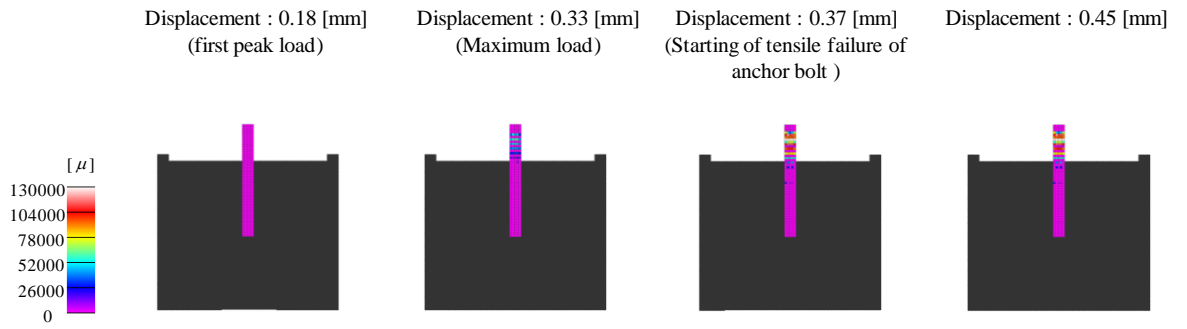
**Figure 4-6:** Pull-out analysis result of anchor bolt ( $h / d = 6$ )



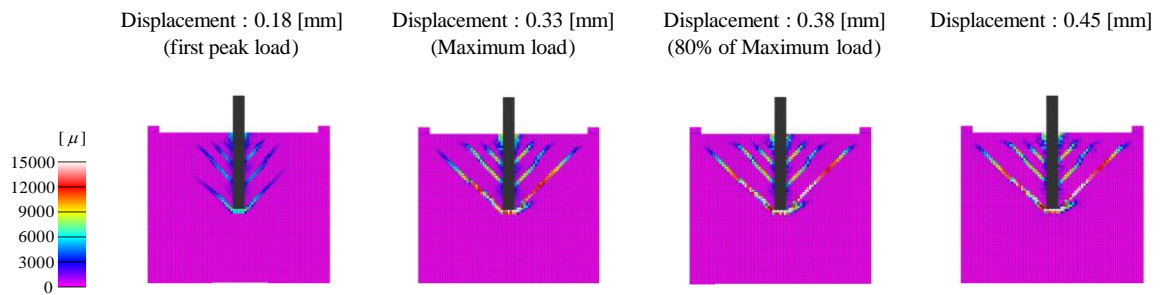
**Figure 4-6:** Pull-out analysis result of anchor bolt ( $h / d = 6$ ) (continued)



**Figure 4-7:** Pull-out analysis result of anchor bolt ( $h / d = 8$ )

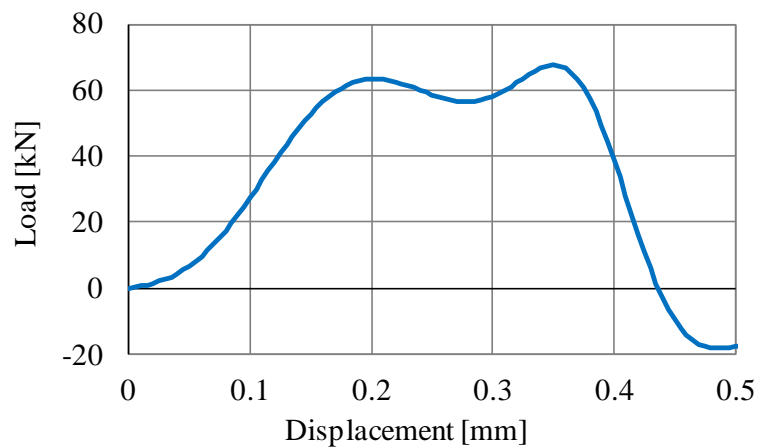


(b) equivalent plastic strain distribution of bolt



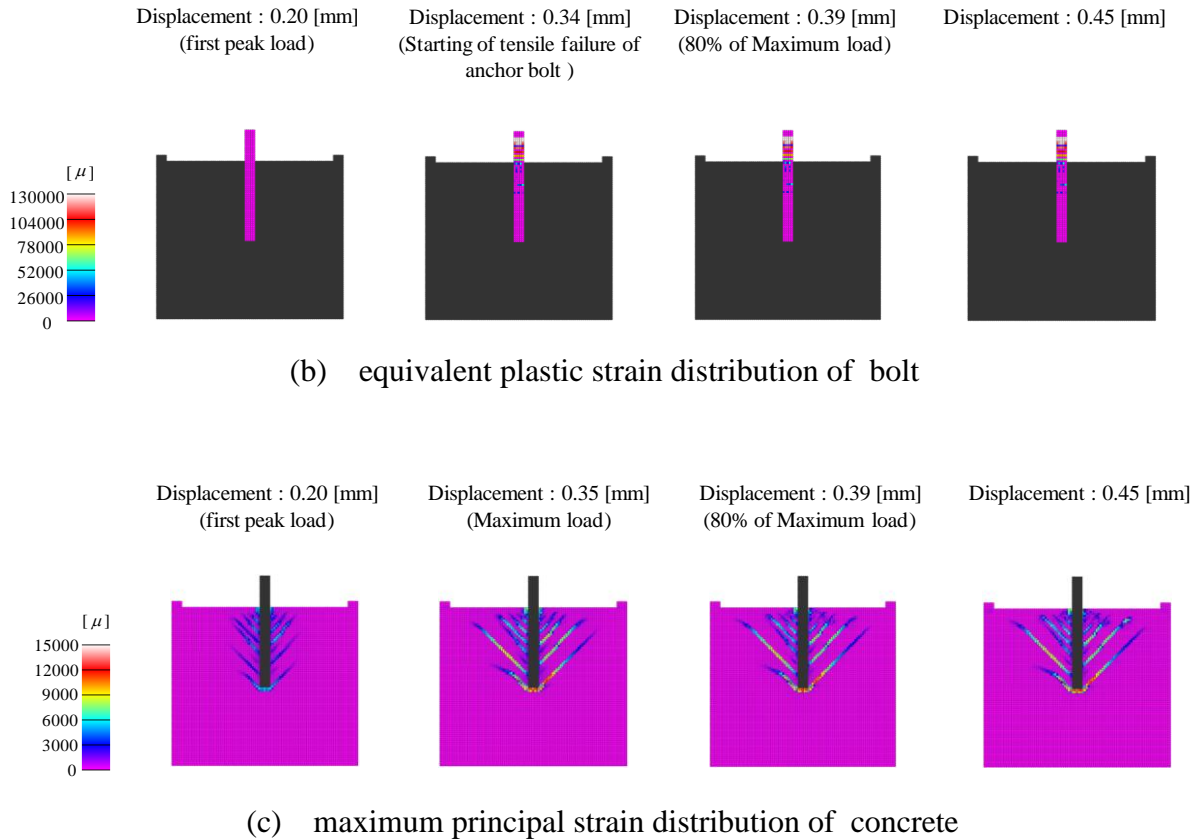
(c) maximum principal strain distribution of concrete

**Figure 4-7:** Pull-out analysis result of anchor bolt ( $h / d = 8$ ) (continued)



(a) relation of reaction force and displacement

**Figure 4-8:** Pull-out analysis result of anchor bolt ( $h / d = 10$ )

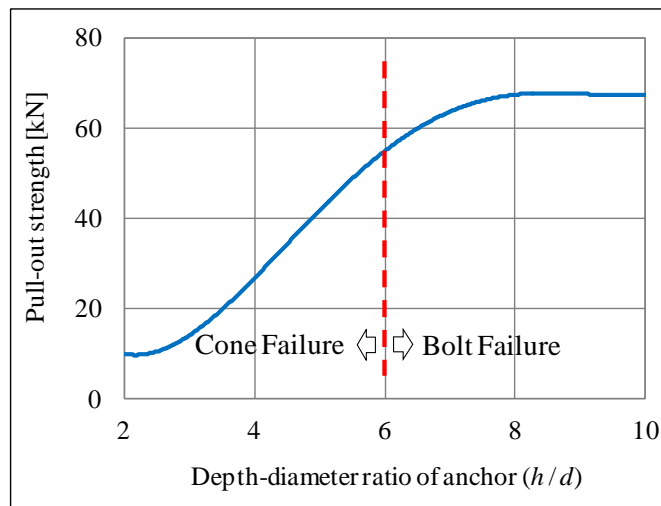


**Figure 4-8:** Pull-out analysis result of anchor bolt ( $h / d = 10$ ) (continued)

The lose-gain-lose strength curve which is observed in Fig. 4-6 (this pattern is not shown in Fig. 4-4 and Fig. 4-5). Since the tensile crack path from not only the bottom, but also the middle of bolt is observed and these crack paths develop at different timing, loading and unloading are shown in this simulation. A sudden reduction of pull-out strength at around 0.55 mm displacement is assumed due to the anchor bolt failure. Considerable maximum principal strain growth of concrete is not recognized during the bolt failure process. So, this case can be evaluated as the bolt failure mode. Finally, as shown in Figure 4-7 and 4-8, the bolt failure patterns which are similar as the result of  $h/d = 6$  are recognized. Furthermore, the tendency that pull-out failure displacement becomes smaller when the embedment depth of bolt is deeper.

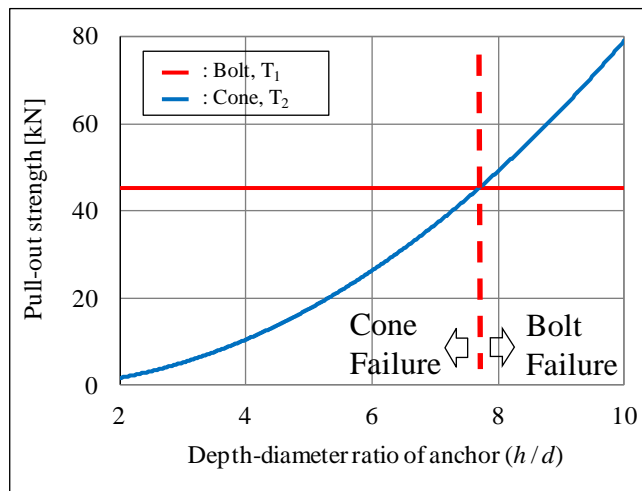
The influence of embedment depth on the load-bearing capacity based on our results is represented in Fig. 4-9. Besides, in Fig. 4-10, the influence of embedment depth on the load-bearing capacity by the design load equation is represented (JSCE, 2010 and Fujikake et al.,

2003). In fact, bonding failure is not considered in this analysis because the perfect bonding between bolt and concrete is assumed in our analysis model. The Fig. 4-9 shows, for the shallow depth of anchor (with  $h/d$  less than 6), the pull-out strength increase significantly in accordance to the increasing of embedment depth. In this range, concrete failure or cone failure of concrete is gained. The significant increasing of reaction force is gained due to the reaction force is directly affected by the depth of anchor. In contrast, when the anchor depth is higher than 6, the graph shows that the reaction force is a relatively constant. It is due to the structure has been in anchor bolt failure condition. So, there is no a significant effect of the depth of anchor bolt to the pull-out strength.



**Figure 4-9:** Influence of embedment depth into load-bearing ability based on the analysis

Furthermore, by comparing between the analysis result and the standard design equation, a similar pattern between them is found. There is a rapid increasing of pull-out strength in accordance to increase in depth of anchor, then followed by a constant strength. And also the failure mode change from cone failure to bolt failure with an increasing of depth-diameter ratio of anchor until a certain depth. However, the analytical pull-out strength due to the cone failure is quite different from design load, it is supposed because several cracks grow at the same time in the numerical analysis. Whereas, the standard design formula assumes only one crack path considered.



**Figure 4-10:** Influence of embedment depth into load-bearing ability based on the design equation

Based on all these figures (Fig. 4-4 ~ 4-10), the trend is that the failure mode can change from cone failure to bolt failure because of increase of embedment depth. In the next step, a quantitative evaluation of pull-out resistance will be constructed by using several parameters such as by considering the bonding character model between concrete and anchor bolt, and we seek to improve the accuracy of design load equation of embedded anchor bolt.

### 4.3 Conclusion

This chapter precisely explains about the numerical calculation setting and presented a numerical example of the analysis of anchor bolt under pull-out load. The effect of variation of anchor bolt depth as a parameter were determined by the proposed numerical method when simulating anchor bolt structure subjected to pull-out load. By adopting the VM model for anchor bolt and DP model for concrete and applying cut-off procedure, the ultimate pull-out strength and failure mechanism can be investigated. The change of load-displacement behavior, failure mode and maximum pull-out strength due to the embedment depth can be expressed by numerical analysis using the SPH method. Moreover, the numerical analysis

results show that the SPH method adequately describes the large deformation of anchor structure failures.

However, bonding failure is not considered in this analysis because the perfect bonding between bolt and concrete is assumed in our analysis model. By ignoring the effect of bond character, the numerical analysis may result a higher pull-out strength and a real failure behavior cannot be gained. According to the characteristics of concrete, steel anchor bolt and bond character between them, the bonding criterion is significantly important to evaluate the pull-out strength and failure mechanism of anchor bolt structure in concrete under pull-out load.

#### 4.4 References

- Etse, G.: Finite element analysis of failure response behavior of anchor bolts in concrete, *Nuclear Engineering and Design*, Vol. 179, pp. 245-252 (1998).
- Fujikake, K. et. al.: Chemically bonded anchors subjected to rapid pullout loading, *ACI Materials Journal*, Vol. 100, No. 3, pp. 246-252 (2003).
- JSCE: Standard specifications for concrete structures-2007, Design, JSCE Guidelines for Concrete No. 15, *Japan Society of Civil Engineers (JSCE)* (2010).
- Ozbolt, J., Orsanic, F. and Balabanic, G.: Modeling pull-out resistance of corroded reinforcement in concrete: Coupled three-dimensional finite element model, *Cement & Concrete Composites*, Vol. 46, pp. 41-55 (2014).
- Ozbolt, J., Rah, K.K. and Mestrovic, D.: Influence of loading rate on concrete cone failure, *International Journal of Fracture*, Vol. 139, pp. 239-252 (2006).
- Periskic, G., Ozbolt, J. and Eligehausen, R.: 3D Finite Element analysis of stud anchors with large head and embedment depth, *Proceedings of FraMCos-6 Catania, Italy* (2007).





## CHAPTER V

### NUMERICAL ANALYSIS WITH CONSIDERING THE BOND CHARACTER

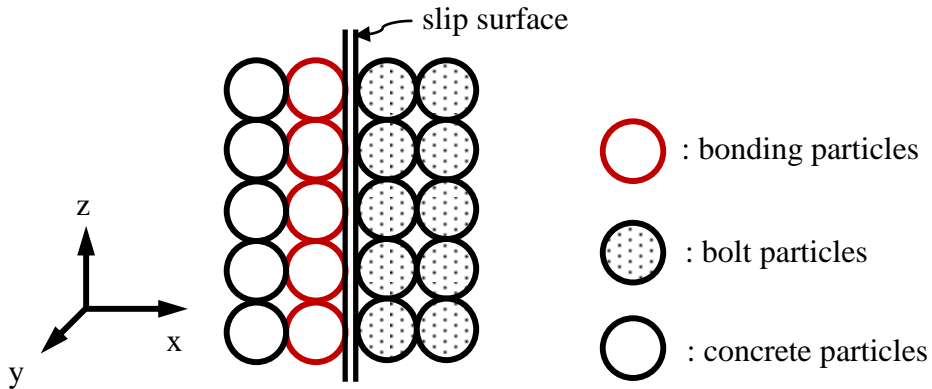
#### 5.1 Introduction

As discussed in Chapter IV, the perfect bonding between concrete and steel anchor bolt was assumed, including the contact surface between concrete and embedded anchors. By assuming the perfect bonding, analysis result shows that only two kinds of failure mode can be distinguished, that is cone failure and bolt failure. However, in real applications the combination of cone and bond failures may be found. This combination of failure mode was also confirmed by the experimental results explained in Chapter II. To improve the numerical model developed in Chapter IV, therefore, the bonding character model will be proposed and applied to all models examined in Chapter IV. These results, then, will be compared to the obtained results on Chapter IV and the comparison will be focused on the loading capacity and failure mode of anchor bolt structures under pull-out loads. Some parameters, such as the constitutive model of materials, size of anchor structures, material properties, and other parameters will be fully adopted from the models investigated in Chapter IV.

#### 5.2 Bonding character model

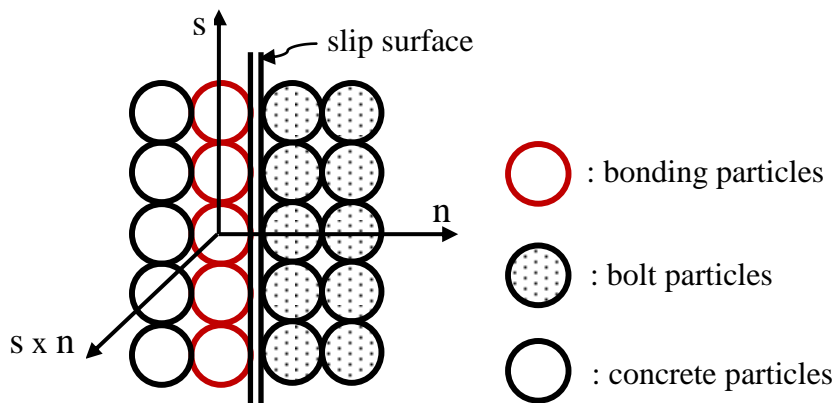
Bonding character model is the constructed model to provide the possibility of bond failure in the interface area between the concrete and anchor bolt particles by conducting a number bonding particles in the interface area. Since the mechanical properties of concrete are significantly lower than the anchor bolt particle, hence it is assumed that the bonding

particles, the particles that may lose in bond or failure due to bond/shear, have the material properties equal to the concrete particles, such as Young's modulus ( $E$ ), density, yield stress, etc. Let us consider Fig. 5-1 describing the schematic of bond elements and slip boundary area in global coordinates.



**Figure 5-1:** Schematic of bond link element and slip boundary

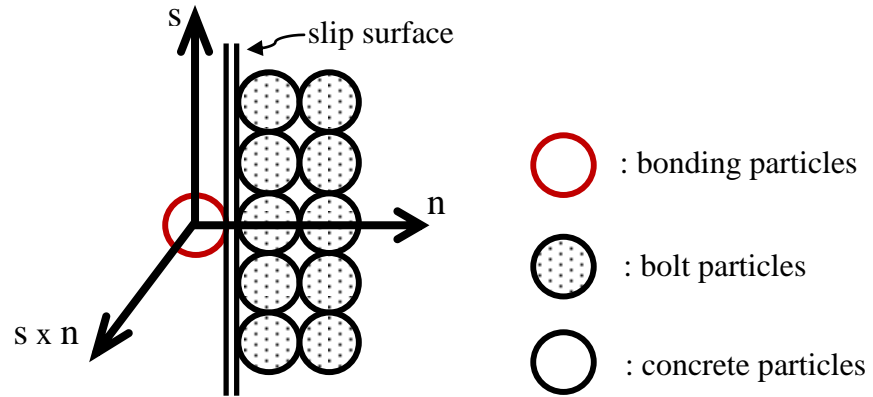
Bonding character is defined by 2 parameters: the bond stress and bond strain relationship, and bond failure expression of bonding particle.



**Figure 5-2:** Schematic of cross product vector of normal and slip vectors

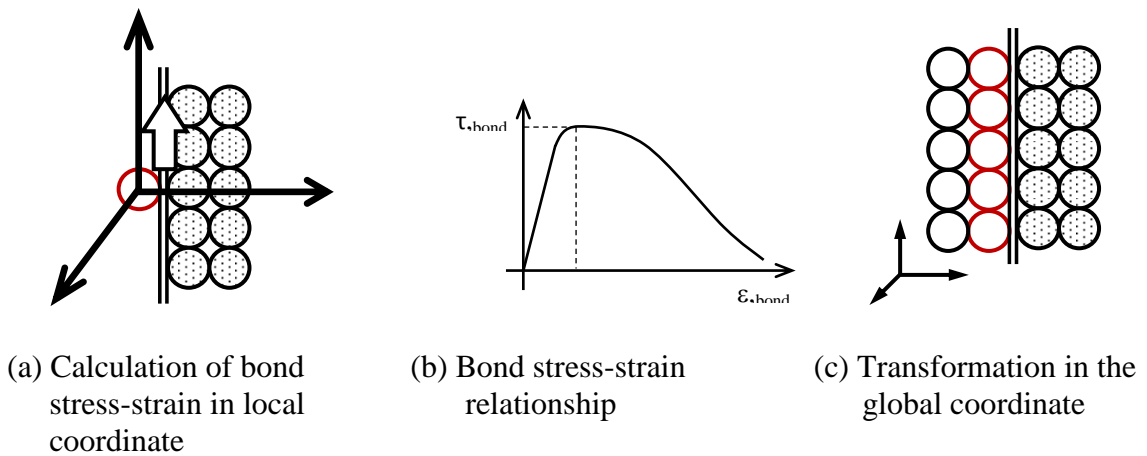
In global space the stress is arranged to normal stress ( $n$ ), shear stress ( $s$ ), and cross product of them ( $s \times n$ ) as shown in Fig. 5-2. However to evaluate the bond condition, the stress in global space should be translated to the local space and divided by 3 vector components: normal

vector of slip surface, slip direction vector of slip surface, and cross product vector as shown in Fig. 5-3.



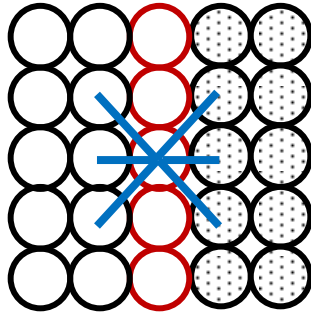
**Figure 5-3:** Schematic of cross product vector in local coordinate

The numerical analysis results of every particle in the local coordinate should be plotted in bond stress-strain relationship and transformed into the global coordinate, see Fig. 5-4.



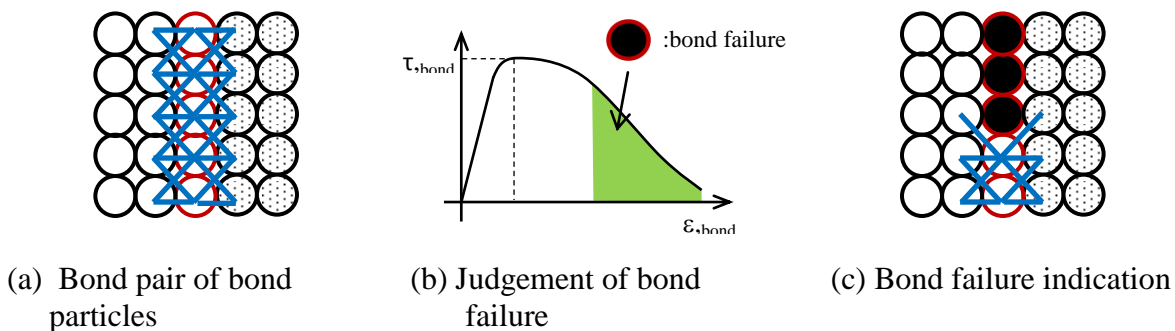
**Figure 5-4:** Transformation of bond stress and bond strain from local to global coordinate

To evaluate the bond condition, the particle approximation is treated as a continuum. In the SPH method, the neighbor particles are bound to the target particle (the bonding particle), see Fig. 5-5.



**Figure 5-5:** Particle pair of bonding particle

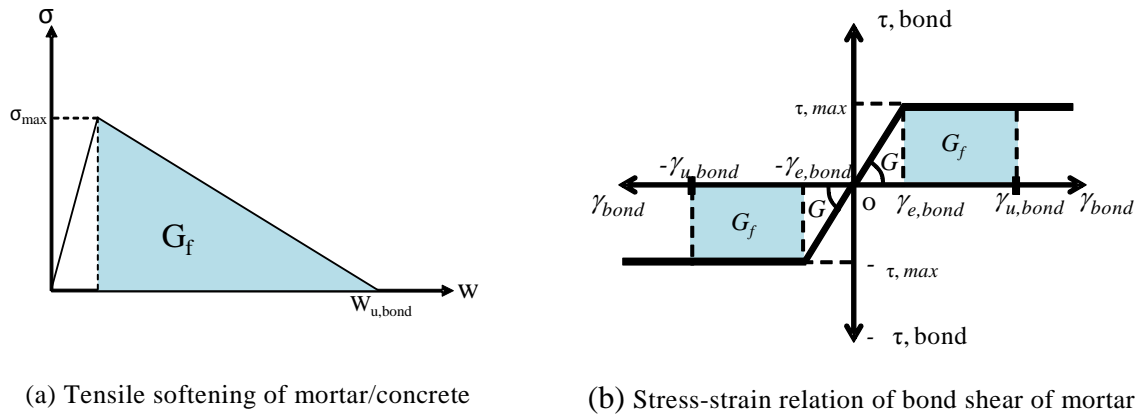
The modified bond stress-strain relationship as well as the condition bond of pair between bond particles and other particles around them can be illustrated, see Fig. 5-6(a). In order to define bond stress and bond strain, we transform the stress and strain tensor from global to local system (slip coordinate system) to verify the bond condition in slip surface direction. When the ultimate bond strain of particle is exceeded, which is in the green area in the Fig. 5-6(b), the bond failure is occurring which is indicated by vanishing the line of the bond particle pair as shown in Fig. 5-6(c). The judgement of bond failure considering the contact state is determined by taking into account the friction (Coulomb friction) with the coefficient of friction ( $\mu$ ) = 0.6 (Sonoda *et al.*, 1995).



**Figure 5-6:** Procedures of bond failure judgement

Pull-out loading transferred from anchor bolt to concrete generate a shear stress at the bonding shear zone. In this analysis, the fracture energy obtained by shear is assumed equal to the fracture energy of tension. Under the pull-out load on the anchor, the bonding shear may reach an ultimate stress and generate a bond failure. The failure of bond may occur when the ultimate bond strain is reached which is taken account of perfect elastic-plastic approach (see

Fig. 5-7(b)). On the other hand, the ultimate tensile strain is counted between the elastic zone having no crack and the completely cracked portion,  $w_{cr}$ . The fracture energy ( $G_f$ ) of tensile fracture is projected as the area below the curve correspond to the maximum elastic tensile strain ( $\sigma_{max}$ ) towards the completely cracked portion ( $w_{cr}$ ) (see Fig. 5-7(a)). Verification for safety of concrete under shear are considered in a fracture process zone. The fracture energy ( $G_f$ ) of shear is equal to the energy required to form a unit area of completely sliding crack and a loose bond. That is the area under the curve, which is a perfect-plastic shear curve expressing the relationship between the transferred stress and sliding crack (see Fig. 5-7(b)). Since the fracture energy obtained by tensile and shear is assumed equal, as a result the limit shear strain in a particle ( $\gamma_{u,bond}$ ) can be obtained.



**Figure 5-7:** Stress-strain relation of bond shear and bonding shear softening of mortar

For general application, refer to Ikki *et al.* (1996), the maximum shear strength of concrete is shown in Eq. 5.1. This equation was obtained by testing the embedded reinforce steel bar in concrete under static pull-out load. The maximum shear stress between concrete and reinforce steel bar ( $\tau_{max}$ ) may be calculated as,

$$\tau_{max} = 0.9 f'_c \frac{2}{3} \tag{5.1}$$

where,  $f'_c$  is the compressive strength of concrete (MPa). While the shear modulus ( $G$ ) can be found by the following equation.

$$G = \frac{E}{2(1+\nu)} \quad 5.2$$

where,  $E$  is Young's elastic modulus of concrete (MPa), and  $\nu$  is poisson's ratio of concrete. Based on elasticity principles, the elastic strain ( $\gamma_e$ ) is as follows,

$$\gamma_e = \frac{\tau_{\max}}{G} \quad 5.3$$

The total of the fracture energy ( $G_f$ ) of shear is assumed equal to the tensile fracture (as described in Eq. A.31, Appendix 2), so the ultimate bond strain ( $\gamma_{u,bond}$ ) can be computed as,

$$G_f = \frac{1}{2} \sigma_{\max} w_{u,bond} \text{ (for tensile)} \quad \leftrightarrow \quad G_f = \tau_{\max} (\gamma_{u,bond} - \gamma_e) \text{ (for shear)} \quad 5.4$$

Finally, the bond ultimate strain of concrete is;

$$\gamma_{u,bond} = \frac{G_f}{\tau_{\max} \times d^\phi} + \gamma_e \quad 5.5$$

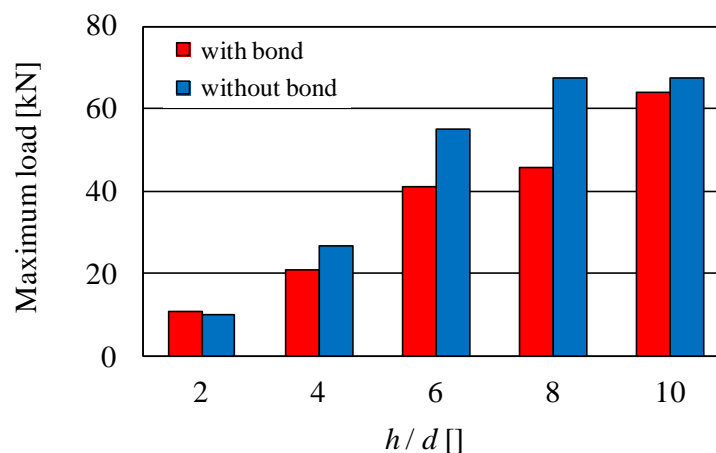
where,  $d^\phi$  is the diameter particle model of concrete (mm). The detail calculation of the bond ultimate strain of concrete for numerical model will be explained in Sub-chapter A-5, Appendix 2.

### 5.3 Comparison between the analysis model with and without considering bonding character

#### 5.3.1 Load carrying capacity

The loading capacity and the failure mode of anchor bolt structures will be investigated in this chapter. Five various anchor depths will be observed as examined in Chapter IV. The variation of embedment depth with  $h/d = 2, 4, 6, 8, 10$  are used in this simulation.

Figure 5-8 shows the maximum loading capacity of various anchor bolt depths. The figures illustrate that for model without bond character, the loading capacity increases rapidly in accordance to increasing the ratio of anchor depth between 2 to 6 and followed by a small increase in the ratio 6 to 8, then finally a relatively constant load is notified between the ratio 8 and 10. The rapid increase of loading capacity indicates that the failure mode may be the cone failure. On the other hand, the bolt failure may be gained when the constant loading capacity of structures is detected. These analyses have been explained in detail in Chapter IV. By applying the bond character, a significant change in the performance of loading capacity is reported. Almost all of the ratio of anchor depths have smaller loading capacity compared to the model without considering the bond character, except the ratio equal to 2. However, a relatively linear increasing of loading capacity is achieved by implementing bond character in accordance with the increasing of ratio depth to diameter of the anchor bolt. This linear increasing of loading capacity indicates that all models may have an identical failure mode.

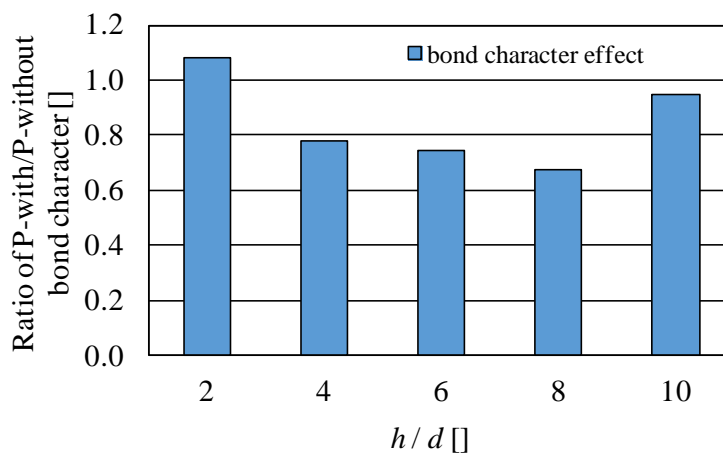


**Figure 5-8:** Maximum loading capacity of various anchor bolt depths



Effect of applied bond character for the model can be examined by the ratio of loading capacity with bond character to without bond character as shown in Fig. 5-9. In general the loading capacity with considering bond character should have a lower loading capacity than without considering the bond character, so that the ratio of loading capacity should be less than or equal to 1.0. It is due the bond character is applied to get a possibility bond failure on the model. However, a strange result is gained on the ratio of anchor depth equal to 2 which is the ratio of loading capacity higher than 1. This condition occur may due to the shock effect of reflection load, because of the applied load is the dynamic pull-out load and the size of model is a small model and very shallow anchor depth. For further analysis of the effect of bond character, the ratio of anchor depth equal to 2 will be ignored.

Figure 5-9 demonstrates that the ratio of loading capacity decreases in accordance with the increasing ratio of anchor depth until  $h/d$  equal to 8. It indicates that the bond character may have a significant effect on developing the combination of the failure mode, which may be constructed between bond and cone failure. Moreover, the depth of bond failure may increase in accordance with the increasing ratio of anchor depth. However, the ratio of loading capacity returns to a high value even nearly to 1.0 for the ratio of anchor depth equal to 10. It means that for the deeper anchor the bond character will not affect to the loading capacity and it also may not affect to the development of bolt failure.



**Figure 5-9:** Ratio of loading capacity between with and without considering bond character

### 5.3.2 Failure mode

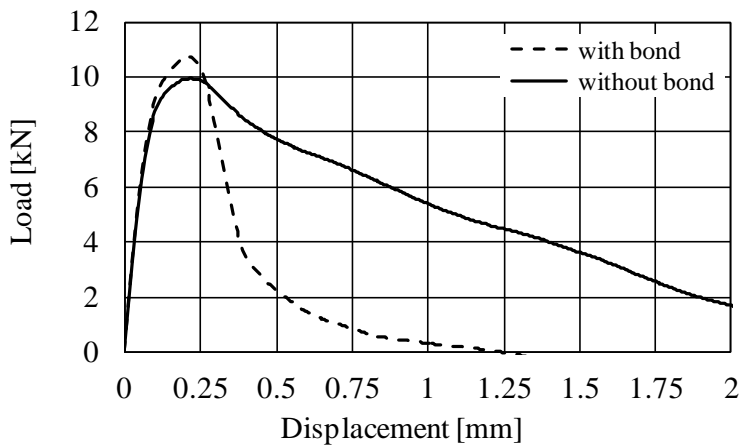
Figures 5-10, 5-13, 5-16, 5-19, and 5-22 show the relation of load-displacement of various anchor bolt depths. In this analysis result, the behavior of anchor structures under low dynamic in constant velocity pull-out load is calculated by time integration scheme. Hence, oscillation of reaction force is recorded. However, a filter by implementing the average frequency is applied to make easier on identifying the trend of the graph.

Figures 5-11, 5-12, 5-14, 5-15, 5-17, 5-18, 5-20, 5-21, 5-23, and 5-24 show the failure mode of various anchor bolt depths. These figures also display the distributions of a maximum principle strain of concrete, the equivalent plastic strain of anchor bolt, and the bond of pair between bond particles and other particles. These figures represent the investigation in two conditions, that is with and without bond character at the displacement of each maximum loading capacity. Figures in the red color boxes (□) represent the result with bond character, whereas the figures in the blue color boxes (□) represent the result without bond character. Each figure consists of three rows, the top row represents the distributions of a maximum principle strain of concrete, the middle row corresponds to the equivalent plastic strain of anchor bolt, and the bottom row represents the bond of pair between bond particles and bolt particles. The cut-off procedures for concrete material is still adopted from the models in Chapter IV, which is concrete particles in black color represent cut-off treatment due to the tensile failure of concrete. The white color of anchor bolt indicates the particle of bolt already in a failure condition. And vanishing of the line in bond pair particles indicates the bond failure occur.

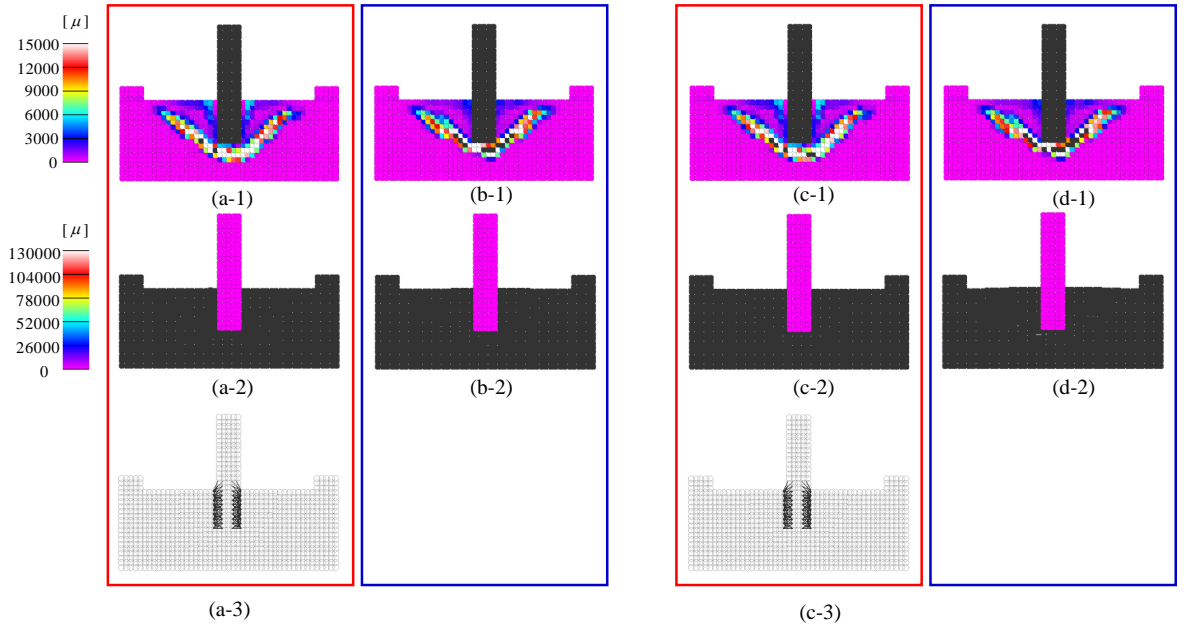
Considering the Fig. 5-10 ~ 5-15, it can be seen the results of the shallow depth of anchor that are  $h/d = 2$  and 4. Both of these models have a similar trend which is in the relation load-displacement, a linearly decreasing on the loading capacity is found in the model without bond character. However, a difference performance is shown after applying the bond character in the model. In the model  $h/d=2$ , the displacement of the maximum loading capacity is relatively constant around 0.21 mm (see Fig. 5-10 and 5-11). On the other hand, a significant decreasing on the displacement of the maximum loading capacity in the model

$h/d=4$ , that is 0.305 mm for model without bond character to be 0.16 mm after applying bond character (see Fig. 5-13 and 5-14).

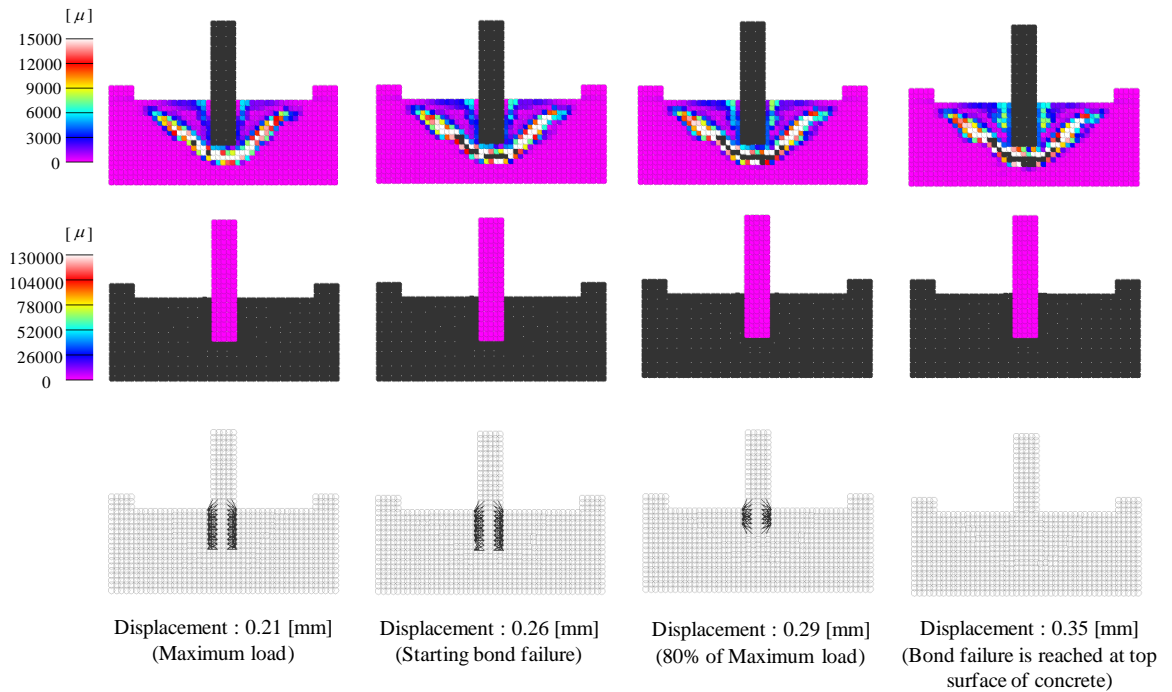
Analysis of the failure mode shows an obvious result that by applying the bond character, a bond failure is gained in the both models. In addition, a smaller displacement on the bond failure is found in the deeper of anchor (see Fig. 5-12 and 5-15). Finally, by combining the result between with and without bond character we can predict the real failure of anchors. A fully cone failure or bond failure may be found in the model  $h/d=2$ , on the other hand, based on bond character effect a combination failure between the bond and cone failure may be gained on the model  $h/d=4$ .



**Figure 5-10:** Load-displacement of Model  $h/d = 2$



**Figure 5-11:** Displacement on the maximum load of Model  $h/d = 2$



**Figure 5-12:** Failure mode analysis considering bond character for Model  $h/d = 2$

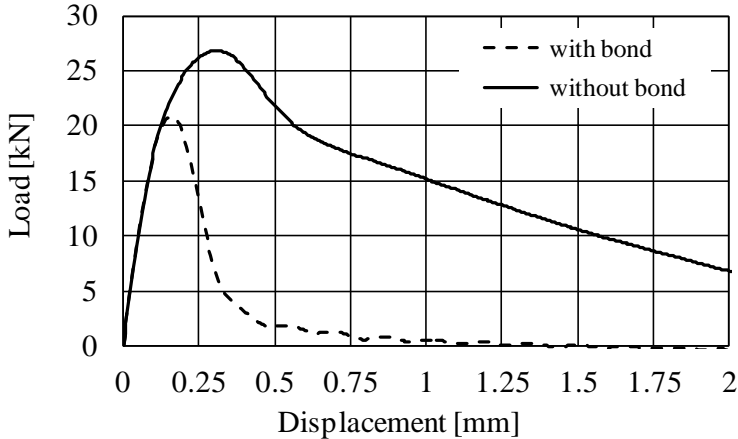
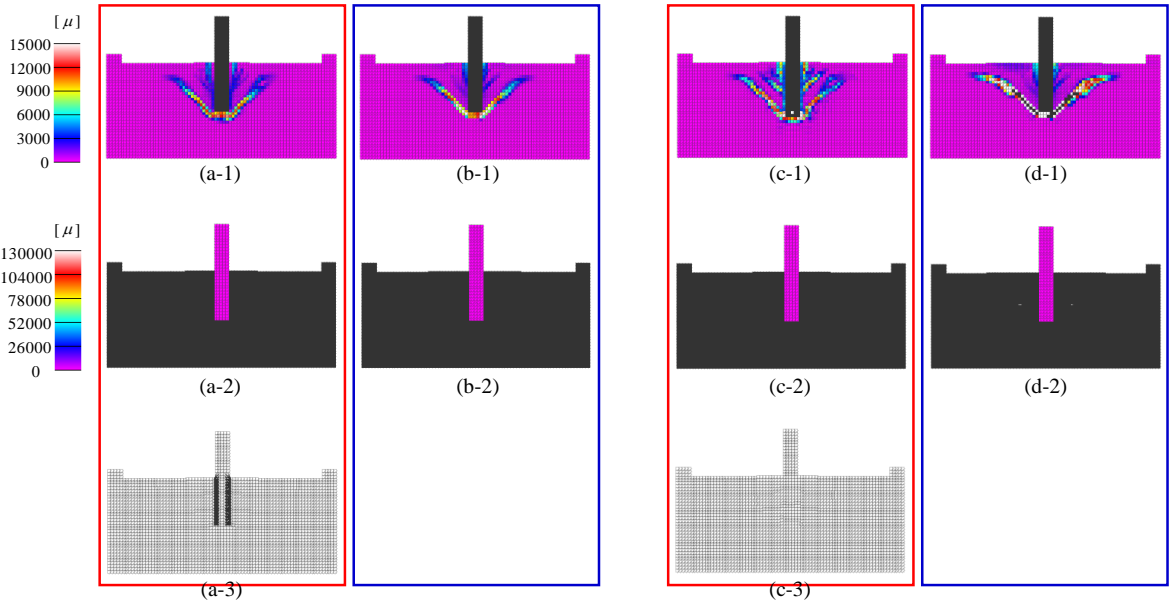
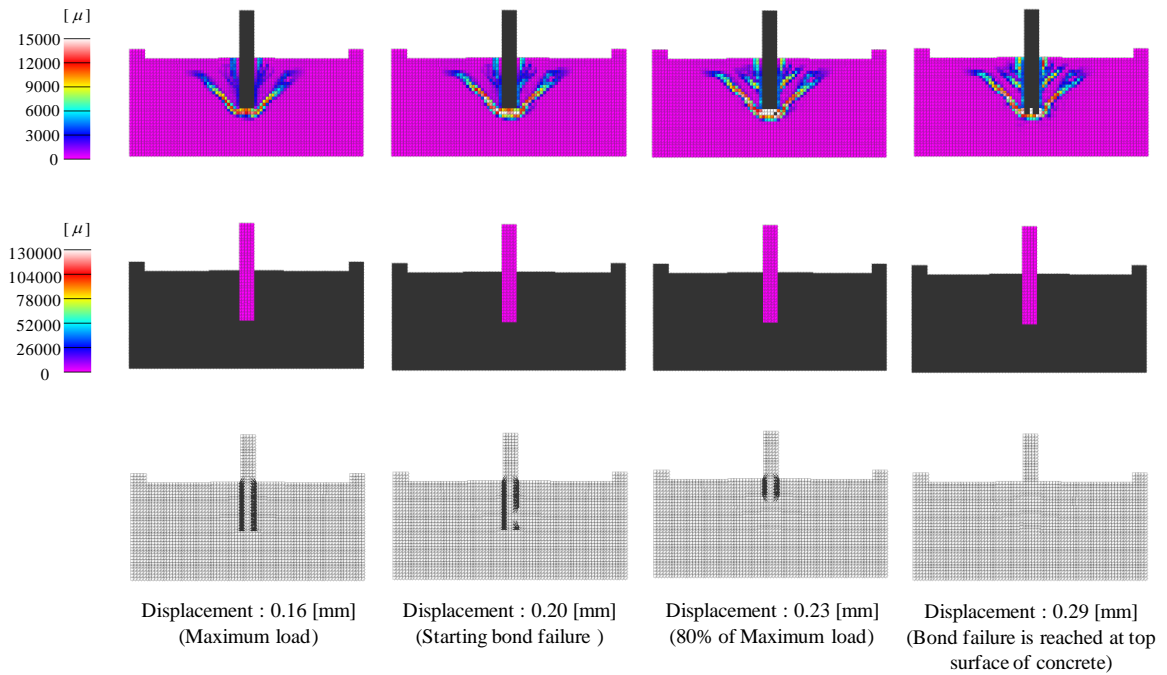


Figure 5-13: Load-displacement of Model  $h/d = 4$



(a) Displacement: 0.16 mm (maximum load of with bond character)      (b) Displacement: 0.305 mm (maximum load of without bond character)

Figure 5-14: Displacement on the maximum load of Model  $h/d = 4$



**Figure 5-15:** Failure mode analysis considering bond character for Model  $h/d = 4$

Figures 5-16 ~ 5-18 show the results of the anchor depth  $h/d = 6$ . A fluctuated loading capacity is found in the model without considering the bond character. While the premature failure in small displacement and low loading capacity is found by applying the bond character to the model. The displacement of the maximum load reduces from 0.37 mm to be 0.17 mm for without and with bond character respectively (see Fig. 5-16 and 5-17). A significant declining on the maximum loading capacity is also found from 54.94 kN to be 40.88 kN after applying the bond character.

An evident result is presented with an analysis of the failure mode. For the model without bond character, even though the final failure mode is bolt failure, however the maximum loading capacity is gained before developing the bolt failure (see Fig. 5-16 and Fig. 5-17). In contrast, a bond failure is obtained by applying the bond character in the model (see Fig. 5-18). Finally, by combining the result between with and without bond character we can estimate the real failure of anchors. Considering the maximum load of model without bond character, which is found in smaller displacement than of bolt failure displacement, and also bond character effect, a combination failure between the bond and cone failure may be gained on the model  $h/d = 6$ .

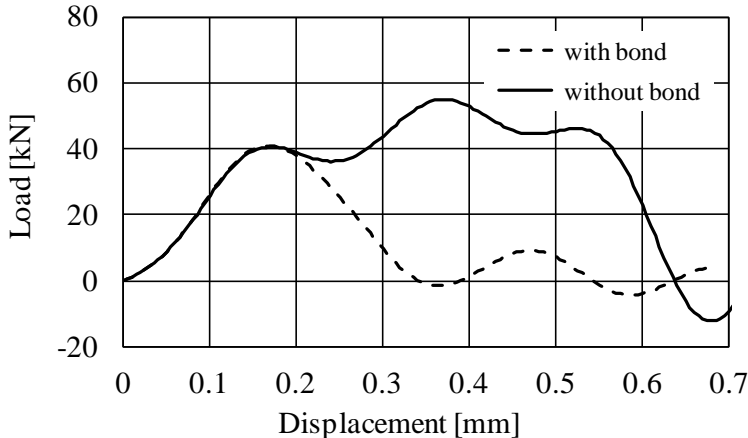
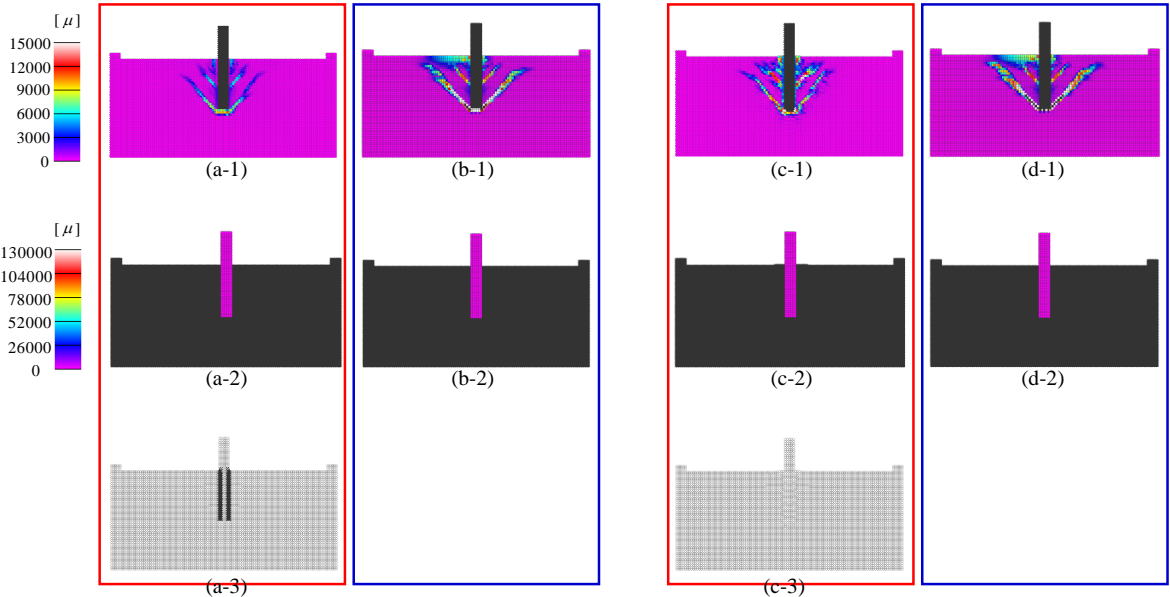
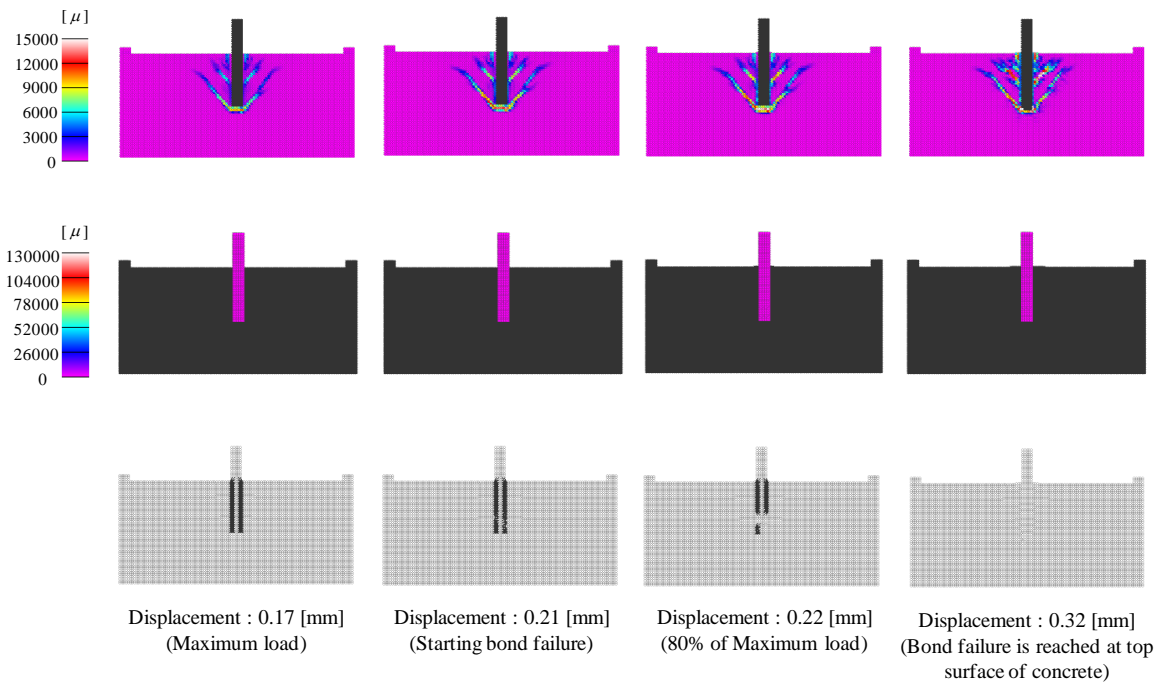


Figure 5-16: Load-displacement of Model h/d = 6



(a) Displacement: 0.17 mm (maximum load of with bond character) (b) Displacement: 0.37 mm (maximum load of without bond character)

Figure 5-17: Displacement on the maximum load of Model h/d = 6



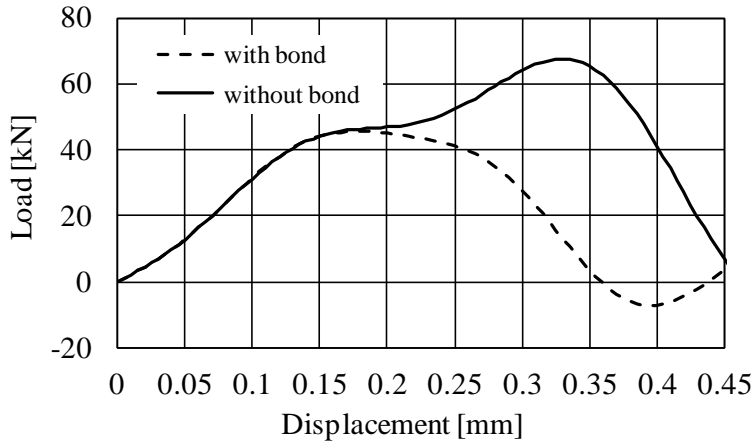
**Figure 5-18:** Failure mode analysis considering bond character for Model  $h/d = 6$

Considering the Fig. 5-19 ~ 5-24, it can be seen that the results of the various depths of anchor that are  $h/d = 8$  and 10. Both of these models have a similar trend which is in the relation load-displacement, a suddenly decreasing on the loading capacity is found in the both models with and without bond character. A lower loading capacity and displacement on this loading is exhibited after applying the bond character in the model. In the model  $h/d=8$ , there is a significant decreasing in displacement of the maximum loading capacity from 0.33 mm to 0.175 mm for without and with bond character respectively (see Fig. 5-19 and 5-20). On the other hand, even though having a similar maximum load, however the differences of the displacement are significantly high in the model  $h/d=10$ , that is 0.35 mm for model without bond character to be 0.20 mm for applying bond character (see Fig. 5-22 and 5-23).

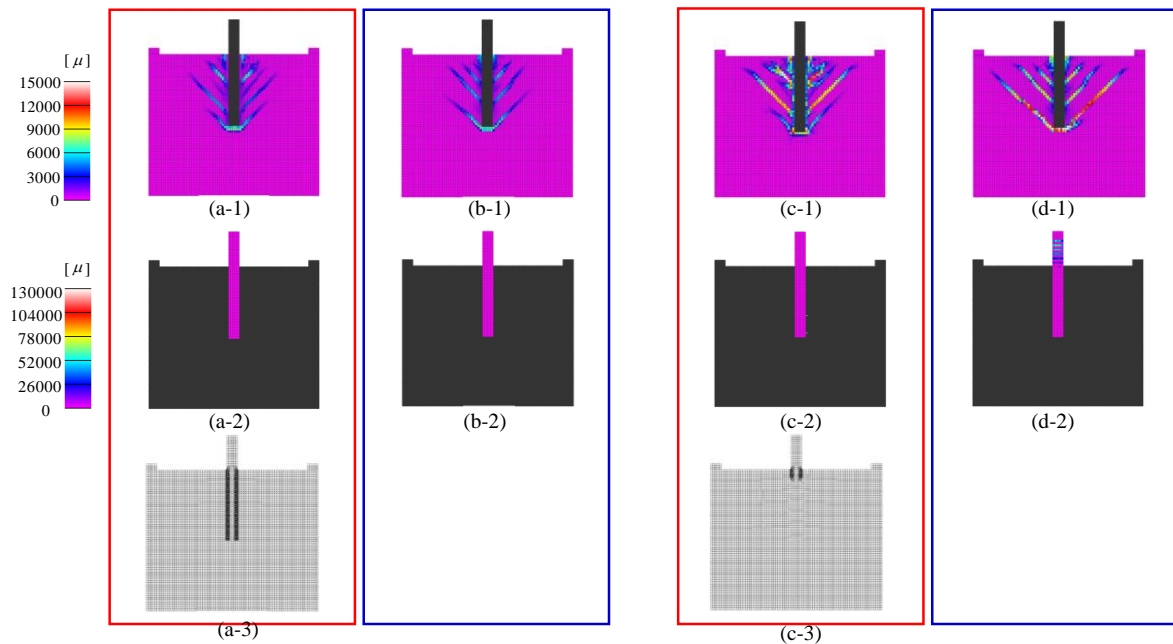
By applying the bond character, an undoubted result is exhibited on analysis of the failure mode, that is gained the bond failure in the both models (see Fig. 5-21 and 5-24). Finally, by combining the result between with and without bond character the real failure of anchors can be predicted. A combination failure between the bond and cone failure may be gained on the model  $h/d=8$ . However, a fully bolt failure or combination between the bond and cone failure may be found on the model  $h/d=10$ , due to the bond character effect is nearly



1.0, the load-displacement pattern is almost coincident between with and without bond character, and the bolt particles show the changing color toward bolt failure (see Fig. 5-22 and 5-24).

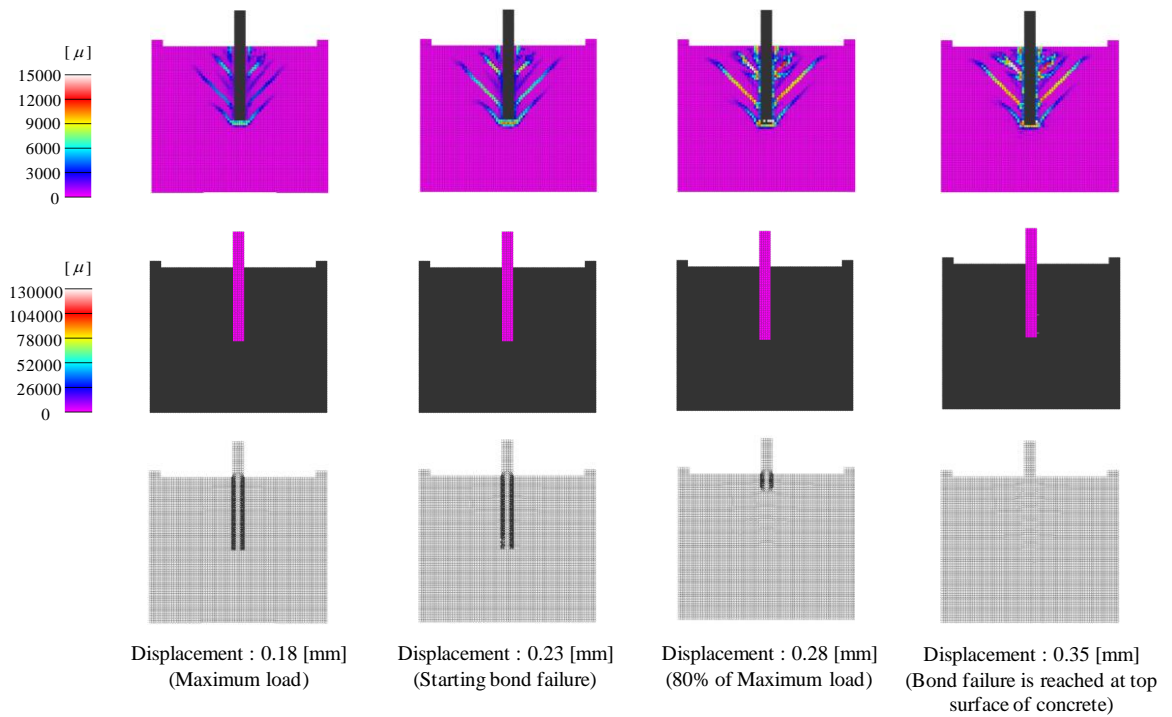


**Figure 5-19:** Load-displacement of Model  $h/d = 8$

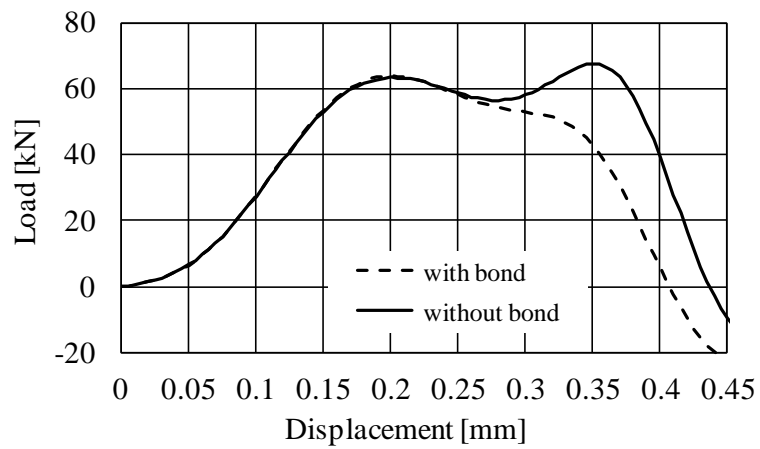


(a) Displacement: 0.175 mm (maximum load of with bond character)      (b) Displacement: 0.33 mm (maximum load of without bond character)

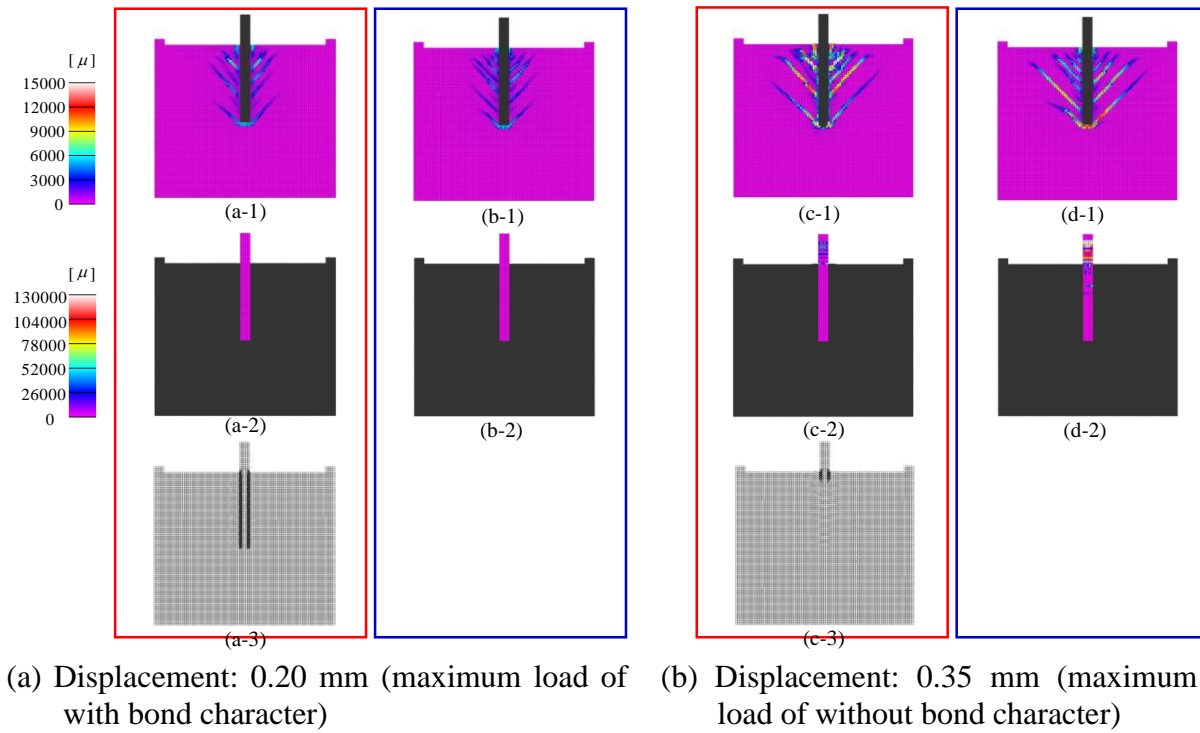
**Figure 5-20:** Displacement on the maximum load of Model  $h/d = 8$



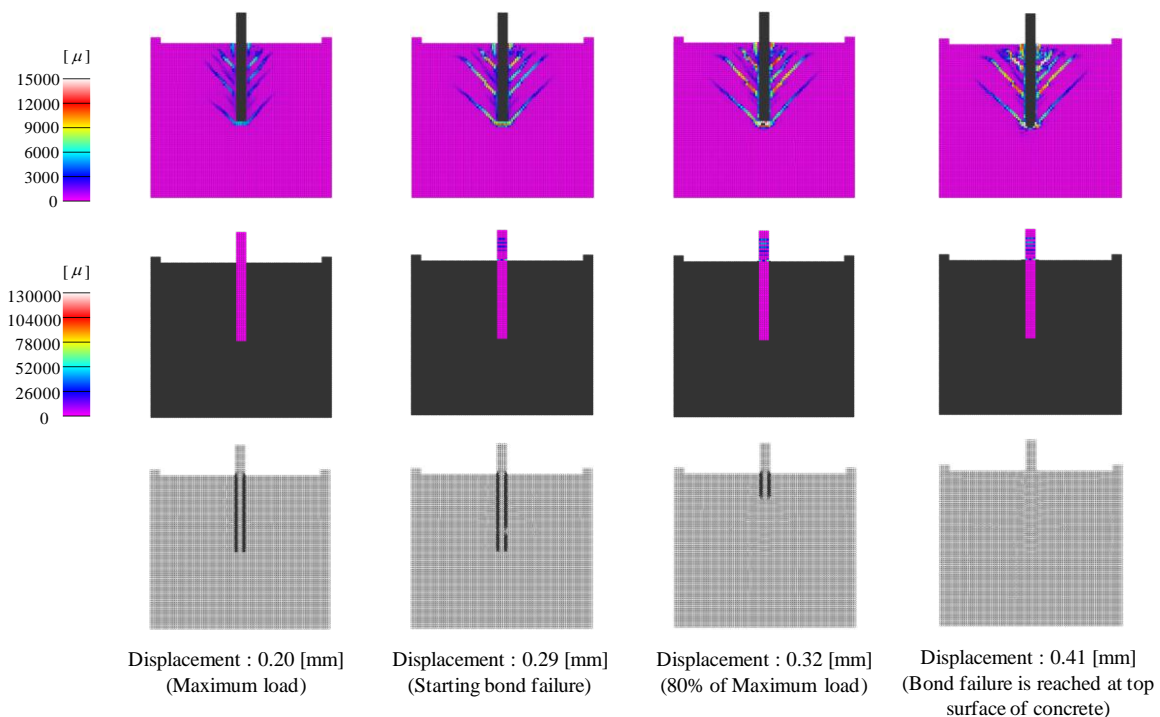
**Figure 5-21:** Failure mode analysis considering bond character for Model  $h/d = 8$



**Figure 5-22:** Load-displacement of Model  $h/d = 10$

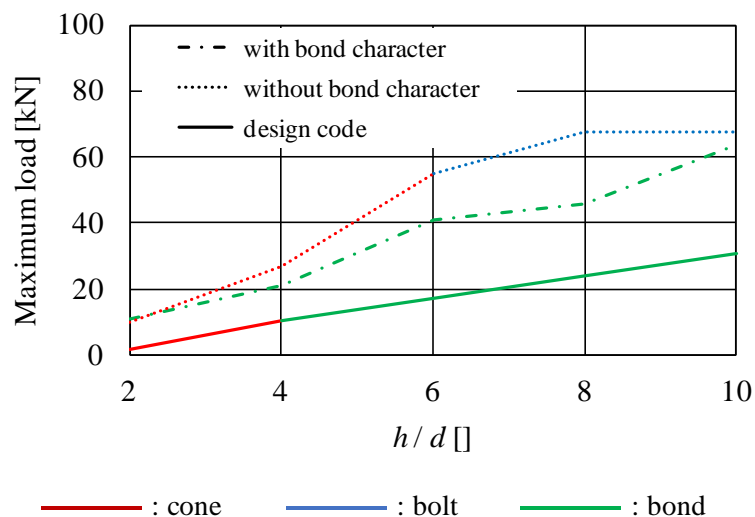


**Figure 5-23:** Displacement on the maximum load of Model  $h/d = 10$



**Figure 5-24:** Failure mode analysis considering bond character for Model  $h/d = 10$

Figures 5-10 ~ 5-21 (for  $h/d \leq 8$ ) indicate that the bolt particles does not generate a plastic deformation, therefore, equivalent plastic strain of the bolt is not observed. From these results, cone failure or bond failure of concrete may develop and need to further investigate. In contrary, since the bolt particles generate a plastic deformation in the model  $h/d=10$ , therefore the bolt failure may occur in this model and need further investigation (see Fig 5-23 and 5-24). Considering all these figures, only Fig. 5-11 and 5-12 (for  $h/d=2$ ) that represent the cut-off procedure which is indicated by the black color on concrete particles. However, this cut-off condition does not reach the surface of concrete. It means that the cone failure may not occur in model  $h/d=2$ . Let us consider the bond pair particles on each figure. The bond failure is recognized in all models with  $h/d = 2 \sim 10$  which is shown by Fig. 5-10 ~ 5-24, even though the Fig. 5-24 indicates the development of bolt failure.



**Figure 5-25:** Maximum loading capacity considering to various of the anchor depths

Figure 5-25 shows the summary of the maximum load capacity considering to various of the anchor depths. The graph depicts the numerical analysis without considering bond character has a higher loading capacity than others in all depths of anchor, following by the numerical analysis with bond character and design standard code. In this term, only the Japanese design standard code is considered (JSCE, 2010; Fujikake *et al.*, 2003). Regarding the failure mode, the bond failure mode is gained for all of anchor depths with the numerical analysis considering the bond character. In the contrary, the changing of failure mode is found

in the numerical analysis without considering the bond character, that is a change from cone failure to be bolt failure when the depth of anchor more than 6. A similar tendency is also notified in the design standard results, that is a change from cone failure to be bond failure.

#### 5.4 Conclusion

The bond character of numerical model was proposed in Chapter V, since a combination failure between bond failure and cone failure is generally found in anchor structures. In order to solve the phenomenon, a modified constitutive model was constructed and applied to simulate the effects of the bonding zone on developing cracks around the contact surface between anchor bolt and concrete. All models analyzed in Chapter IV were re-investigated by applying the bond character. Then, the numerical analysis results between without and with considering bond character were compared and reviewed. The result shows that by applying the bond character model, the loading capacity of all anchor bolt structure models reduced. Furthermore, the effect of applying bond character to the failure mode, the bond failure mode was gained on all models, and only bolt particles of  $h/d=10$  sample generated a plastic deformation. By integrating the failure mode between with and without bond character, a combination failure between the bond and cone failure might be gained on all models, even a fully bolt failure also might be occur in the model  $h/d=10$ . By comparing among numerical model with bond character, without bond character, and design standard, the failure mode of some models had been changed. The model with  $h/d \leq 4$  calculated by design standard and with  $h/d \leq 6$  of numerical analysis without considering bond character showed cone failure, however the failure of this model was changed to be bond failure after applying bond character model. The model with  $h/d > 6$  and without considering bond character exhibited the bolt failure mode, whereas the design standard with  $h/d > 4$  showed the bond failure. On the other hand, the bond failure was gained for the numerical analysis by considering the bond character in all models.

## 5.5 References

- Fujikake, K. et. al.: Chemically bonded anchors subjected to rapid pullout loading, *ACI Materials Journal*, Vol. 100, No. 3, pp. 246-252 (2003).
- Ikki, N., Kiyomiya, O., and Yamada, M.: Experimental study on the effects of numerous factors on bond-slip relationship, *Proceedings of JSCE*, Vol. 33, No. 550, pp. 73-83 (1996).
- JSCE: Standard specifications for concrete structures-2007, Design, JSCE Guidelines for Concrete No. 15, *Japan Society of Civil Engineers (JSCE)* (2010).
- Sonoda, K., Kitoh, H., and Nakajima, K.: An experimental study on the bond characteristics of embossed steel plates, *The 3rd Symposium on Research and Application of Hybrid and Composite Structures*, (in Japanese), November (1995).



## CHAPTER VI

### NUMERICAL-EXPERIMENTAL COMPARISON

#### 6.1 Introduction

In order to verify the numerical analysis results, we need to compare the numerical analysis and the experimental results. The detail procedures and results of the experimental program have been explained in Chapter II. Thus, this chapter more focus on numerical analyzing on the earlier chapter, then comparing and verifying the analysis results to the experimental result at the end of the chapter.

The simulation of failure mechanism of anchor bolt under pull-out is more complex than generally a tensile failure of beam because it is affected by properties of concrete and bond performance. According to the design standards (ACI 318, 2011; and JSCE, 2010), the bond character between concrete and steel anchor bolt is still not considered. Commonly the bond failure is considered only as a standalone failure without combining to the cone failure. Consequently, the pull-out strength of anchor bolt may be overestimated and it may cause an early failure as well as reducing the safety of structures. Even though many researchers have studied the anchor bolt structures by either numerical analysis or experimental test, however, they did not clearly evaluate the bond character phenomena. Whereas, the combination failure between bond and cone failure commonly occurs in the real application of anchor bolt structures.

The aim of this chapter is to simulate the tensile failure under pull-out load on anchor bolt structures with and without considering the bond character. By considering the bond character between concrete material and anchor bolt in the numerical analysis, then verifying



the analysis result to the experimental results, a real-like failure mechanism could be found and finally a reliable numerical analysis can be gained. This chapter also presents the derivation of the proposed constitutive model of shear bond failure to demonstrate the shear stress of concrete material at the interface zone. It is assumed that all stress components have an elastic shear limit, and the failure of bond may occur when the ultimate bond strain is reached which is taken account of perfect elastic-plastic approach, and concrete completely lose its shear strength. In this analysis, the fracture energy obtained by shear is assumed equal to the fracture energy of tension. The issue in the numerical analysis of shear bond failure and its solutions will be discussed later. The effectiveness of considered bond character in the proposed numerical scheme will be studied by simulating numerically the experimental model. There are three experimental results that will be compared to the numerical analysis results, that is loading capacity, displacement, and failure mode.

## **6.2 Bonding mechanism**

In this research, we investigate the numerical model of the anchor bolt structure using two assumptions, namely perfect bonding and bond character considered between mortar concrete and anchor bolts. The correlation between mortar concrete and steel anchor surface on the perfect bonding model is assumed that without a slip or shear failure at the interface area between anchor and mortar concrete. The possibility failure is taken into account by considering the ultimate strain of steel or concrete. Hence, the probability failure of the anchor bolt structure is cone failure or anchor bolt failure only.

Bonding shear between concrete and steel anchor is unavoidable phenomena in the anchor structure mainly due to pull-out load on the anchor. The transfer of load at the steel anchor/mortar bond interfaces is shown in Fig. 6-1. The bond shear between concrete and anchor is directly applied on the cast-in-place anchor. The pull-out load is transferred from the threaded rod into the mortar concrete. Some researchers have studied on bonding behavior of anchor. Cook et al. (1998) compared the worldwide database of behavioral models of single

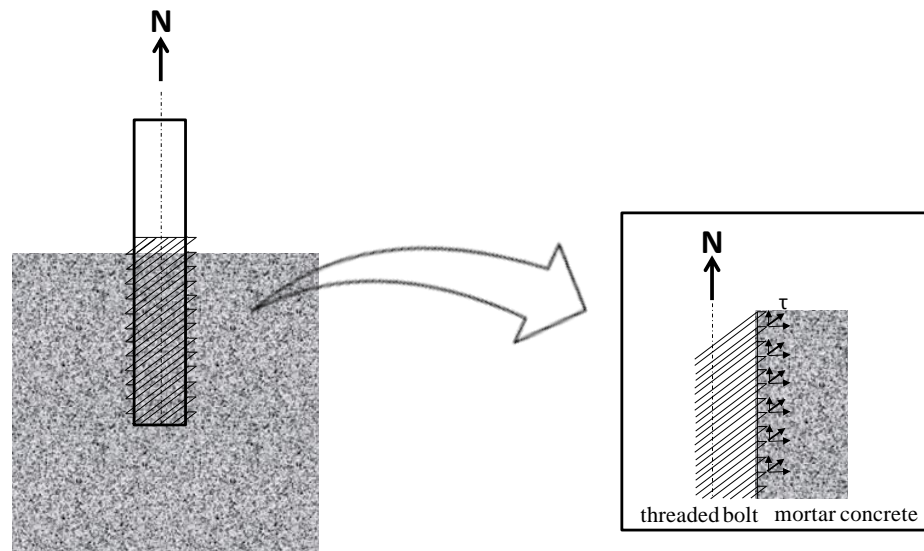
anchors. The result indicates that their failure load might be approached by a uniform bond stress model. The uniform bond stress model ( $N_\tau$ ) for cast-in-place anchor is:

$$N_\tau = \tau \pi d_a h_{ef} \quad 6.1$$

The uniform bond stress is valid for  $4 \leq h_{ef}/d_a \leq 20$  and  $d_a \leq 50$  mm with the bond area  $\pi d_a h_{ef} \leq 58,000$  mm<sup>2</sup>.

Investigation of Eligehausen *et al.* (2006), however, indicated that the actual bond stress distributing along the embedment length at peak load is nonlinear with higher bond stresses at the embedded end of the anchor and the lower bond stresses in the concrete surface. The shear stress distribution of bonding area is calculated as below.

$$\tau_{\max} = \frac{4.7 f_c^{0.5} h_{ef}^{0.5}}{d_a} \quad 6.2$$



**Figure 6-1:** Mechanism of load transfer of anchor bolt

The above equation (Eq. 6.2) was based on bonded anchor research and taken account of the effective depth of anchor bolt ( $h_{ef}$ ) and diameter of anchor ( $d_a$ ). However, for general application, refer to Ikki *et al.* (1996) the maximum shear strength of mortar concrete is shown in Eq. 5.1 in Chapter V. Then the limit shear strain in a particle ( $\gamma_{u,bond}$ )

based on the fracture energy has been explained in Eq. 5.1 to Eq. 5.5 in Chapter V. The example of calculating the tensile ultimate strain and the bond ultimate strain of mortar for the experimental model is explained in Appendix 2, in Sub-chapter A-4 and Sub-chapter A-6 respectively.

### **6.3 Numerical analysis of experimental model**

The model as same size and properties as the experimental sample performed in this study can be seen in Fig. 6-2. A model series consisted of a concrete block in which a straight threaded anchor bolt with a diameter size 16 mm bar were installed with an embedment depth 3.5 times to the diameter anchor bolt size, that is 56 mm. The compressive and tensile strength of mortar used in this model is 48.18 MPa and 3.31 MPa, respectively which corresponds to the experimental test result. The constant velocity rate of pull-out load applied to the top of anchor bolt particles is 0.05 m/s. The diameter size of each particle (mortar concrete and anchor bolt) is 4 mm in this model. Regarding the boundary condition of analytical models, the vertical displacement restraint is applied on the four sides of the top surface as displayed in Fig. 6-2. The pull-out loading capacity is calculated as the total load on these four sides. In addition, to calculate an accurate loading capacity, a similar method of dummy particles which is shown in Figure 3-21 (in Chapter III) are also applied to the lateral sides of the anchor bolt. The bonding condition between anchor bolt and concrete is assumed as both the perfect bond condition and the bond character considered. Figure 6-3 shows a schematic of the stress-strain curve of concrete and steel material based on experimental results as explained in Chapter II.

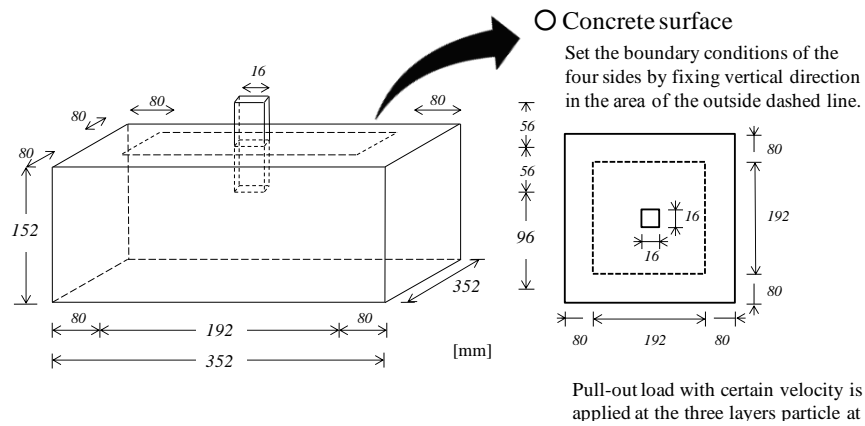


Figure 6-2: Model of the anchor bolt structure

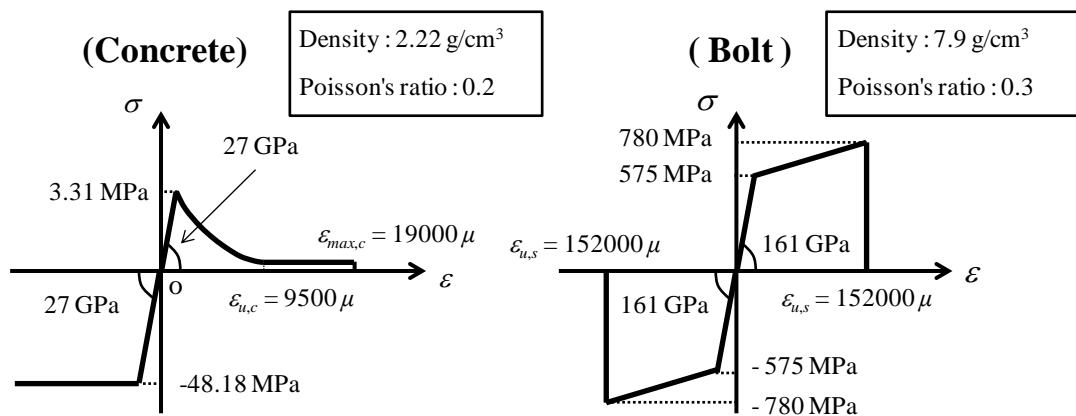


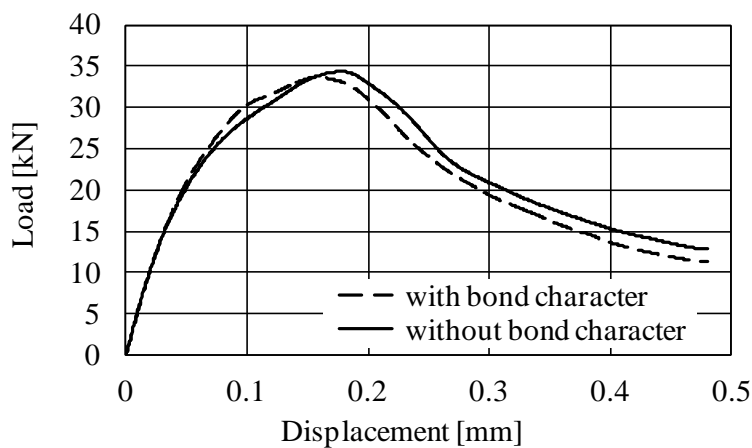
Figure 6-3: Stress-strain relation of mortar and steel anchor.

### 6.3.1 Numerical analysis of experimental model with and without considering the bond character

#### 6.3.1.1 Loading capacity and displacement

The loading capacity and displacement analyzed is for both perfect bonding model (without bond character) and bond character considered model (with bond character). Figure 6-4 depicts a correlation between loading capacity and displacement of anchor bolt with and without bond character model. It shows that the loading capacity of model without bond

character is slightly higher than model with bond character and even they are almost same, they are about 34.34 kN to 33.61 kN respectively. Furthermore, this condition is also found on the displacement of the maximum loading capacity, an insignificant longer displacement is obtained on the model without bond character which is 0.1775 mm. It is longer than the model with bond character which is only 0.156 mm. Even though having lower maximum strength and also shorter its displacement, however, it can be noted that the model with bond character has a slightly higher on its stiffness.

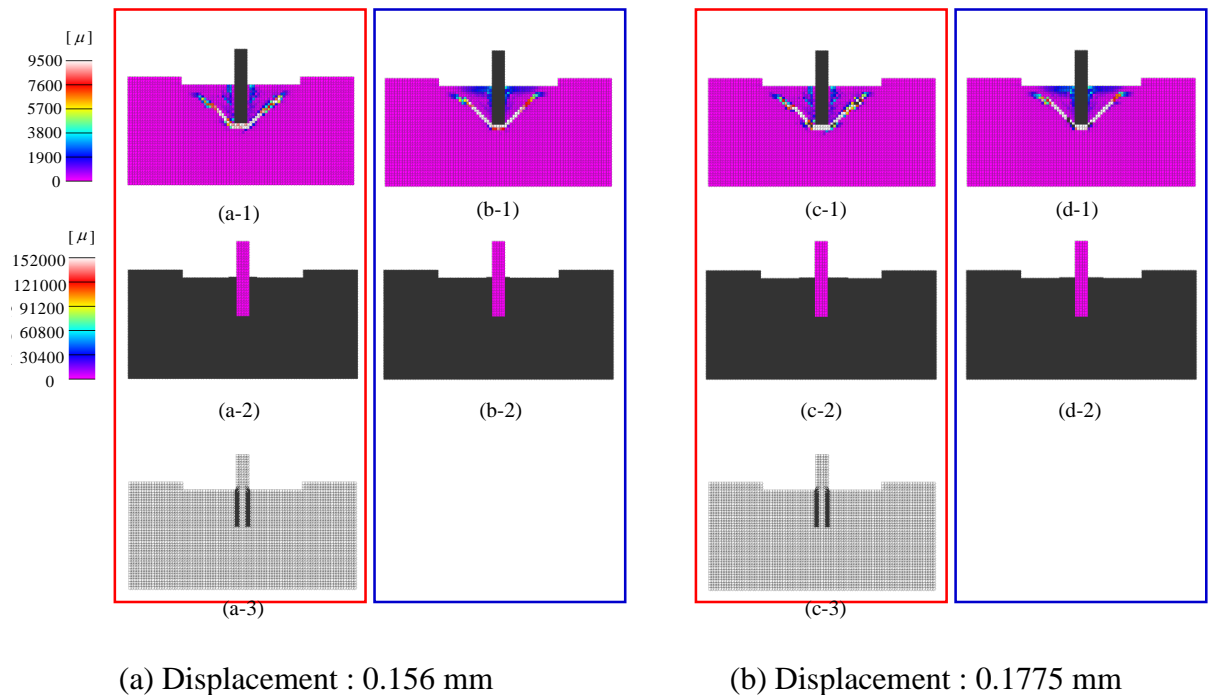


**Figure 6-4:** Load-displacement of the experimental model anchor bolt under pull-out load

### 6.3.1.2 Failure mode of anchor bolt structure

Figure 6.5 interprets the distributions of a maximum principle strain of concrete, the equivalent plastic strain of anchor bolt, and bond condition of the particle pair between concrete and anchor bolt particle. Figures in the red color boxes (□) represent the result with bond character, whereas the figures in the blue color boxes (□) represent the result without bond character. The plot analysis model was conducted by the model with the size of model structure and material properties equivalent to the experimental test. In this figure, we investigate the result in two conditions, with and without bond character at the maximum displacement of each maximum loading capacity. The equivalent plastic strain of anchor bolt figures (Fig. 6-5 (X-2)) indicate that the bolt does not generate a plastic deformation,

therefore, equivalent plastic strain of the bolt is not further observed. Moreover, the bond condition between bond pair, the figures (Fig. 6-5 (X-3)) demonstrate that no bond failure occur on the maximum loading capacity. Eventhough the cut-off procedure does not show in the figures (Fig. 6-5 (X-1)), however it can be presumed that cone failure is the most probable failure mode in both with and without bond character model.



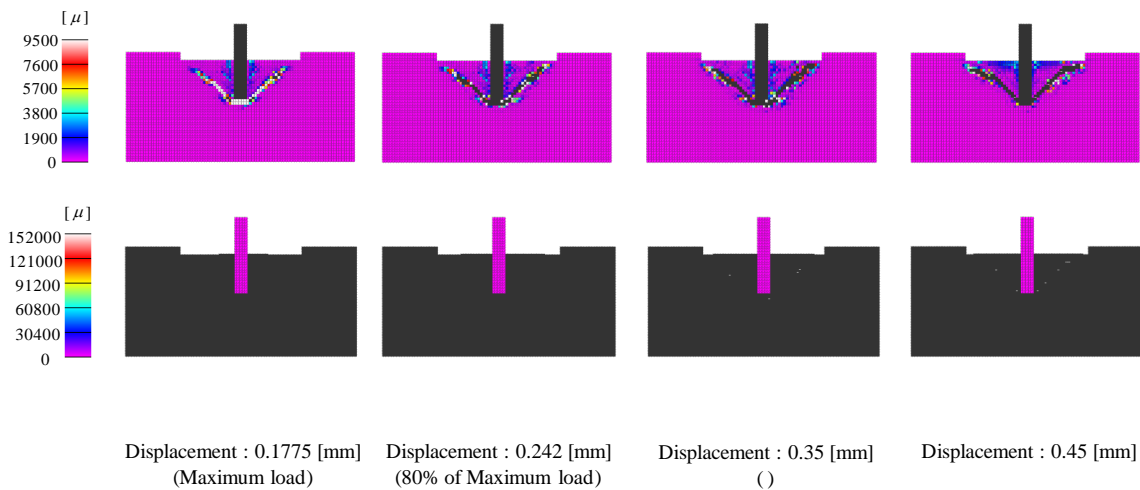
**Figure 6-5:** Displacement on the maximum load of the experimental model

Note :

- |                      |  |
|----------------------|--|
| Figure (a-) and (c-) | : with bond character model  |
| Figure (b-) and (d-) | : without bond character model   |
| Figure (a-) and (b-) | : at the maximum displacement of with bond character model (0.156 mm)      |
| Figure (c-) and (d-) | : at the maximum displacement of without bond character model (0.1775mm)   |
| Figure (-1)          | : maximum principal strain distribution of concrete                        |
| Figure (-2)          | : equivalent plastic strain distribution of anchor bolt                    |
| Figure (-3)          | : bond of particle pair between concrete particle and anchor bolt particle |

Analysis of the failure mode of the sample without bond character can be seen in Fig. 6-6. The bottom figures of Fig. 6-6 obviously reveal that the anchor bolt particle is still in elastic condition since the color of these particles remain in purple color as the lowest indicator of strain. And, when the top figures of Fig. 6-6 are deeply considered, the fracture of concrete propagate from the bottom of anchor bolt and develop a cone form of fracture. Then

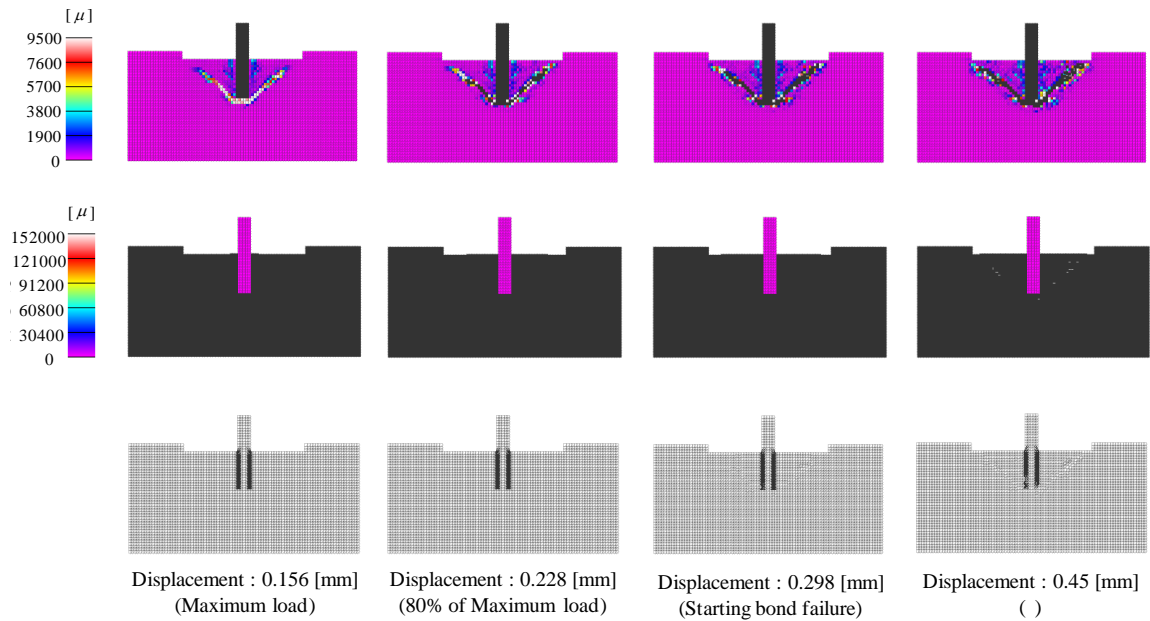
finally it reached nearly the concrete surface at the time of maximum strength. When the cone failure is approximately generated, loading capacity reaches to the maximum pull-out resistance, and followed by a gradual decline. The decreasing of pull-out load is due to the development of tensile failure of concrete particles. It can be concluded that only the cone failure of concrete occurs in the model without considering the bond character. However, the complete separation of the concrete blocks have not been finally expressed. In the figures, concrete particles in black color represent cut-off treatment due to the tensile failure of concrete. It is presumed that cone failure is the most probable failure mode.



**Figure 6-6:** Failure mode analysis without considering bond character for the experimental model

By applying the bond character between anchor bolt and concrete to the model, a similar failure mode result is gained. Analysis of the failure mode of the sample with bond character is shown in Fig. 6-7. This figure definitely shows that the anchor bolt particle is still in elastic condition. The figure also indicates that the bolt does not generate a plastic deformation, therefore, equivalent plastic strain of the bolt will not be further observed. A simultaneous failure between cone failure and bond failure was found, it indicates a possibility of distributing the load. Furthermore, cracking on concrete particle is developed, and the cut-off particles of the cone fracture surface are released, and the cracking of concrete reach the top surface of concrete. In addition, based on the load-displacement graph (Fig. 6-4),

it can be clearly notified that the loading capacity gradually decrease after the maximum load, it indicates that the cone failure occurs by this model.



**Figure 6-7:** Failure mode analysis considering bond character for the experimental model

By considering deeply on the bottom figures of Fig. 6-7, it is undoubtedly that the vanishing process of bond on the particle pair in the concrete interface area (the bond between bonding particles and other particles) are found. However, the starting bond failure arises after the maximum displacement, and until the end of considered analysis only a few bond pairs vanished. Considerable the bond failure process is recognized during the maximum principal strain growth of concrete. So, this case can be recognized as the cone failure mode. This failure mode is evidenced by the bottom figures of Fig. 6-7 that the bond failure does not reach the top surface of concrete by the end of considered analysis. Finally, it can be recognized that there is no significant effect by applying the bond character, and even the cone failure mode is obtained which is similar to the without bond character model.

Comparison of experimental model between with and without considering the bond character, the failure mode shows an obvious result that by applying the bond character a similar failure mode, that is cone failure, is gained. Based on bond character effect, a combination failure between the bond and cone failure may be gained on the experimental



model when the depth anchor is varied or the numerical model is modified, so it will correspond to the laboratory experimental result.

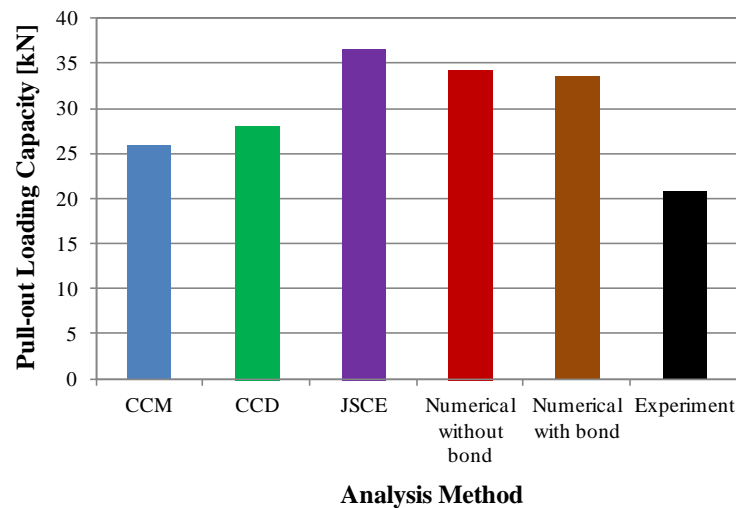
### **6.3.2 Comparison between experimental results and numerical model**

A high pull-out loading capacity is one of the most expected on the anchor bolt structure. However, due to a complexity of factors affecting the capacity, some approached methods still need to be evaluated to find a reliable design, either by experimental program or numerical method. Here is a comparison of pull-out loading capacity between the experimental results, numerical model, and design standard. The result of each approached method has been discussed in the previous chapter.

The typical load-displacement graphs for all experiment samples and numerical results indicate that the maximum loading of the numerical analysis, both with and without considering bond character are higher than experimental results and design standard, except the JSCE standard which is having the highest loading capacity. Even though their loading capacities are higher than others, that is around 30 to 35 kN for experimental model with and without bond character respectively, however the differences of displacement show a significant gap which is only 0.15 to 0.18 mm for the numerical analysis and in contrary around 2 to 2.5 mm for the experimental results. This disparity probably due to the relaxation of the top support plate of the experimental sample, since it is difficult to make the sample in a flat condition during experimental test, consequently we used the wedges and put the wedge under the top support plate to solve the problem. As a result, the displacement of the experimental result cannot be used and directly compared to the numerical analysis result.

The comparison of maximum loading capacity between the design standard, numerical analysis and experimental results is plotted in Fig. 6-8. Three well known design standard method will be considered as a comparison, namely CCM method (Eligehausen *et al.*, 2006), CCD method (Fuch *et al.*, 1995; ACI 318, 2011) and Japanese method (JSCE, 2010; Fujikake *et al.*, 2003). The graph clearly shows that the experiment results have the lowest strength than others. The numerical analysis shows that the closest result in the design standard is the

JSCE method. On the other hand, the JSCE method has the highest strength than other design standard. The loading capacity of the experimental result is around a half of JSCE design standard and the numerical analysis. The CCM and CCD design standard is the closest to the experimental result.



**Figure 6-8:** The comparison of pull-out loading capacity between experimental, numerical and design standard

Considering deeply to the numerical analysis results in Fig. 6-8, it is clearly shown that by applying the bond character the pull-out loading capacity reduces 2% from 34.34 kN to 33.61 kN. And if we compare between the numerical analysis result with bond character and the experimental result, the loading capacity of numerical result is higher around a half (61%) than the experimental result, that is 33.61 kN and 20.87 kN respectively. In this research, the loading capacity of JSCE and CCD method is 75% and 34% higher than the experimental result that is 36.60 kN, 28.03 kN and 20.87 kN respectively. Based on this comparison, it can be concluded that when the numerical analysis will be applied to the design and analysis of structure, a certain correction/safety factor should be used to get a reliable numerical method in analyzing the anchor bolt structures and to get a safe structure. The numerical analysis also needs a correction factor when it is compared to the CCD method which is adopted by ACI 318 and might be adopted also by other design standard, to get a reliable strength.

## 6.4 Conclusion

This chapter presents a comparison between the numerical results, design standard, and experimental results. Constitutive model applied in the numerical model consisted of the von Mises for steel anchor bolt and Drucker Prager for concrete. The size and material properties of model were fully adopted from the experimental tests in Chapter II. The numerical model, in this chapter, was divided by the model with and without considering the bond character. In addition, the perfect elastic-plastic for bonding characteristic was applied with the calculation of the limit ultimate strain of shear by considering the fracture energy which is equal to the fracture energy of tensile softening. By applying the bond character, the change condition was found in the bonding properties of the particle pair in the concrete interface area. The vanishing process of bond on the particle pair in the concrete interface area (the bond between bonding particles and other particles) were found. However, the starting bond failure arose after the maximum loading capacity, and until the end of considered analysis only a few bond pairs vanished. Moreover, the concrete particle in the cracking path reached an ultimate strain and cut-off procedure was applied (it was confirmed by black color in concrete particles). So, this case can be recognized as the cone failure mode. This failure mode was evidenced by the figures that the bond failure does not reach the top surface of concrete by the end of considered analysis.

The numerical analysis results were compared to the experimental results and the design standard equation to verify the accuracy of results. Comparison of the numerical analysis results between with and without considering bond character shown that by applying the bond character the pull-out loading capacity reduced 2%. On the other hand, the numerical analysis result with bond character showed higher around a half (61%) of loading capacity than the experimental result. In general, it can be concluded that the certain correction factor should be used when the numerical analysis will be applied to the design and analysis of anchor bolt structures. Moreover, the numerical analysis also needs a correction factor when it is compared to the CCD method, which is adopted by ACI 318 and might be adopted also by other design standard, to get a reliable strength. Finally, the proposed numerical method may

reliable to use for design and analysis the anchor bolt structures, and the correction factor should be used to get the safe structures.

## 6.5 References

- ACI Committee 318, Building code requirements for structural concrete (ACI 318-11) and commentary (318M-11), *American Concrete Institute* (2011).
- Cook, R.A., Kunz, J., Fuchs, W., and Konz, R.C.: Behavior and design of single adhesive anchors under tensile load in uncracked concrete, *ACI Structural Journal*, Vol. 95, No. 1, pp. 9-26 (1998).
- Eligehausen, R., Cook, R. A., and Appl, J.: Behavior and design of adhesive bonded anchors, *ACI Structural Journal*, Vol. 103, No. 6, pp. 822-831 (2006).
- Eligehausen, R., Mallee, R., and Silva, J. F.: Anchorage in Concrete Construction, First edition, *Ernst & Sohn*, Berlin (2006).
- Fuchs, W., Eligehausen, R., and Breen, J. E.: Concrete Capacity Design (CCD) approach for fastening to concrete, *ACI Structural Journal*, Vol. 92, No. 1, pp. 73-94 (1995).
- Fujikake, K. et. al.: Chemically bonded anchors subjected to rapid pullout loading, *ACI Materials Journal*, Vol. 100, No. 3, pp. 246-252 (2003).
- Ikki, N., Kiyomiya, O., and Yamada, M.: Experimental study on the effects of numerous factors on bond-slip relationship, *Proceedings of JSCE*, Vol. 33, No. 550, pp. 73-83 (1996).
- JSCE: Standard specifications for concrete structures-2007, Design, JSCE Guidelines for Concrete No. 15, *Japan Society of Civil Engineers (JSCE)* (2010).



## CHAPTER VII

### CONCLUSIONS AND RECOMMENDATIONS FOR FUTURE RESEARCH

#### 7.1 Conclusions

A certain conclusion of each chapter has been described precisely in the appropriate chapter. However, to give an overview of all conclusions, the following paragraphs will briefly illustrate the phase of this study as well as the individual achievement for every chapter.

In Chapter I, the main objective and scope of the study were declared. A literature review of the design formulas to predict the ultimate pull-out capacity of anchors was provided. After that, the assumed problems in the design and analysis of anchor bolt structures in the design standards were presented. Then, following by a concise review of mesh-free methods and explanations of the essence of SPH formulations.

The experimental part of this study was described in Chapters II. The shallow depth of anchors and the normal strength of mortar was conducted to investigate the failure mechanisms of the anchors. A series of anchor mortar blocks were cast and static load was applied to all samples. The failure mode, loading capacity, and concrete cone stress of the anchor bolt structure were presented and discussed. Finally, a comparison between the experimental results and design standard has been presented. The experimental results show that: 1) The experiment resulted the combination failure mode, cone failure and bond failure, of anchor bolt under pull-out loading test. Furthermore, the degree of cone slope ( $\alpha$ ) for the inner side area and outside area is significantly lower than the design standard assumed, that is around  $15^\circ \sim 23^\circ$  for experiment compare to  $35^\circ \sim 45^\circ$  for design standard. 2) The cone

stress of the experimental result is extremely lower than the design standard, this is either in inner side area or outside area. It is even less than half of the standard, either CCM and CCD or JSCE standard. This phenomena were predicted due to the cracking of samples of the experimental result spread widely with a lower cone slope and resulted wider cone area than the design standard. It was also should be noted that the stress of experimental result less than half of the standard, either CCM and CCD or JSCE standard. The average of cone stress is 0.94, 1.45, 3.04 and 3.33 MPa for the outside area, inner side area of experimental results, JSCE, and CCM and CCD standard, respectively. 3) The loading capacity of experimental result is significantly lower than the design standard, even almost a half of JSCE standard. It may due to in the standard design the crack pattern is assumed a single crack and the cracks propagate from end of the anchor to the concrete surface. Moreover, in the design standard it is absolutely assumed that the failure mode is cone failure only without considering bond failure. While, the experimental result clearly shows that the failure is a combination between cone failure and bond failure, so that the cone failure part is a shallow depth and the angle of cone slope is smaller than design standard.

In Chapter III, the numerical calculation setting and a solution of the particle deficiency problem around the boundary area in the SPH method was presented. A basic formulation and calculation procedure of SPH were expressed. Constitutive model consists of von Mises and Drucker-Prager were also described in this chapter. Dummy particles apply to solve the boundary problem on the anchor bolt since it is a slender rod and only a few particles constructed on its cross section, so it may generate inaccurate result and difficult to justify the failure mode of the anchor bolt. The result shows that the distribution of the dummy particles around the boundary area is very useful to solve mechanical problems under the free surface condition.

In Chapter IV, the numerical calculation setting and several examples of the analysis on the strength of anchor bolt under pull-out load were precisely explained. The effect of anchor bolt depths were investigated by the proposed numerical method. By adopting the VM model for anchor bolt and DP model for concrete and applying cut-off procedure, the ultimate pull-out strength and failure mechanism can be evaluated. The change of load-displacement

behavior, failure mode and maximum pull-out strength due to the embedment depth can be expressed by using the proposed SPH analysis and it adequately describes the large deformation and failures of concrete structure with the anchor bolt. However, bonding failure between bolt and concrete was not considered in this analysis. By ignoring the effect of bond character, the numerical analysis may give a higher pull-out strength and it is preferable to consider the possibility of bond failure in the next step.

The bond character of numerical model was proposed in Chapter V, since a combination failure between bond failure and cone failure is generally found in anchor structures. In order to solve the phenomenon, a modified constitutive model was constructed and applied to simulate the effects of the bonding zone on developing cracks around the contact surface between anchor bolt and concrete. All models analyzed in Chapter IV were re-investigated by applying the bond character. Then, the numerical analysis results between without and with considering bond character were compared and reviewed. The result shows that by applying the bond character model, the loading capacity of all anchor bolt structure models reduced. Furthermore, the effect of applying bond character to the failure mode, the bond failure mode was gained on all models, and only bolt particles of  $h/d=10$  sample generated a plastic deformation. By integrating the failure mode between with and without bond character, a combination failure between the bond and cone failure might be gained on all models, even a fully bolt failure also might be occur in the model  $h/d=10$ . By comparing among numerical model with bond character, without bond character, and design standard, the failure mode of some models had been changed. The model with  $h/d \leq 4$  calculated by design standard and with  $h/d \leq 6$  of numerical analysis without considering bond character showed cone failure, however the failure of this model changed to be bond failure after applying bond character model. The model with  $h/d > 6$  and without considering bond character exhibited the bolt failure mode, whereas the design standard with  $h/d > 4$  showed the bond failure. On the other hand, the bond failure was gained for the numerical analysis by considering the bond character in all models.

In Chapter VI, a comparison between the numerical results, standard design, and experimental results were presented. Constitutive model applied in the numerical model



consisted of the von Mises for steel anchor bolt and Drucker Prager for concrete. The size and material properties of model were fully adopted from the experimental program in Chapter II. The numerical model, in this chapter, was divided by the model with and without considering the bond character. In addition, the perfect elastic-plastic for bonding characteristic was applied with the calculation of the limit ultimate strain by considering the fracture energy which is equal to the fracture energy of tensile softening. The result shows that by applying the bond character, the change condition was found in the bonding properties of the particle pair in the concrete interface area. On the other hand, there was no concrete particle that reaches an ultimate strain (no black color in concrete particles). It can be recognized that the bond failure mode was obtained. Comparison of the numerical analysis results between with and without bond character considered shown that by applying the bond character the pull-out loading capacity reduced 2%. On the other hand, the numerical analysis result with bond character showed a higher around a half (61%) of loading capacity than the experimental result. In general, it can be concluded that the certain correction factor should be used when the numerical analysis will be applied to the design and analysis of structure. Moreover, the numerical analysis also needs a correction factor when it is compared to the CCD method, which is adopted by ACI 318 and might be adopted also by other standard design, to get a reliable strength. Finally, the proposed numerical method may reliable to use for design and analysis the anchor bolt structures, and the correction factor should be used to get the safe structures.

## **7.2 Recommendations for future research**

In order to obtain more reasonable and realistic estimation of loading capacity and failure mode of anchor bolt in concrete under pull-out load, further study on SPH calculations and other numerical technique should be conducted numerously, especially when involving in the large deformation state. Considering on some limitations such as time constraints,

expensive cost in term of providing experimental tests, inadequate or difficulties on laboratory activities, some general recommendations are as follows;

- 1) Firstly, the experimental tests can be conducted on various anchor mortar blocks to validate further numerical simulation by respecting in a different way designed anchors. Some improvement in term of providing the appropriate loading support on frame or changing the testing method is necessary to avoid significant deviation on displacement.
- 2) When formulating the tensile and compressive softening technique for the concrete materials, the parameters such as the limit ultimate strain and cut-off procedure should be designated appropriately to enhance the failure mode estimation. Indeed, prior to perform the numerical method, the test data of materials should be able to support the development of constitutive material models.
- 3) An advanced modification of the bond character should be developed prior to achieve more realistic results of failure mode, and combination of failure mode can be gained in accordance to the experimental result.
- 4) Some discrepancies between numerical and experimental results such as displacement and failure mode can be improved by modifying the bond character model and yield criteria of the constitutive parameter model. However, improvement of yield criteria requires the increase of parameter identification.
- 5) Since the advantage of SPH methods is very suitable to simulate problems with large deformations, further studies can be applied in those fields such as anchor bolt in concrete under various dynamic loads by implementing the proposed model.



## APPENDIX 1 - Derivation of notation

Some notations are used to simplify the derivation of stress increments of elastic plastic constitutive equations as well as its derivation of constitutive matrix forms for each yield model. This appendix chapter presents some of the derivation of notation that used in the yield criterion derivation. Besides, solving of some equations is also presented.

### A-1 Notation used in the von Mises criterion derivation

Now, let consider the fourth-tensor of elastic stiffness in Eq. 2.49 (Chapter II) and multiply it to the deviatoric stress  $\sigma'_{kl}$  to form

$$D_{ijkl}^e \sigma'_{kl} = [\lambda(\delta_{ij} \delta_{kl}) + \mu(\delta_{ik} \delta_{jl} + \delta_{il} \delta_{jk})] \sigma'_{kl} \quad \text{A.1}$$

Substitute Eq. 2.42(b) (Chapter II) into Eq. A.1 to get

$$D_{ijkl}^e \sigma'_{kl} = [\lambda(\delta_{ij} \delta_{kl}) + \mu(\delta_{ik} \delta_{jl} + \delta_{il} \delta_{jk})] \left( \sigma_{kl} - \frac{1}{3} \sigma_{mm} \delta_{kl} \right) \quad \text{A.2}$$

Expand Eq. A.2

$$D_{ijkl}^e \sigma'_{kl} = \mu \sigma_{kl} (\delta_{ik} \delta_{jl} + \delta_{il} \delta_{jk}) - \frac{1}{3} \sigma_{mm} \delta_{kl} (\delta_{ik} \delta_{jl} + \delta_{il} \delta_{jk}) + \lambda \sigma_{kl} \delta_{ak} \delta_{al} \delta_{ij} - \frac{1}{3} \sigma_{mm} \delta_{kl} \delta_{ak} \delta_{al} \delta_{ij} \quad \text{A.3}$$

By noting that

$$\sigma_{kl}\delta_{ik}\delta_{jl} = \sigma_{ij}, \sigma_{ij} = \sigma_{ji}, \sigma_{kl}\delta_{kl} = \sigma_{kl}\delta_{ak}\delta_{al} \text{ and } \delta_{ij} \cdot \delta_{ij} = 3 \quad \text{A.4}$$

Solve Eq. A.3,

$$D_{ijkl}^e \sigma'_{kl} = \mu \sigma_{kl} (\delta_{ik}\delta_{jl} + \delta_{il}\delta_{jk}) - \frac{1}{3} \sigma_{mm} \delta_{kl} (\delta_{ik}\delta_{jl} + \delta_{il}\delta_{jk}) + \underbrace{\lambda \sigma_{kl} \delta_{ak} \delta_{al} \delta_{ij} - \frac{1}{3} \sigma_{mm} \delta_{kl} \delta_{ak} \delta_{al} \delta_{ij}}_0 \quad \text{A.5}$$

One can be written as

$$D_{ijkl}^e \sigma'_{kl} = \mu (\sigma_{ij} + \sigma_{ji}) - \frac{1}{3} \mu \sigma_{mm} (\delta_{ij} + \delta_{ji}) \quad \text{A.6}$$

Finally, solve Eq. A.6 by substituting the relationships of deviatoric stress in Eq. 2.42(b) (Chapter II), yield to

$$D_{ijkl}^e \sigma'_{kl} = 2\mu \sigma_{ij} - \frac{2}{3} \mu \sigma_{mm} \delta_{ij} = 2\mu \left( \sigma_{ij} - \frac{1}{3} \mu \sigma_{mm} \delta_{ij} \right) = 2\mu \sigma'_{ij} \quad \text{A.7}$$

In this study, the materials are considered to follow associated flow rules of plasticity. This means that the yield function,  $f$  can be assumed to be the same.

$$f(J_{2D}) = J_{2D} - k^2 = 0 \quad \text{A.8}$$

where

$$J_{2D} = \frac{1}{2} \sigma'_{ij} \sigma'_{ij} \quad \text{A.9}$$

and by substituting Eq. 2.52 (Chapter II) and Eq. A.9 into Eq. A.8, the function can be expressed

$$f = \frac{1}{2} \sigma'_{ij} \sigma'_{ij} - \frac{1}{3} \sigma_{eqs}^2 = 0 \quad \text{A.10}$$

Finally, we write the notation as below

$$\sigma'_{ij} \sigma'_{ij} = \frac{2}{3} \sigma_{eqs}^2 \quad \text{A.11}$$

By considering the normality rule as in Eq. 2.44, which is the plastic potential function is assumed to be the same with the function,  $f$ . We substitute Eq. A.8 and A.9 into the differentiation form as well as change the index notation; it can be written as below

$$\frac{\partial f}{\partial \sigma_{ij}} = \frac{\partial f(J_{2D})}{\partial \sigma_{ij}} = \frac{\partial f}{\partial \sigma_{ij}} \left( \frac{1}{2} \sigma'_{kl} \sigma'_{kl} - k^2 \right) \quad \text{A.12}$$

Differentiate Eq. A.12

$$\frac{\partial f}{\partial \sigma_{ij}} = \underbrace{\frac{\partial f}{\partial \sigma'_{mn}} \left( \frac{1}{2} \sigma'_{kl} \sigma'_{kl} - k^2 \right)}_{\text{LHS}} \underbrace{\left| \frac{\partial \sigma'_{mn}}{\partial \sigma_{ij}} \right|}_{\text{RHS}} \quad \text{A.13}$$

Firstly, solve the LHS of Eq. A.13

$$\frac{\partial f}{\partial \sigma'_{mn}} \left( \frac{1}{2} \sigma'_{kl} \sigma'_{kl} - k^2 \right) = 2 \cdot \frac{1}{2} \sigma'_{kl} \frac{\sigma'_{kl}}{\sigma'_{mn}} \quad \text{A.14}$$

where

$$\frac{\partial \sigma'_{kl}}{\partial \sigma'_{mn}} = \delta_{km} \delta_{ln} \quad \text{A.15}$$

Then, the differentiation of LHS can be written as

$$\frac{\partial f}{\partial \sigma'_{mn}} \left( \frac{1}{2} \sigma'_{kl} \sigma'_{kl} - k^2 \right) = \sigma'_{kl} \delta_{km} \delta_{ln} = \sigma'_{mn} \quad \text{A.16}$$

Now, solve the RHS of Eq. A.13 by substituting Eq. 2.42(b) and considering Eq. A.15 leads to

$$\frac{\partial \sigma'_{mn}}{\partial \sigma_{ij}} = \frac{\partial}{\partial \sigma_{ij}} \left( \sigma_{mn} - \frac{1}{3} \sigma_{rr} \delta_{mn} \right) = \left( \delta_{mi} \delta_{nj} - \frac{1}{3} \delta_{ri} \delta_{rj} \delta_{mn} \right) \quad \text{A.17}$$

By noting that

$$\sigma'_{ij} \delta_{ij} \delta_{jl} = \sigma_{ii} \quad \text{A.18}$$

Finally, combine the solution of LHS and RHS as in Eq. A.16 and A.17, respectively. Thus, the differentiation of Eq. A.13 can be expressed as

$$\frac{\partial f}{\partial \sigma_{ij}} = \sigma'_{mn} \left( \delta_{mi} \delta_{nj} - \frac{1}{3} \delta_{ri} \delta_{rj} \delta_{mn} \right) = \sigma_{ij} - \frac{1}{3} \sigma_{mm} \delta_{ij} = \sigma'_{ij} \quad \text{A.19}$$

## A-2 Notation used in the Drucker Prager criterion derivation

Noting that

$$\sigma_{ij} \sigma'_{ij} = \left( \sigma'_{ij} + \frac{\sigma_{mm}}{3} \delta_{ij} \right) \underbrace{\sigma'_{ij}}_0 \quad \text{A.20}$$

$$\sigma'_{ij} \sigma'_{ij} = 2 \frac{\sigma'_{ij} \sigma'_{ij}}{2} = 2J_{2D} \quad \text{A.21}$$

$$\sigma'_{ij} \cdot \delta_{ij} = \sigma_{ii} = 0, \delta_{ij} \cdot \delta_{ij} = 3 \quad \text{A.22}$$

Solve the following plastic multiplier for Drucker Prager,  $\lambda_{dp}$ ;

$$\lambda_{dp} = \frac{\left( \frac{\sigma'_{ij}}{2\sqrt{J_2}} + \alpha \delta_{ij} \right) (\lambda (\delta_{ij} \delta_{kl}) + \mu (\delta_{ik} \delta_{jl} + \delta_{il} \delta_{jk})) d\varepsilon_{kl}}{\left( \frac{\sigma'_{ab}}{2\sqrt{J_2}} + \alpha \delta_{ab} \right) (\lambda (\delta_{ab} \delta_{mn}) + \mu (\delta_{am} \delta_{bn} + \delta_{an} \delta_{bm})) \left( \frac{\sigma'_{mn}}{2\sqrt{J_2}} + \alpha \delta_{mn} \right) + \left[ 2\alpha^2 + \frac{2}{3} \right] \sigma_{eqs}(H) \left[ \alpha + \frac{1}{\sqrt{3}} \right]} \quad \text{A.23(a)}$$

By using the notation in Eq. A.22 and Eq. A.22, we can solve Eq. A.23(a) as;

$$\lambda_{dp} = \frac{\left( \frac{\mu\sigma_{ij}\delta_{ik}\delta_{jl}}{2\sqrt{J_2}} + \frac{\mu\sigma_{ij}\delta_{il}\delta_{jk}}{2\sqrt{J_2}} + \alpha\delta_{ij}\delta_{ij}\delta_{kl}\lambda + \alpha\delta_{ij}\delta_{ik}\delta_{jl}\mu + \alpha\delta_{ij}\delta_{il}\delta_{jk}\mu \right) d\varepsilon_{kl}}{\left( \frac{\mu\sigma_{ab}\delta_{an}\delta_{bn}}{2\sqrt{J_2}} + \frac{\mu\sigma_{ab}\delta_{an}\delta_{bm}}{2\sqrt{J_2}} + \alpha\delta_{ab}\delta_{ab}\delta_{mn}\lambda + \alpha\delta_{ab}\delta_{an}\delta_{bm}\mu + \alpha\delta_{ab}\delta_{an}\delta_{bm}\mu \right) \left( \frac{\sigma'_{mn}}{2\sqrt{J_2}} + \alpha\delta_{mn} \right) + \left[ 2\alpha^2 + \frac{2}{3} \right] \sigma_{eqs}(H) \left[ \alpha + \frac{1}{\sqrt{3}} \right]} \quad \text{A.23(b)}$$

$$\lambda_{dp} = \frac{\left( \frac{\mu\sigma'_{kl}}{2\sqrt{J_2}} + \frac{\mu\sigma'_{lk}}{2\sqrt{J_2}} + \alpha 3\delta_{kl}\lambda + \alpha\delta_{kl}\mu + \alpha\delta_{lk}\mu \right) d\varepsilon_{kl}}{\left( \frac{\mu\sigma'_{mn}}{2\sqrt{J_2}} + \frac{\mu\sigma'_{nm}}{2\sqrt{J_2}} + \alpha 3\delta_{mn}\lambda + \alpha\delta_{mn}\mu + \alpha\delta_{nm}\mu \right) \left( \frac{\sigma'_{mn}}{2\sqrt{J_2}} + \alpha\delta_{mn} \right) + \left[ 2\alpha^2 + \frac{2}{3} \right] \sigma_{eqs}(H) \left[ \alpha + \frac{1}{\sqrt{3}} \right]} \quad \text{A.23(c)}$$

$$\lambda_{dp} = \frac{\left( \frac{2\mu\sigma'_{kl}}{2\sqrt{J_2}} + \alpha(3\lambda + 2\mu)\delta_{kl} \right) d\varepsilon_{kl}}{\left( \frac{2\mu\sigma'_{mn}}{2\sqrt{J_2}} + \alpha(3\lambda + 2\mu)\delta_{mn} \right) \left( \frac{\sigma'_{mn}}{2\sqrt{J_2}} + \alpha\delta_{mn} \right) + \left[ 2\alpha^2 + \frac{2}{3} \right] \sigma_{eqs}(H) \left[ \alpha + \frac{1}{\sqrt{3}} \right]} \quad \text{A.23(d)}$$

$$\lambda_{dp} = \frac{\left( \frac{2\mu\sigma'_{kl}}{2\sqrt{J_2}} + \alpha(3\lambda + 2\mu)\delta_{kl} \right) d\varepsilon_{kl}}{\left( \frac{\mu\sigma'_{mn}\sigma'_{mn}}{2\sqrt{J_2}\sqrt{J_2}} + \alpha(3\lambda + 2\mu)\delta_{mn}\alpha\delta_{mn} \right) + \left[ 2\alpha^2 + \frac{2}{3} \right] \sigma_{eqs}(H) \left[ \alpha + \frac{1}{\sqrt{3}} \right]} \quad \text{A.23(e)}$$

$$\lambda_{dp} = \frac{\left( \frac{2\mu\sigma'_{kl}}{2\sqrt{J_2}} + \alpha(3\lambda + 2\mu)\delta_{kl} \right) d\varepsilon_{kl}}{\left( \frac{\mu 2J_2}{2J_2} + \alpha^2(3\lambda + 2\mu)3 \right) + \left[ 2\alpha^2 + \frac{2}{3} \right] \sigma_{eqs}(H) \left[ \alpha + \frac{1}{\sqrt{3}} \right]} \quad \text{A.23(f)}$$

and finally it is solved as,

$$\lambda_{dp} = \left[ \frac{\frac{\mu\sigma'_{kl}}{\sqrt{J_2}} + \alpha(3\lambda + 2\mu)\delta_{kl}}{3\alpha^2(3\lambda + 2\mu) + \mu + \left[ 2\alpha^2 + \frac{2}{3} \right] \sigma_{eqs}(H) \left[ \alpha + \frac{1}{\sqrt{3}} \right]} \right] d\varepsilon_{kl} \quad \text{A.24}$$



The general incremental stress relationship ( $d\sigma_{ij}$ ) is solved as follows,

$$d\sigma_{ij} = D_{ijkl}^e (d\varepsilon_{kl} - d\varepsilon_{kl}^p) = D_{ijkl}^e d\varepsilon_{kl} - \underbrace{D_{ijkl}^e \lambda_{dp} \frac{\partial f_{DP}}{\partial \sigma_{ij}}}_{[D]^p} \quad \text{A.25}$$

Substitute the derivation form in Eq. 2.59 into Eq. A.25,

$$d\sigma_{ij} = D_{ijkl}^e d\varepsilon_{kl} - \underbrace{D_{ijkl}^e \lambda_{dp} \left( \frac{\sigma'_{ij}}{2\sqrt{J_2}} + \alpha \delta_{ij} \right)}_{[D]^p} d\varepsilon_{kl} \quad \text{A.26}$$

Develop the plastic stiffness matrix,

$$[D]^p = D_{ijkl}^e \left( \frac{\sigma'_{ij}}{2\sqrt{J_2}} + \alpha \delta_{ij} \right) d\varepsilon_{kl} \lambda_{dp} \quad \text{A.27}$$

Substitute  $D_{ijkl}^e$  in Eq. 2.62 for expanding  $[D]^p$  in Eq. A.27,

$$[D]^p = \left[ \lambda (\delta_{ij} \delta_{kl}) + \mu (\delta_{ik} \delta_{jl} + \delta_{il} \delta_{jk}) \right] \left( \frac{\sigma'_{kl}}{2\sqrt{J_2}} + \alpha \delta_{kl} \right) d\varepsilon_{kl} \lambda_{dp} \quad \text{A.27(a)}$$

$$[D]^p = \left[ \lambda \delta_{ij} \delta_{kl} \frac{\sigma'_{kl}}{2\sqrt{J_2}} + \lambda \alpha \delta_{ij} \delta_{kl} \delta_{kl} + \mu \delta_{ik} \delta_{jl} \frac{\sigma'_{kl}}{2\sqrt{J_2}} + \mu \alpha \delta_{ik} \delta_{jl} \delta_{kl} + \mu \delta_{il} \delta_{jk} \frac{\sigma'_{kl}}{2\sqrt{J_2}} + \mu \alpha \delta_{il} \delta_{jk} \delta_{kl} \right] d\varepsilon_{kl} \lambda_{dp} \quad \text{A.27(b)}$$

$$[D]^p = \left[ 0 + \lambda \alpha 3 \delta_{ij} + \mu \frac{\sigma'_{ij}}{2\sqrt{J_2}} + \mu \alpha \delta_{ij} + \mu \frac{\sigma'_{ji}}{2\sqrt{J_2}} + \mu \alpha \delta_{ji} \right] d\varepsilon_{kl} \lambda_{dp} \quad \text{A.27(c)}$$

$$[D]^p = \left[ \alpha (3\lambda + 2\mu) \delta_{ij} + \mu \frac{\sigma'_{ij}}{\sqrt{J_2}} \right] d\varepsilon_{kl} \lambda_{dp} \quad \text{A.27(d)}$$

Substitute  $\lambda_{dp}$  in Eq. A.24 into  $[D]^p$  in Eq. A.27(d), and modify the index notation.

$$[D]^p = \left[ \frac{\left[ \frac{\mu\sigma'_{kl}}{\sqrt{J_2}} + \alpha(3\lambda + 2\mu)\delta_{kl} \right] \left[ \frac{\mu\sigma'_{mn}}{\sqrt{J_2}} + \alpha(3\lambda + 2\mu)\delta_{mn} \right]}{3\alpha^2(3\lambda + 2\mu) + \mu + \left[ 2\alpha^2 + \frac{2}{3} \right] \sigma_{eqs}(H) \left[ \alpha + \frac{1}{\sqrt{3}} \right]} \right] \delta_{mk} \delta_{nl} d\varepsilon_{kl} \quad \text{A.27(e)}$$

Then expand  $d\sigma_{ij}$  in Eq. A.26, finally the constitutive equation of DP can be expressed as;

$$d\sigma_{ij} = \underbrace{D_{ijkl}^e}_{[D]^e} d\varepsilon_{kl} - \underbrace{\left[ \frac{\left[ \frac{\mu\sigma'_{kl}}{\sqrt{J_2}} + \alpha(3\lambda + 2\mu)\delta_{kl} \right] \left[ \frac{\mu\sigma'_{mn}}{\sqrt{J_2}} + \alpha(3\lambda + 2\mu)\delta_{mn} \right]}{3\alpha^2(3\lambda + 2\mu) + \mu + \left[ 2\alpha^2 + \frac{2}{3} \right] \sigma_{eqs}(H) \left[ \alpha + \frac{1}{\sqrt{3}} \right]} \right]}_{[D]^p} \delta_{mk} \delta_{nl} d\varepsilon_{kl} \quad \text{A.28}$$



## APPENDIX 2 - Calculation of ultimate strain, $\varepsilon_{crc}$

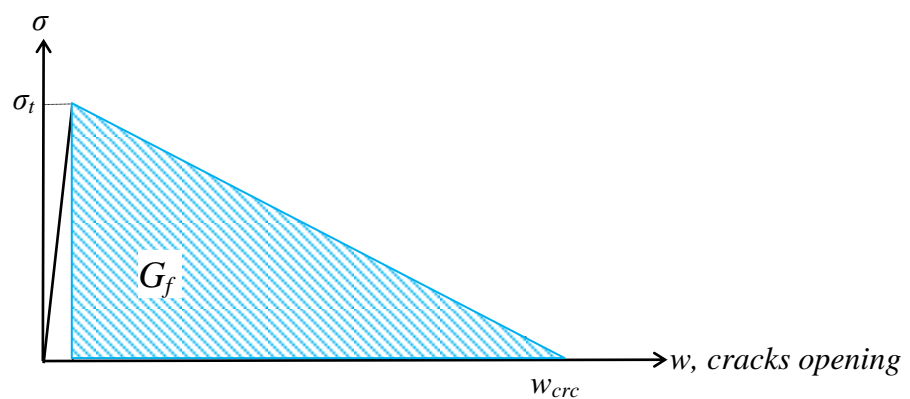
In order to restrain the cracking of concrete and mortar material, ultimate strain  $\varepsilon_{crc}$  is calculated by fracture energy,  $G_f$  and depend on the particle size. In this thesis, anchor bolt in concrete and mortar block were used for the validation of numerical analysis. The fracture energy of concrete and mortar are calculated, refer to JSCE standard.

### A-3 Calculation of ultimate tensile strain of concrete material for the numerical model

Use the formulation as below,

$$G_f = \int_0^{\infty} \sigma d\varepsilon \quad \text{A.29}$$

and use the relationships between stress and crack opening relationships in Fig. A-1



**Figure A-1:** Relationships between stress cracking zone and crack opening

Thus,

$$G_f = \frac{1}{2} \sigma_t w_{crc} \quad \text{A.30}$$

where  $w_{crc}$  is ultimate crack opening. Refer to JSCE standard, based on tension softening of normal concrete, the fracture energy ( $G_f$ ) may be obtained as,

$$G_f = 10(d_{\max})^{\frac{1}{3}} f_c^{\frac{1}{3}} \quad \text{A.31}$$

then, the ultimate strain ( $\varepsilon_{crc}$ ) can be calculated as,

$$\varepsilon_{crc} = \frac{w_{crc}}{d^\phi} \quad \text{A.32}$$

where  $d_{\max}$  is the maximum size of aggregate (mm),  $f_c$  is the characteristic compressive strength of concrete (MPa), and  $d^\phi$  is the particle diameter of material model. If the compressive strength of concrete is assumed 24.5 MPa and maximum diameter of aggregate is 20 mm. Thus, the fracture energy is;

$$G_f = 10(20)^{\frac{1}{3}} 24.5^{\frac{1}{3}} = 79.37 \text{ N/m} \quad \text{A.33}$$

meanwhile, the tensile strength,  $\sigma_t$  is  $3.57 \times 10^6 \text{ N/m}^2$ . Therefore,

$$79.37 = \frac{1}{2} (3.57 \times 10^6) w_{crc} \quad \text{A.34}$$

Get the ultimate crack opening

$$\therefore w_{crc} = 4.446 \times 10^{-5} \text{ m} \quad \text{A.35}$$

Finally, the ultimate strain can be calculated as below if the particle size,  $d^\phi$  is 0.003 m,

$$\varepsilon_{crc} = \frac{w_{crc}}{d^{\phi}} = \frac{4.446 \times 10^{-5}}{0.003} 10^6 = 14,820 \mu \approx 15,000 \mu \quad \text{A.36}$$

#### A-4 Calculation of ultimate tensile strain of mortar in the experimental model

Calculation of the ultimate strain for the numerical analysis of experimental model is as follows.

From the experimental test data, the compressive strength of mortar is 48.18 MPa and maximum diameter of aggregate is 5 mm. Thus, the fracture energy is;

$$G_f = 10(5)^{\frac{1}{3}} 48.18^{\frac{1}{3}} = 62.22 \text{ N/m} \quad \text{A.37}$$

meanwhile, the tensile strength,  $\sigma_t$  is  $3.31 \times 10^6 \text{ N/m}^2$ . Therefore,

$$62.22 = \frac{1}{2} (3.31 \times 10^6) w_{crc} \quad \text{A.38}$$

Get the ultimate crack opening

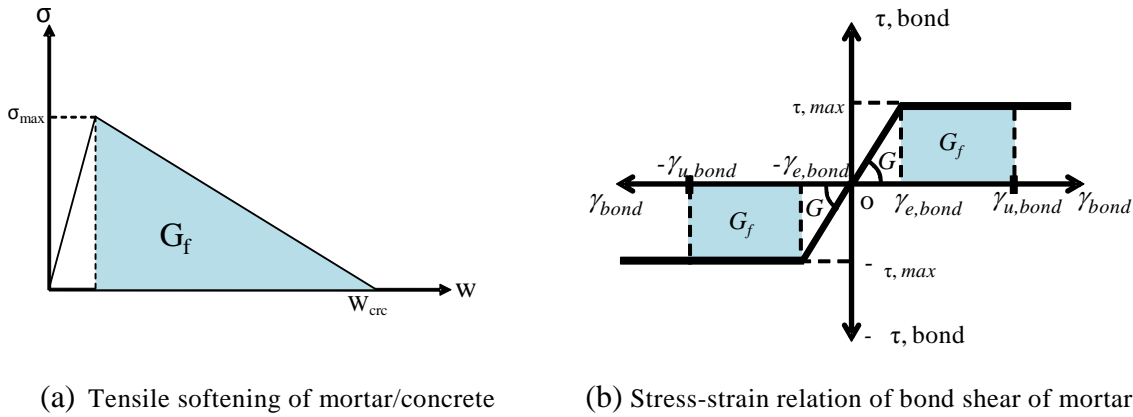
$$\therefore w_{crc} = 3.760 \times 10^{-5} \text{ m} \quad \text{A.39}$$

Finally, the ultimate strain can be calculated as below if the particle size,  $d^{\phi}$  is 0.004 m,

$$\varepsilon_{crc} = \frac{w_{crc}}{d^{\phi}} = \frac{3.760 \times 10^{-5}}{0.004} 10^6 = 9,399 \mu \approx 9,500 \mu \quad \text{A.40}$$

### A-5 Calculation of ultimate shear strain of concrete material for the numerical model

The ultimate tensile strain is counted between the elastic zone having no crack and the completely cracked portion,  $w_{cr}$ . The fracture energy ( $G_f$ ) of tensile fracture is projected as the area below the curve correspond to the maximum elastic tensile strain ( $\sigma_{max}$ ) towards the completely cracked portion ( $w_{cr}$ ) (see Fig. A-2(a)). A shear softening curve expresses the relationship between the transferred stress and sliding crack, and the area below the curve correspond to the fracture energy ( $G_f$ ) of shear, which is equal to the energy required to form a unit area of completely sliding crack and a loose bond (see Fig. A-2(b)). In this analysis the fracture energy obtained by tensile and shear is assumed equal, as a result the limit shear strain in a particle ( $\gamma_{u,bond}$ ) can be obtained as below.



**Figure A-2:** Stress-strain relation of bond shear and bonding shear softening of mortar

Refer to Ikki *et al.* (1996), the maximum shear strength of mortar concrete is shown in Eq. A.41. The maximum shear stress between concrete and reinforce steel bar ( $\tau_{max}$ ) may calculate as,

$$\tau_{max} = 0.9 f'_c \frac{2}{3} = 0.9 \times 24.5 \frac{2}{3} = 7.59 \text{ N/mm}^2 \quad \text{A.41}$$

where,  $f'_c$  is the compressive strength of concrete (MPa). While the shear modulus ( $G$ ) can be found by the following equation.

$$G = \frac{E}{2(1+\nu)} = \frac{21,000}{2(1+0.2)} = 8,750 \text{ N/mm}^2 \quad \text{A.42}$$

where,  $E$  is Young's elastic modulus of concrete (MPa),  $\nu$  is poisson's ratio of concrete. Based on elasticity principles, the elastic strain ( $\gamma_e$ ) is as follows,

$$\gamma_e = \frac{\tau_{\max}}{G} = \frac{7.59}{8,750} = 8.67 \times 10^{-4} \quad \text{A.43}$$

Calculation of fracture energy ( $G_f$ ) of shear is equal to the tensile fracture. Based on Eq. A.31 and A.33, so the ultimate bond strain ( $\gamma_{u,bond}$ ) can be computed. Finally, the bond ultimate strain of concrete is;

$$\gamma_{u,bond} = \frac{G_f}{\tau_{\max} \times d^{\phi}} + \gamma_e = \frac{79.37 \times 10^{-3}}{7.59 \times 3} + 8.67 \times 10^{-4} = 4.35 \times 10^{-3} \quad \text{A.44}$$

#### A-6 Calculation of ultimate shear strain of mortar in the experimental model

In this analysis the fracture energy obtained by tensile and shear is assumed equal, as a result the limit shear strain in a particle ( $\gamma_{u,bond}$ ) can be obtained. Refer to Ikki *et al.* (1996), the maximum shear strength of mortar concrete is shown in Eq. A.45. The maximum shear stress between concrete and reinforce steel bar ( $\tau_{max}$ ) may calculate as,

$$\tau_{\max} = 0.9 f'_c{}^{\frac{2}{3}} = 0.9 \times 48.18^{\frac{2}{3}} = 11.92 \text{ N/mm}^2 \quad \text{A.45}$$

where,  $f'_c$  is the compressive strength of mortar (MPa). While the shear modulus ( $G$ ) can be found by the following equation.

$$G = \frac{E}{2(1+\nu)} = \frac{27,000}{2(1+0.2)} = 11,250 \text{ N/mm}^2 \quad \text{A.46}$$



where,  $E$  is Young's elastic modulus of concrete (MPa),  $\nu$  is poisson's ratio of concrete. Based on elasticity principles, the elastic strain ( $\gamma_e$ ) is as follows,

$$\gamma_e = \frac{\tau_{\max}}{G} = \frac{11.92}{11,250} = 1.06 \times 10^{-3} \quad \text{A.47}$$

Calculation of fracture energy ( $G_f$ ) of shear is equal to the tensile fracture. Based on Eq. A.37, so the ultimate bond strain ( $\gamma_{u,bond}$ ) can be computed. Finally, the bond ultimate strain of concrete is;

$$\gamma_{u,bond} = \frac{G_f}{\tau_{\max} \times d^{\phi}} + \gamma_e = \frac{62.22 \times 10^{-3}}{11.92 \times 4} + 1.06 \times 10^{-3} = 2.36 \times 10^{-3} \quad \text{A.48}$$